Spermine-functionalized Perylene Bisimide Dyes: Synthesis and Self-assembly in Water

Dissertation zur Erlangung
des naturwissenschaftlichen Doktorgrades
der Julius-Maximilians-Universität Würzburg

vorgelegt von
Stefanie Margarete Rehm, geb. Krauß
aus Mellrichstadt

Würzburg 2015

Eingereicht am

bei der Fakultät für Chemie und Pharmazie

Gutachter der schriftlichen Arbeit:

1. Gutachter:

2. Gutachter:

Prüfer des öffentlichen Promotionskolloquiums:

1. Prüfer:

2. Prüfer:

3. Prüfer:

Datum des öffentlichen Promotionskolloquiums:

Doktorurkunde ausgehändigt am:

für meine Familie

List of abbreviations

AFM	atomic force microscopy
ATP	adenosine triphosphate
CD	circular dichroism
DCC	*N*,*N*'-dicyclohexylcarbodiimide
DCTB	*trans*-2-[3-(4-*tert*-butylphenyl)-2-methyl-2-propenylidene]malononitrile
DIPEA	diisopropylethylamine (Hünig's base)
DMF	dimethyl formamide
DMSO	dimethyl sulfoxide
DNA	deoxyribonucleic acid
ESI	electro spray ionization
FT-IR	Fourier transformation – infrared
HEPES	2-[4-(2-hydroxyethyl)piperazin-1-yl]ethanesulfonic acid
HOBt	*N*-hydroxybenzotriazole
HPLC	high-performance liquid chromatography
HRMS	high resolution mass spectrometry
LD	linear dichroism
LDI	laser desorption ionization
MALDI	matrix assisted laser desorption ionization
MES	2-(*N*-morpholino)ethanesulfonic acid
MOPS	3-morpholinopropane-1-sulfonic acid
m.p.	melting point
NMR	nuclear magnetic resonance
PBI	perylene bisimide
PET	photoinduced electron transfer
RNA	ribonucleic acid
RT	room temperature
^{t}Boc	*tert*-butyloxycarbonyl
TEM	transmission electron microscopy
TFA	trifluoroacetic acid
TLC	thin layer chromatography
TMS	tetramethylsilane
TOF	time of flight
TRIS	2-amino-2-hydroxymethyl-propane-1,3-diol
UV/Vis	ultraviolet/visible

Table of Contents

Chapter 1

Introduction and Aim of the Thesis

Nature's amazing portfolio of molecular and supramolecular designs inspires researchers of numerous disciplines to mimic these. Understanding the underlying principles and developing advanced functional applications by rational design are major objectives.

Amphiphilic and bolaamphiphilic molecules – characterized by hydrophobic and hydrophilic structural elements – and their supramolecular assemblies are ubiquitous in nature and essential for life, for example as membranes formed by lipid bilayers.[1] There are incredibly many possibilities to covalently link hydrophobic and hydrophilic structural elements for designing artificial amphiphilic and bolaamphiphilic molecules and just as much options to vary the external conditions of assembly. Perylene tetracarboxylic bisimide (PBI, Figure 1) as the hydrophobic part and the naturally occurring polyamine spermine (**1**, Figure 1) as the hydrophilic component can be covalently connected to form such bolaamphiphilic molecules. In water these bolaamphiphiles form supramolecular systems. The synthesis of those building blocks and the investigation of their self-assembly behavior in water are the objectives of this thesis. This work though contributes to understanding the principles of self-assembly of perylene bisimide dyes in water and so should help to develop applications of those systems.

In the last decade perylene bisimide dyes, the most prominent members of the rylene chromophore class, were widely used for the construction of supramolecular aggregates based on their affinity for extensive π-stacking.[2] Bay-unsubstituted PBIs are planar molecules which interact with each other by strong hydrophobic interactions. Furthermore, PBIs exhibit a strong quadrupol moment which delivers additional binding strength between the polyaromatic compounds.[3] A large variety of substituents can be linked with the chromophore, either in the bay- or *ortho*-positions or in the imide-positions via the central nitrogen atoms (Figure 1).[2,4–11] The substituents are necessary due to mainly two reasons: first, they act as solubility enhancing groups for the appropriate solvent used and, second, their intrinsic structure (steric hindrance, chirality, charged or other functional groups, ...) has an immediate impact on the size, the structure and the function of both the monomeric building block and the resulting supramolecular aggregate.

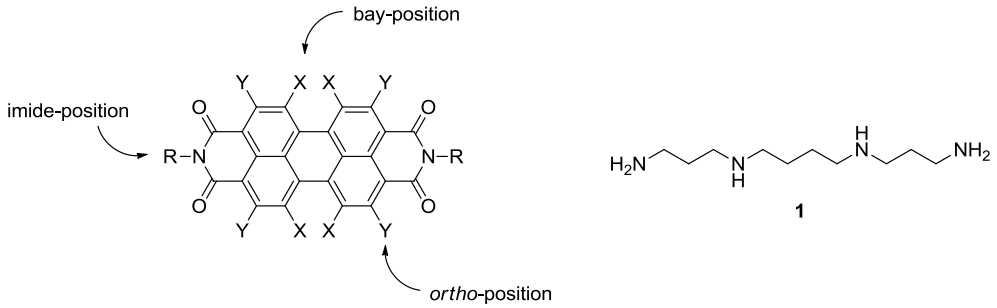

Figure 1. General chemical structure of perylene bisimide dyes and the diverse anchor points for substituents (left). Naturally occurring polyamine spermine (**1**, right).

Water is a special solvent[12] and it is the solvent of life.[13,14] Achieving solubility of PBIs in water is a challenge. It can be successful by introducing ionic or polar residues to the PBI core. The high polarity of water molecules and their ability to act simultaneously as hydrogen bond donor and acceptor results in weakened electrostatic and dipole interactions. In organic solvents these forces are considered to be the most important ones due to their directionality, specificity and strength.[15,16] Therefore both the process of self-assembling molecules and the design of tailor-made supramolecular structures need to be redirected on the properties of water as solvent.

The set of non-covalent interactions delivers also forces which can be very strong in polar and protic solvents as in case of amphiphilic phospholipids. The consequent

separation of hydrophobic parts (alkyl chains) from hydrophilic parts (polar or even charged head groups) is the basis for the construction of double-layered cell membranes.[17] As extension of this natural architecture the attachment of a second polar head group at the free end of the hydrophobic alkyl chain results in a building block with a bolaamphiphilic structure. The unpolar segment or core is surrounded by a polar or even charged environment (Figure 2).[18–20]

The main driving force for the self-assembly process of such building blocks is based on the hydrophobic collapse of the core elements. Their all-over unpolar chemical characteristics avoid the close contact with water molecules and push the monomers into an aggregate state by weak intermolecular forces, e.g. van-der-Waals or π-π-stacking interactions. Beside these mutual interactions the reintegration of loosely ordered water molecules from the surface of the hydrophobic molecules into the hydrogen-bond network of the bulk solvent delivers additional binding energy. With this concept at hand highly specific structures can be built either by the variation of the hydrophobic part or by introducing different polar groups.[3,21–27]

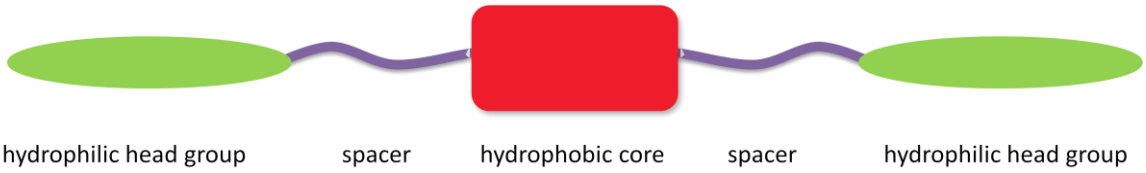

Figure 2. Schematic illustration of a bola-amphiphilic building block: hydrophilic head groups (polar or charged residues) connected via spacers to the central hydrophobic core.

Spermine, present in virtually all living cells, is a linear alkyl amine with four amino groups. It is fully protonated at physiological pH (approx. 7.4; pK_a (spermine) = 10.86, 10.05, 8.82, 7.95) and is hence highly polar and hydrophilic. Spermine as a polycation interacts with (poly)anions. In the cell such (poly)anions are nucleic acids (DNA, RNA), adenosine triphosphate (ATP), phospholipids (in membranes) or specific proteins.[28] As a result of this interaction, spermine plays important roles in cell physiology including effects on the structure of cellular macromolecules, gene expression, protein function, nucleic acid and protein synthesis, regulation of ion channels, and providing protection from oxidative damage.[28–30]

Spermine as substituent for PBI enhances the solubility in polar solvents, forming amphiphilic or bolaamphiphilic molecules. Their aggregation behavior in water is of great fundamental interest and biological or medicinal applications of spermine-PBI amphiphiles could be kept in mind.

The aim of this project is the self-assembly of supramolecular structures in water via solubilization of hydrophobic perylene bisimide chromophores by the introduction of the oligoamine spermine via the imide position. These functional residues, which become water-soluble upon protonation, are connected to the hydrophobic dye by different types of spacers, achiral ones of varying length and chiral ones with diverse steric hindrance (Figure 3). In case of the chiral bola-amphiphiles also neutral analogues with dodecyl alkyl chains are synthesized in order to compare the self-assembly process of charged and uncharged building blocks in water and chloroform as organic solvent, respectively.

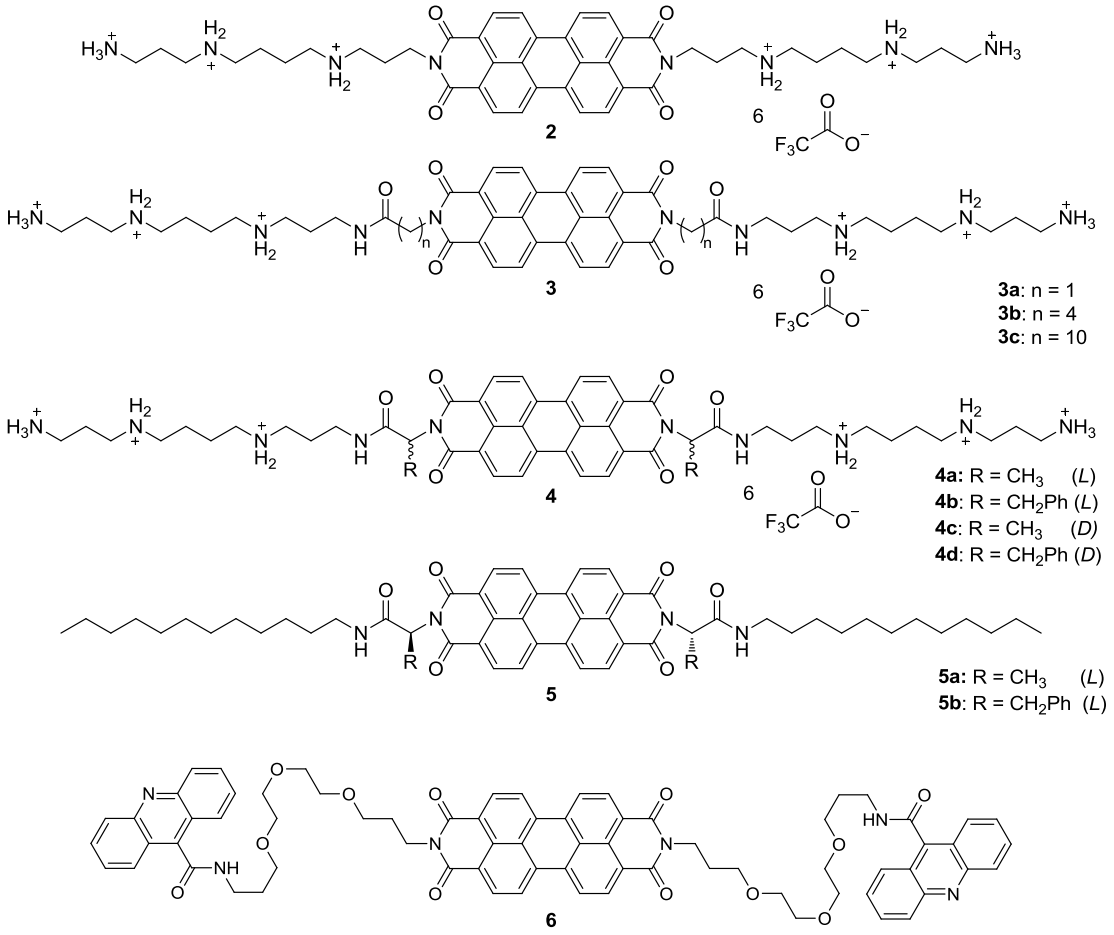

Figure 3. Overview on the perylene bisimide based building blocks synthesized, analyzed and discussed in this thesis.

The results presented in this thesis provide a new route for the synthesis of water-soluble perylene bisimide dyes, give a deeper insight into the aggregation behavior of the highly fluorescent bola-amphiphiles and discuss the possibility to control the aggregate architecture by the structural characteristics of the spacer moieties.

Chapter 2 presents a literature survey on perylene bisimide dyes with amino- and polyamino substituents in the imide-positions. Optical properties, solubility and aggregation behavior are considered particularly. Applications are presented as well.

In **Chapter 3** the synthesis of four perylene bisimide dyes is discussed which were made water-soluble by the introduction of protonatable spermine residues as substituents in the imide position of the chromophore. The bola-amphiphilic character of these dyes was controlled by the introduction of hydrophobic alkylcarbonyl linkers with different length between the chromophore and the polyamine. The aggregation behavior of these six-fold positively charged PBIs was investigated with several spectroscopic and microscopic methods whose results were used for the development of a model of the PBI aggregates formed in pure water.

Chapter 4 describes the synthesis of two chiral pairs of perylene bisimide dyes. Chiral centers were introduced by α-amino acids utilized as linkers between the chromophore and the solubility-enhancing groups. Both enantiomers of alanine and phenylalanine were used for the water-soluble PBI derivatives with spermine chains. Parallel experiments with uncharged PBI derivatives carrying dodecyl alkyl chains as solubility-enhancing groups for unpolar organic solvents were performed only with the *L*-configured enantiomers. The impact on aggregation by chirality and steric hindrance of the amino acid linkers was surveyed with several spectroscopic and microscopic methods focusing here especially on the detection of PBI stacks with a predominant helicity.

In **Chapter 5** the synthesis of a twofold acridine functionalized perylene bisimide dye is described. The aromatic parts are bridged by oligoethylene glycol linkers. First spectroscopic results give a small impression of the aggregation mode in organic solvent.

A summary is given in English (**Chapter 6**) and in German (**Chapter 7**) afterwards.

The experimental section in **Chapter 8** documents materials and methods as well as synthesis and characterization of the compounds described in Chapters 3 to 5.

Chapter 2

Perylene Bisimide Dyes with Amine containing Side Chains

Abstract: In the introductory **Chapter 2** a survey on perylene bisimide dyes with amine containing side chains is given. The role of protonation or quaternization of these amino groups for aggregation and optical properties is presented as well as other influencing parameters. Applications of PBIs with amine containing side chains are mostly based on aggregation – deaggregation processes and accompanied changes in the optical properties. Furthermore literature known PBIs with spermine substituents are presented in this chapter.

2.1 Basic Considerations

As mentioned in the introduction, there are many possibilities to covalently link hydrophobic and hydrophilic structural elements for designing artificial amphiphilic and bolaamphiphilic molecules. The intrinsic properties of the structural elements and the outer conditions like nature and polarity of the solvent, concentration, temperature and possible co-solutes determine the properties of the system.

Molecules with a similar structure as the target molecules bearing a PBI core and two imide-substituents with amino groups can exist in principle as monomers in solution or can interact non-covalently with other PBI molecules forming dimers or higher aggregates. Interactions with other molecules than PBIs are possible as well. The π-surface of the perylene and the amino or positively charged ammonium groups respectively present themselves for non-covalent interactions. Hence, molecules which as well own π-surfaces or anionic molecules or a combination of both are ideal interaction partners for PBIs with amine containing side chains. Most likely the interplay of π-π- and electrostatic interactions is mainly responsible for the resulting system. In this chapter a closer look should be taken on the systems originating from the non-covalent interaction of PBIs with amine containing side chains with itself and other species by giving examples from literature.

Two points play an important role for understanding. These are 1. the distinction of monomeric, dimeric and aggregated PBI by spectroscopic measurements and 2. the ways of quenching fluorescence. It is not intended to discuss these points in detail here, but to refer to literature sources.[3,31–33]

2.2 Perylene Bisimides with Amino-Functionalities in the Imide Positions

Perylene bisimide dyes with amine containing substituents in both imide positions combine the hydrophobic perylene unit and hydrophilic amino or ammonium groups and thus can be regarded bolaamphiphilic molecules. Not all of the compounds presented below are soluble in water and not for all of them the bolaamphiphilic character was the reason for investigating them. Nevertheless, the overview on PBIs with amine containing imide substituents should give the reader an idea about how manifold the structural designs and properties of this type of PBIs are – with main

attention on optical properties, solubility and aggregation behavior. Further, it should be revealed how different parameters, experimental conditions and methods of investigation affect the results and possible applications.

Only symmetrically substituted perylene bisimide dyes will be included into the discussion as the additional discussion of unsymmetrically substituted PBIs would be too far reaching with regard to the compounds addressed in this thesis.

2.2.1 Factors influencing the Fluorescence Quantum Yield

PBIs with the general structure shown in Figure 4 are the amino-functionalized PBIs by far the most represented in the literature.

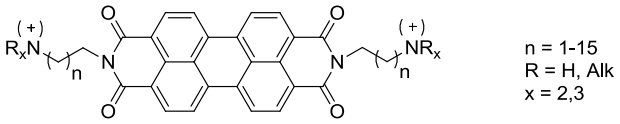

Figure 4. General structure of amino-functionalized PBIs

While in the mid 1990s the synthesis and basic (optical) properties of PBIs **7**–**9** (Figure 5) and of related structures were objects of research, more detailed studies of PBIs **7**–**9** and their applications were in the centre of interest after the turn of the millennium. Especially the influence of alkylation and protonation of the amine functionalities on the fluorescence properties has been considered.

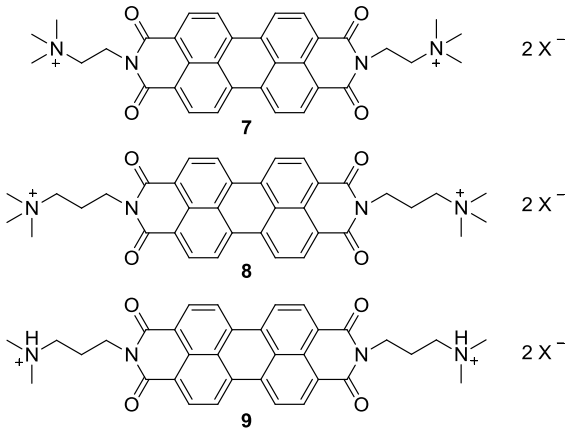

Figure 5. Alkylated or protonated amino-alkyl functionalized PBIs **7**–**9**.

In 1994 *Deligeorgiev et al.* reported about the synthesis and basic optical properties of a series of amino alkylated PBIs (general structure shown in Figure 6) including PBIs **7**–**9**.[34] The distance between the imide nitrogen and the amino groups is either two or three methylene groups. One part of the series bears amino groups, the other part ammonium groups as a result of alkylation with methyl or ethyl halides. The authors recorded UV/Vis and fluorescence spectra of the PBI series in dimethylsulfoxide and acetonitrile. All compounds show similar absorption bands with three distinct peaks between 440 and 520 nm with molar extinction coefficients between 70000 and 80000 $Lmol^{-1}cm^{-1}$. This indicates the presence of monomeric PBI in the utilized organic solvents.

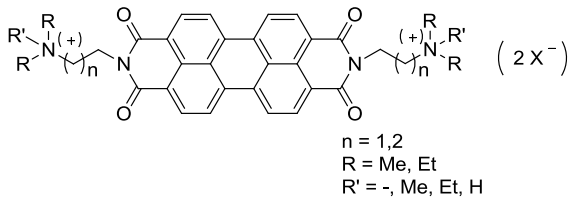

Figure 6. General structure of amino alkylated PBIs **7**–**15**. For substituents, see Table 1.

Table 1. Fluorescence quantum yields of **7**–**15**.

Compound	R	R'	n	solvent	Φ_{fl}
9	Me	-	3	acetonitrile	0.001
10	Me	-	2	acetonitrile	0.001
11	Et	-	2	acetonitrile	0.001
12	Et	-	3	acetonitrile	0.001
9H$^+$	Me	H	3	acetonitrile+ $HClO_4$	0.79
10H$^+$	Me	H	2	acetonitrile+ $HClO_4$	0.86
11H$^+$	Et	H	2	acetonitrile+ $HClO_4$	0.80
12H$^+$	Et	H	3	acetonitrile+ $HClO_4$	0.81
7	Me	Me	2	acetonitrile	0.84
8	Me	Me	3	acetonitrile	0.88
13	Me	Et	3	acetonitrile	0.80
14	Et	Et	2	acetonitrile	0.76
15	Et	Me	3	acetonitrile	0.84

Comparing the shapes and positions of the absorption and emission spectra of the neutral compounds **9–12** and the cationic compounds **7**, **8**, and **13–15**, there are only little significant variations. But while the neutral compounds PBIs **9–12** show almost no fluorescence in acetonitrile, their protonated counterparts (in acetonitrile with perchloric acid, **9H$^+$–12H$^+$**) and alkylated counterparts (**7**, **8**, **13–15**) fluoresce with quantum yields of 0.76-0.88. Compared to the protonated and the quaternized PBIs, **9–12** must have a nonradiative deactivation pathway or fluorescence must be quenched otherwise. This can be explained by photoinduced electron transfer (PET, Figure 7a). Molecular systems owning a fluorophore (e.g. perylene bisimide) and an ion receptor (e.g. amines) are known to undergo photoinduced electron transfer as their π- and n-electron systems weakly interact with each other.[35] The ion receptor as the photo electron donor and the fluorophore as the acceptor are therefore covalently connected by a σ-bonded spacer. When the fluorophore is photoexcited, electron transfer from the ion receptor to the excited fluorophore is usually favored over fluorescence. The suppression of the photoinduced electron transfer can be achieved by ionization of the ion receptor (e.g. by protonation or alkylation of the amino group, Figure 7b) as the oxidation potential of the donor is raised. Fluorescence of the acceptor is recovered.[35]

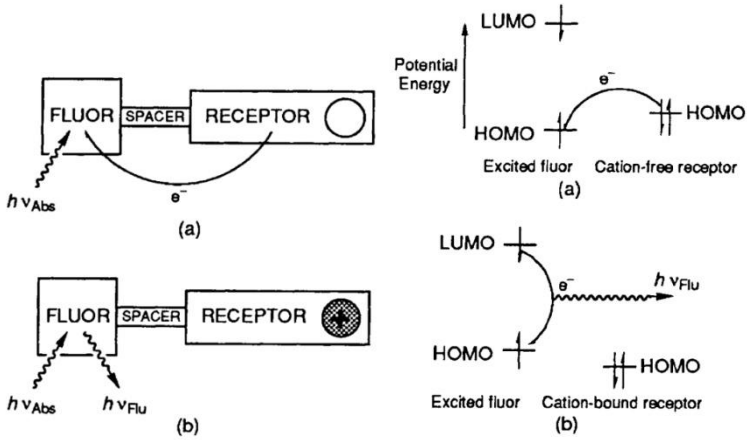

Figure 7. Schematic representation (left) and frontier orbital energy representation (right) of photoinduced processes in a 'fluoro-spacer-receptor' signaling system (a) when cation-free and (b) when cation-bound. Reproduced from ref. [35] with permission of The Royal Society of Chemistry.

Daffy et al. found fluorescence enhancement values between factors 2.6 and 46 on protonation of PBIs **11**, **12**, (Figure 6) and **16** (Figure 8) at low pH compared to the non-protonated (neutral) compounds at higher pH.[36] **16** with primary amine functionalities shows the weakest effect on decreasing pH in aqueous solution as primary amines are

less oxidizable respectively than tertiary ones. **12** exhibits a 46 times higher fluorescence intensity at low pH than at high pH. For **11** the effect is significant (fluorescence enhancement = 11) but smaller than for **12**. This indicates the relevance of amine residues (H or alkyl) and the spacer length between the perylene bisimide and the amino group.

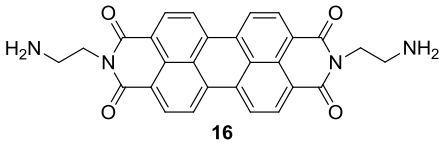

16

Figure 8. PBI **16**, showing fluorescence enhancement on protonation.

PBIs **8** and **9**/**9H**$^+$ were part of a series of PBIs which were presented by *Schnurpfeil et al.* in 1995.[37] The relevant PBI derivatives of this series with amino or ammonium functionalities are shown in Figure 9. The main variations in this series concern the alkyl chain length between the imide-N and the amino functionality and the residues at the amino and ammonium groups respectively. Those derivatives with uncharged amino groups are soluble in organic solvents such as DMSO, DMF and dichloromethane. This also applies for the PBIs of the series which own quaternized ammonium functionalities. With increasing chain length of the quaternizing alkyl groups the solubility decreased significantly. PBI **8**, which is quaternized with methyl iodide, is soluble in water. The authors also found that different amino-alkyl substituents in the imide positions do not influence the position of the absorption and emission spectra but they influence the fluorescence quantum yields. Fluorescence quantum yields of **8** and **19a–c** were determined in DMSO. PBI **8** shows the lowest (0.28) compared to **19a–c** (with Φ_{fl} = 0.44, 0.41, 0.62, respectively) with longer terminal alkyl chains. The authors explain this increase in fluorescence quantum yield by the shielding effect of increasing chain length of the alkylated amine.

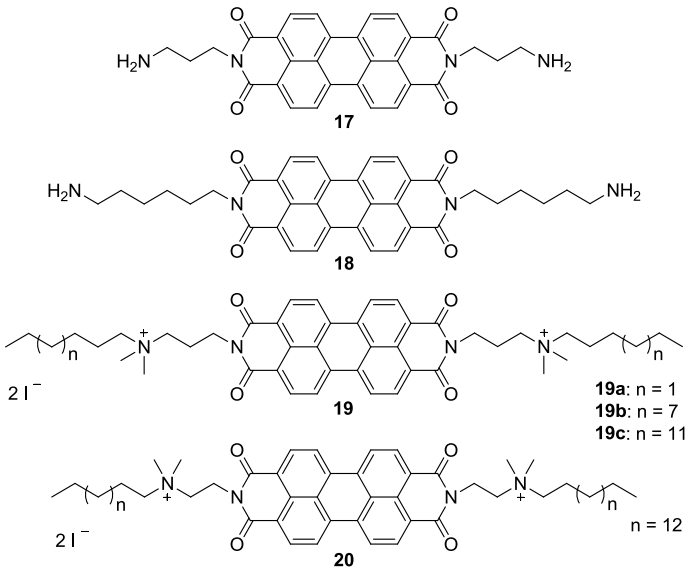

Figure 9. PBIs **17**–**20** with amino- and ammonium groups in the imide positions.

The influence of quaternization of the amino groups on the fluorescence quantum yields of PBI derivatives was described by *Nagao et al.* in 1997 for **7** and its non-methylated version **10**.[38] **10** was almost non fluorescent in acetonitrile whereas **7** showed a considerable quantum yield of 0.84 (in acetonitrile, too). When PBI **10** is quaternized with hexadecyl iodide instead of methyl iodide, the resulting PBI **20** (Figure 9) reaches a fluorescence quantum yield of 0.62 in DMSO, which is very similar to the results of *Schnurpfeil et al.* for **19c** with one methyl group less between the imide-N and the amino-N.

Georgiev et al.[39] applied branched tails with polar groups as substituents in the imide positions. Resulting PBI **21** (Figure 10) is equipped with a tertiary amino group, two amide functionalities and two terminal amino groups at each imide substituent. This makes **21** soluble in water, alcohols, DMF and DMSO but not in chlorinated hydrocarbons such as dichloromethane or chloroform.

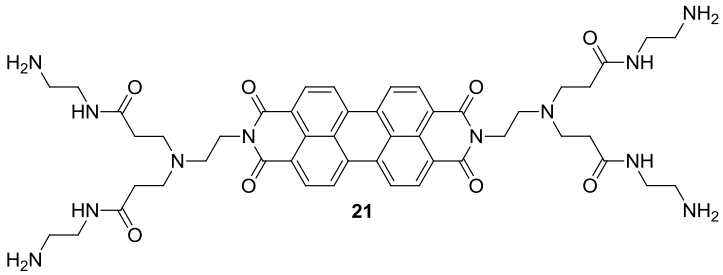

Figure 10. PBI **21** with branched polar tails.

Fluorescence of **21** in DMF is quite low. The authors explain this with a possible photoinduced electron transfer from the tertiary amino groups to the PBI which would cause fluorescence quenching. Protonation of the amino group in turn prevents this photoinduced electron transfer. Fluorescence of **21** in a water/DMF mixture (1:1, v/v) was measured in a pH range between 1 and 10. In acidic medium fluorescence is about 6 times higher than in alkaline medium which the authors call *switched on* (pH 1) and *switched off* (pH > 6). Beside the prevented photoinduced electron transfer enhanced fluorescence is attributed to the reduced aggregation as the protonation of the terminal primary and tertiary amino groups leads to electrostatic repulsion. The charges reduce the attraction between the perylene moieties. PBIs with the described properties seem to be potential sensors not only for protons (pH) but for metal ions, too, as **21** shows selectively increased fluorescence in the presence of certain metal ions.

The amino-imidazole-armed PBI **22** (Figure 11) has been reported by *Zhang et al.* very recently.[40] It was investigated by UV/Vis and fluorescence spectroscopy in aqueous solution in the pH range from 4 to 7.

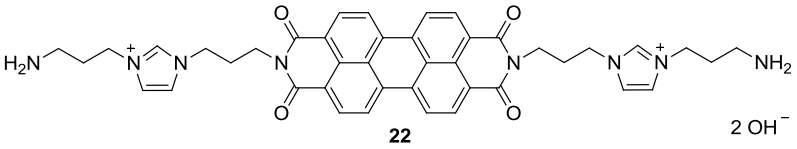

22

Figure 11. Amino-imidazole-armed PBI **22**.

The UV/Vis spectra of **22** (1×10^{-6} M; MOPS [= 3-(N-morpholino)propanesulfonic acid] buffer) show aggregated species for all pH values, but to varying degrees. The lowest pH value (= 4) corresponds to the least aggregated species of **22** which explains the results of fluorescence measurements as well. The solution with the lowest pH showed the highest fluorescence as it is least aggregated. Fluorescence could only be detected for solutions of **22** below pH 7 as fluorescence is quenched in highly aggregated states.[31] TEM images of **22** at different pH are in accordance with the results from UV/Vis and fluorescence investigations. At pH 4.0 and 5.0 PBI **22** forms smaller supramolecular structures (short nanobelts of 50 nm length, Figure 12A and B). At pH 6.0 and 7.0 larger structures were observed (hybranched longer nanobelts, Figure 12C and D).

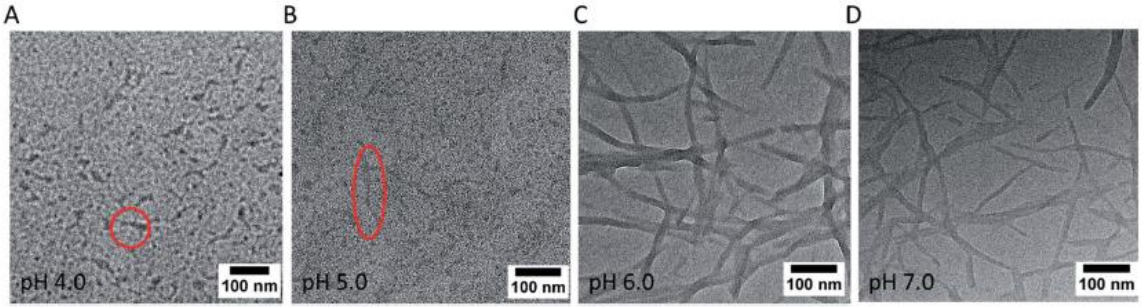

Figure 12. TEM images of **22** at pH 4 (A), 5 (B), 6 (C), and 7 (D). Reproduced from ref. [40] with permission of The Royal Society of Chemistry.

The results show that the extent of protonation of the terminal amino groups (which is higher at lower pH values) influences the aggregation behavior of the PBI dyes which can be explained by intermolecular electrostatic and dispersion interactions. The lower the pH, the higher the protonation and the higher the electrostatic repulsion among the imide substituents which in turn counteracts the π-π-interaction of the PBI. This sensitive pH responding self-assembly of **22** is reversible and could be applied for sensing purposes (see 2.2.2).

Quaternization and protonation of aminoalkyl functionalized PBIs lead to an increase of the fluorescence quantum yields. This seems to be a result of the interplay between reduced aggregation on the one hand and hampered photoinduced electron transfer on the other hand. It is not clear what effect plays the major role. To clarify this question **23** (Figure 13) with tertiary amine groups and two additionally carboxylic acid groups was synthesized and investigated by the Hirsch group.[41] The authors analyzed the optical properties of **23** in four different solvent systems with surprising results for the fluorescence intensity in aqueous solution (Table 2). **23** is strongly aggregated both in acidic and basic aqueous solution even at low concentration (5 x 10^{-6} M). Aggregation in diluted $HCl_{(aq)}$ is even more pronounced than in diluted $NaOH_{(aq)}$ which can be derived from the shape of the UV/Vis spectra (Figure 14). In basic solution (pH ~ 11) the four carboxylic acid functions are deprotonated, the amine is neutral.

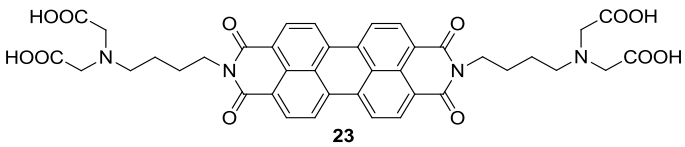

23

Figure 13. PBI **23** with tertiary amine groups and carboxylic acid groups.

Table 2. Optical properties of **23** in aqueous and organic solvents. Adapted from ref. [41] by permission of The Royal Society of Chemistry.

property	diluted $HCl_{(aq)}$	diluted $NaOH_{(aq)}$	DMSO	DMSO with TFA
ε_{max}	17800	24000	33900	57500
$\lambda_{abs,\ max}$ (nm)	549, 481	543, 500	528, 494, 460	528, 494, 460
$\lambda_{fluo,\ max}$ (nm)	587, 546	587, 546	580, 543	580, 543
Φ_{fl}	0.27	2.3	9.1	64
PET possible	No	Yes	Yes	No
aggregation	strongest	strong	less	least

Aggregation of the PBI cores of **23** is suggested to take place in a rotational way so that electrostatic repulsion by the negative charges is minimized. Under acidic conditions (pH ≈ 3) the carboxylic acid functions with an isoelectric point of 2 are only partly protonated which possibly has as a consequence that electrostatic repulsion cannot sufficiently hinder aggregation by π-π-stacking (positive charges at the amines and remaining negative charges at the carboxylic acid groups may neutralize each other). Additionally, intermolecular hydrogen bonds between the protonated carboxylic acid groups might support aggregation. While the tertiary amines are protonated under acidic conditions and the free electron pair is therefore not available for photoinduced electron transfer, it is available for photoinduced electron transfer under basic conditions. These results suggest that the fluorescence quenching by aggregation prevails over inhibition of quenching by amine protonation.

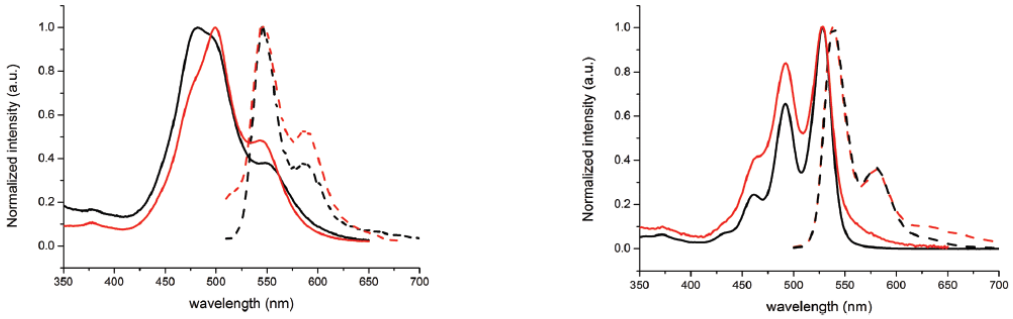

Figure 14. Absorption and fluorescence spectra of **23** in $NaOH_{aq}$ (red curve) and in HCl_{aq} (black curve), c = 5 x 10^{-6} M (left). Absorption and fluorescence spectra of **23** in DMSO (red curve) an in acid-DMSO (black curve), c = 5 x 10^{-6} M (right). Reproduced from ref. [41] with permission of The Royal Society of Chemistry.

In pure DMSO the solubility is enhanced compared to aqueous solutions. The UV/Vis spectrum (c = 5 x 10^{-6} M) shows vibrational fine structure where the ratio between the 0-0 and the 0-1 band is 1.2 (Figure 14, right, red curve). This is evidence for the co-existence of monomer and aggregate. The fluorescence quantum yield is indeed higher compared to the aqueous solutions but still below 0.1 due to fluorescence quenching by photoinduced electron transfer. Addition of trifluoroacetic acid to the solution of **23** in DMSO leads to deaggregation and an overall increase of the extinction coefficients as well as to a strong increase in fluorescence quantum yield to 0.64. This increase is based on the protonation of the tertiary amines which prevents photoinduced electron transfer and additionally causes repulsion between PBI molecules by the emerging positive charges. Electron transfer processes or rather their prevention play a major role at using the changes in fluorescence intensity of PBIs for sensing purposes (see 2.2.2).

The above mentioned examples demonstrate how photoinduced electron transfer could be prevented by protonation or alkylation of the corresponding donor unit, the amine. *Wu et al.* showed that using ionic liquids as solvents can prevent photo induced electron transfer in those systems as well.[42] Optical properties of PBIs **9** and **10** have been measured in two different ionic liquids (which are on the basis of imidazolium) and in conventional organic solvents for comparison. The shapes of absorption and emission spectra are very similar for all solvents (Figure 15) but the fluorescence quantum yields of **9** and **10** are much higher in ionic liquids (Φ_{fl} between 0.98 and 0.43) compared to the values in organic solvents such as DMF, THF, CH_2Cl_2 and toluene (Φ_{fl} between 0.02 and 0.06). Here again the efficient prevention of a photoinduced electron transfer is likely to be the cause of the increased fluorescence. It is assumed that photoinduced electron transfer occurs mainly from a conformation which is not significantly populated in ionic liquids. Furthermore the viscosity of ionic liquids seems to play a role as well. Interestingly, the nature of the counter-anion of the applied ionic liquid has a significant effect. For both **9** and **10** the quantum yield is around twice as high in the ionic liquid with hexafluorophosphate (PF_6^-) compared to the one with tetrafluoroborate (BF_4^-) counterion. The reason for this effect is not given.

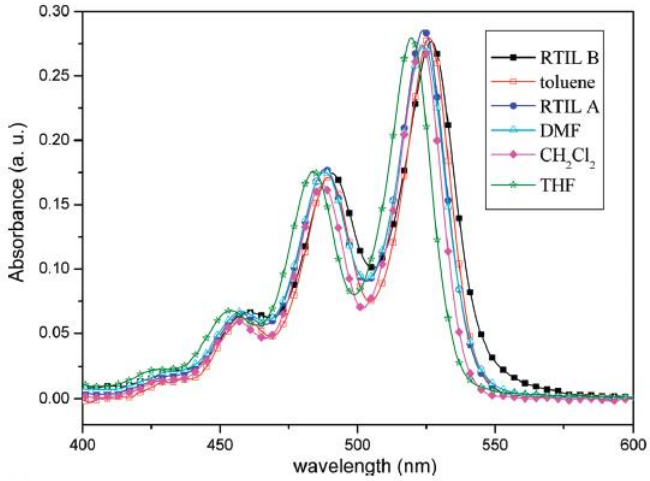

Figure 15. Absorption spectra of **10** in different solvents. Reproduced with permission from ref. [42]. Copyright 2010, American Chemical Society.

2.2.2 Sensing

Changes in the optical properties of dyes due to modified conditions can generally be applied for sensing purposes, for example for sensing of clinically or environmentally relevant species. So it is for perylene bisimide dyes as mentioned briefly before.

PBI **8** for example is widely used as direct or indirect (fluorescence) sensor for diverse species, e.g. metal ions, certain proteins or the detection of cleavage of single stranded DNA. The mechanism is very similar for all these approaches. It makes use of the dependence of the optical properties (first of all the fluorescence properties) of **8** on its aggregation behavior with itself and/or suitable partners in aqueous solution. Exemplary, PBI **8** interacts with a thymine rich, anionic oligonucleotide resulting in strong aggregation and loss of fluorescence intensity of the PBI. Thymine also specifically interacts with Hg^{2+}. Addition of Hg^{2+} to a mixture of **8** and the thymine rich oligonucleotide leads to a decreased aggregation of **8** (because the aggregation promoting oligonucleotide preferably interacts with Hg^{2+}) and to an increase in its fluorescence intensity.[43,44] Fluorescence quenching by oligonucleotide supported aggregation of **8** can be neutralized by metal ions like Hg^{2+}. This can be used as sensor system for those metal ions. Applying another oligonucleotide with specific binding affinity to a certain protein for example results in a sensor system for this protein (e.g. lysozyme[45] or thrombin[46]) as binding of the oligonucleotide to the protein again reduces the aggregation and thus increases fluorescence intensity of **8**. This method is

one of the most sensitive label-free protein detection methods known up to date.[45,46] Fluorescence recovery through the disassembly of **8** from a **8**/DNA ensemble upon DNA cleavage is another possible application. This is for detection of enzymatic or oxidative cleavage of single-stranded DNA.[47] All examples described for application of **8** for sensing purposes are based on the aggregation behavior of the cationic PBI dye, its influencable electrostatic interactions with (poly)anions and the related fluorescence properties and have in common their high sensitivity and selectivity.

PBI derivatives with tris-(2-aminoethyl)amine as basic structure element (Figure 16, top) have been found to selectively sense for Pb^{2+}[48], Al^{3+}[49], Hg^{2+}[50], Fe^{3+}[51], Cu^{2+}[52] or Zn^{2+} and Cd^{2+}[53] with high sensitivity dependent on the exact structure and properties of the residues in the imide position (Figure 16, bottom), the solvent and the pH. Fluorescence is quenched in each case by photoinduced electron transfer from the tertiary amine to the PBI core and/or by strong aggregation. On addition of the suitable cation either photoinduced electron transfer is blocked due to metal-ion binding by the tertiary nitrogen or deaggregation takes place or both processes. This provides fluorescence enhancement. Sensors of this type are therefore called ‘turn-on’ sensors. Solvent and pH are major factors in these systems. Different selectivity was found for example for the same PBI at pH 6 (sensing Zn^{2+}) and pH 9 (sensing Cd^{2+}) and in different solvents like acetonitrile, dimethylformamide/water, acetonitrile/water, water/THF, and aqueous buffer.[53] The solvent influences the aggregation behavior which in turn affects fluorescence intensity. But not only solvent quality and pH influence the fluorescence response of the PBI but the counterions of the metal cations seem to affect the sensing ability as well. This has been shown for PBI-thiophene and different Hg-salts.[50]

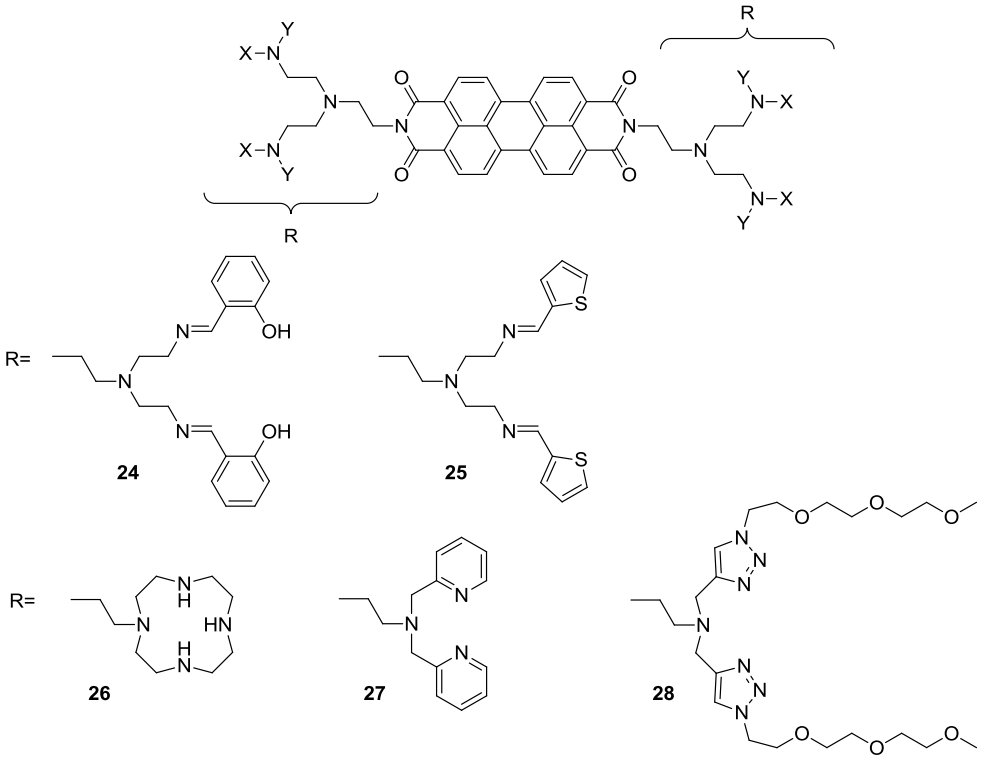

Figure 16. General structure of PBIs with tris-(2-aminoethyl)amine side chains (top) and possible imide substituents (bottom).

In section 2.2.1 PBI **22** has been described to show different aggregation extents at different pH values.[40] Due to this fact, glucose can be indirectly detected in aqueous solution with this PBI dye. Increasing fluorescence intensity is detected with increasing concentration of glucose in the presence of glucose oxidase. Glucose is oxidized by glucose oxidase. The resulting gluconic acid decreases the pH and so increases the degree of protonation of **22**. Thus aggregation is reduced and fluorescence enhanced. Changes in fluorescence quantum yields have been explained here exclusively by aggregation/deaggregation processes due to protonation of the terminal amino functionality but the authors did not enter into the possibility of photoinduced electron transfer as a reason for reduced or completely quenched fluorescence. The free electron pair at the terminal amino group should in principle be able to participate in a photoinduced electron transfer but is possibly too far away. Due to the mesomeric charge distribution the free electron pair at the imidazolium subunit is not available for photoinduced electron transfer.

The varying optical properties of **23** at different pH values have already been described in 2.2.1, as well. This species offers potential for sensing purposes beyond the

acid/base equilibrium as the EDTA-like periphery with the tertiary amine functionalities is able to chelate metal cations.[41] The complexation properties towards metal cations thereby are strongly influenced by the aggregation state of **23** in water and organic solvents. In aqueous solution, where **23** is strongly aggregated from the beginning, fluorescence is quenched in the presence of bi- and trivalent cations, especially for transition metals and lanthanide cations (e.g. Cu^{2+}, Cu^{3+}, Fe^{2+}, Fe^{3+}, Cd^{2+}, Zn^{2+}, Co^{2+}, Hg^{2+}, La^{3+}, In^{3+}, Sc^{3+}). The authors attribute this effect to an energy/electron transfer between the metal (possibly their *d* electrons) and the PBI core. Furthermore, the metal cations possibly cause the formation of extended aggregates by bridging adjacent small PBI aggregates. The addition of the big alkaline cations K^{+} and Cs^{+} in contrast causes an enhancement of fluorescence intensity in aqueous solution as photoinduced electron transfer may be suppressed. On addition of trivalent metal ions (e.g. Fe^{3+}, Al^{3+}, In^{3+}) a long wavelength emission band is observed furthermore, indicating the formation of a new emitting aggregate species (excimer). In DMSO-water mixture (DMSO-rich), where **23** exists almost monomerically, the situation is different. Both the addition of di- and trivalent metal cations results in the formation of aggregates (which can be concluded from the UV/Vis spectra) but **23** is still mainly present as a monomer in solution.

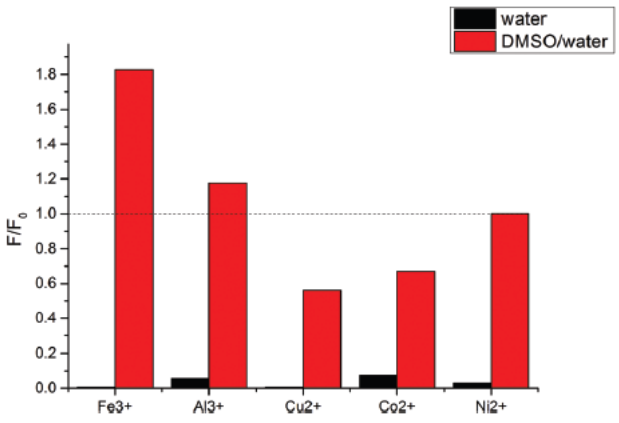

Figure 17. Comparison of the F/F_0 rations for complexes of **23** with M^{2+} and M^{3+} in a DMSO-water mixture (9 : 1) where F is the fluorescence intensity after addition of the cation and F_0 is the fluorescence intensity without metal complexation. Reproduced from ref. [41] with permission of The Royal Society of Chemistry.

Divalent cations such as Cu^{2+} and Co^{2+} cause a decrease in fluorescence emission (most likely due to photoinduced electron transfer from the metal to the PBI) whereas addition of trivalent cations like Fe^{3+} and Al^{3+} here leads to an enhancement of

fluorescence intensity (expressed by a ratio F/F_0 greater than one; see Figure 17) possibly due to the successful interaction of these metal cations with predominant monomeric species, in contrast to the circumstances in aqueous solution, where photoinduced electron transfer processes are suppressed). Overall one can say that the aggregation state of **23** seems to massively influence its complexation properties.

The sensing ability of alkyl-amino functionalized PBIs is based on aggregation – deaggregation processes and/or turned-on or -off photoinduced electron transfer processes. In many examples described in the literature the exact mechanism and the proportion of both processes is not clear and therefore requires more detailed and systematic investigation.

2.2.3 Liquid crystals and Ionic Self-Assembly

Most of the abovementioned investigations have been performed at relatively low concentrations in the range around 10^{-5} M. At much higher concentrations (≈ from 0.1 M onwards) PBIs with alkyl amino or ammonium side chains, respectively, form lyotropic liquid crystalline phases in water. Numerous aromatic compounds with hydrophilic solubilizing groups disposed around the periphery (e.g. dyes, drugs, nucleic acids) form face-to-face aggregates rather than micelles due to their geometry. Those molecules belong to the class of the so called chromonic liquid crystals, a sub class of lyotropic liquid crystals.[54–56] '*Chromonic*' derives from the first chromonic mesogen studied in detail, disodium cromoglycate, which was marketed under the trade name *Chromolyn* in the US.[54]

Tam-Chang and co-workers investigated the properties of different diethylammonium-functionalized PBIs (Figure 18).[57–60] The authors were interested in determining structural factors for liquid crystalline phases as not all amphiphilic or ionic aromatic compounds display liquid-crystalline properties. They wanted to understand the structure-property relationships as this is important for designing novel mesogens, optimizing properties, and designing new applications. In the introduced series of PBIs **11H$^+$**, **29**, and **30H$^+$** just the 'quaternizing groups' (here both alkylation and protonation is intended) and the counterions (chloride or 4-methylbenzenesulfonate = sulf$^-$) alternate.

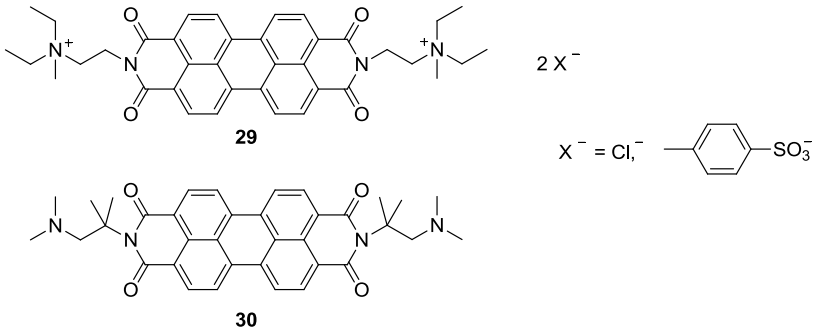

Figure 18. PBI **29** and PBI **30**, showing liquid crystalline phase behavior.

The aggregation behavior at low concentration has been investigated initially. All compounds show similar UV/Vis spectra in water in a concentration range from 10^{-4} to 10^{-7} M. The shapes of the spectra suggest predominantly H-aggregated species of the PBIs – with a greater extent of aggregation for the more concentrated solutions. This behavior is hardly affected by the imide substituents and the counterions. At very much higher concentrations (≈ from 0.1 M onwards) PBI **11H$^+$X$^-$**, **29X$^-$**, and **30H$^+$X$^-$** form liquid crystalline phases. The phase properties were investigated by polarized optical microscopy (Figure 19).

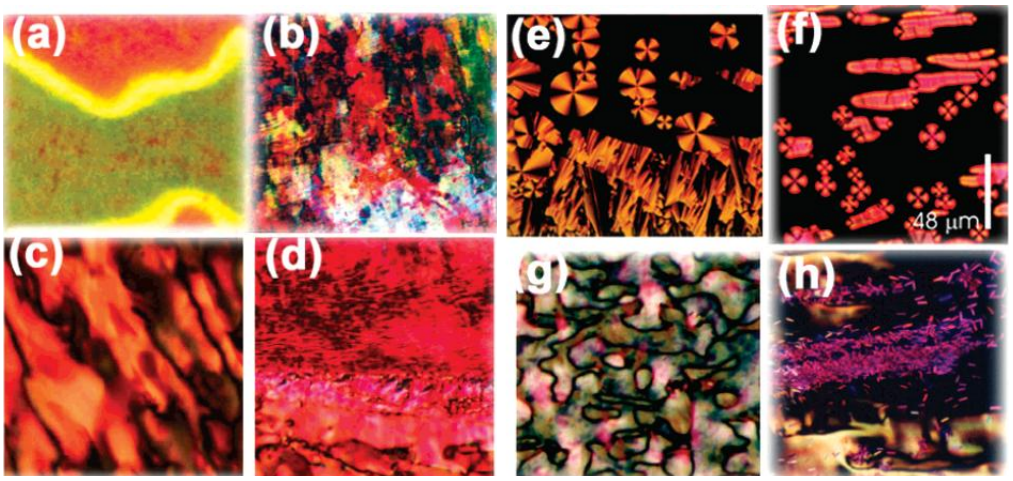

Figure 19. Representative optical textures observed for different chromonic liquid crystalline phases of compounds **11H$^+$X$^-$**, **29X$^-$**, and **30H$^+$X$^-$** in aqueous solutions when viewed between cross polarizers of an optical microscope: (a) Schlieren texture for a N phase of **11H$^+$Cl$^-$**; (b) grainy texture for a M phase of **11H$^+$Cl$^-$**; (c) N phase of **29Cl$^-$** (6.8 wt %); (d) grainy texture for a M phase of **29Cl$^-$** developed upon evaporation of solvent from a solution of **29Cl$^-$** in the N phase; (e) chromonic ribbons (M+I) phase of **11H$^+$sulf$^-$**; (f) chromonic ribbons of **29sulf$^-$**; (g) Schlieren texture for a N phase of **30H$^+$Cl$^-$** (18.8 wt %); and (h) crystals developed upon evaporation of solvent from a solution of **30H$^+$Cl$^-$** in the N phase. Reproduced with permission from ref. [60]. Copyright 2008, American Chemical Society.

11H$^+$Cl$^-$ and **11H$^+$sulf$^-$** with the same imide substituents but different counterions show different phase properties. The same relationship can be observed for **29Cl$^-$** and **29sulf$^-$**. PBI **30** (Figure 18) has two additional methyl groups at the alky chain and its protonated form with chloride counterions was investigated for comparison. It shows similar phase properties like the two other PBIs with chloride counterions for low weight percent mixtures. Hence, the impact of the counterions seems to dominate over the impact of the imide substituents structure. This impressively reveals the importance of the counterions for the supramolecular behavior of PBI aggregates – at least for high concentration ranges where PBIs form liquid crystalline phases. **11H$^+$Cl$^-$** and **29sulf$^-$** have been studied more extensively by this group.[57–59] Thin films with anisotropic oriented dye molecules can be produced from these compounds by a combination of self-organization, mechanically induced orientation, and order-transfer processes from the liquid crystalline to the solid phase. These films, obtained by a bottom-up approach, can be applied as micro-sized sheet polarizers.

Chromonic liquid crystals can also be produced from PBIs with chiral imide substituents, which has been shown by Lee and co-workers.[61] The authors synthesized **31** and, by reaction of this compound with concentrated HCl, **31H$^+$Cl$^-$** was obtained (Figure 20). Whereas the non-protonated **31** is monomerically soluble in chloroform and fluorescent (at 2 x 10^{-7} M), **31H$^+$Cl$^-$** is soluble in water. The broadened spectrum and the lower extinction indicate aggregation in dimers or higher aggregates (at 1.7 x 10^{-6} M). This compound shows liquid crystalline properties at 9-15 weight percent in water.

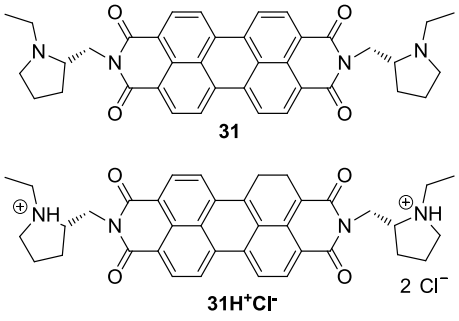

Figure 20. PBIs **31** and **31H$^+$Cl$^-$** with chiral imide substituents.

The Faul group worked with well-known amino ethyl-PBI compound **7** complexed with two more special counter ions which are the anionic surfactants bis(2-ethylhexyl) sulfosuccinate (**AOT**) and dihexadecyl phosphate (**DHP**), shown in Figure 21.[62,63] The properties of the 1:1 charge ratio mixtures were investigated mainly by X-ray crystallography, differential scanning calorimetry, and polarized light microscopy to get an insight into the supramolecular organization and phase behavior. The authors found highly ordered temperature and concentration dependent liquid crystalline materials for the PBI-surfactant mixtures in DMSO driven by electrostatic and π-π-interactions. The phase behavior is determined by the counterion here as well. The **7**-**AOT** mixture with branched alkyl chains at the anion exists in a liquid crystalline phase from - 50 to 200 °C with no evidence for any crystallinity in the material. Complex **7**-**DHP** with long linear alkyl chains in contrast showed reversible transitions from a liquid crystalline phase to a partially crystalline one due to better packing. Anisotropic alignment could be reached by shearing of thin films, hence a mechanically induced orientation, comparable to the approach of Tam-Chang and co-workers.

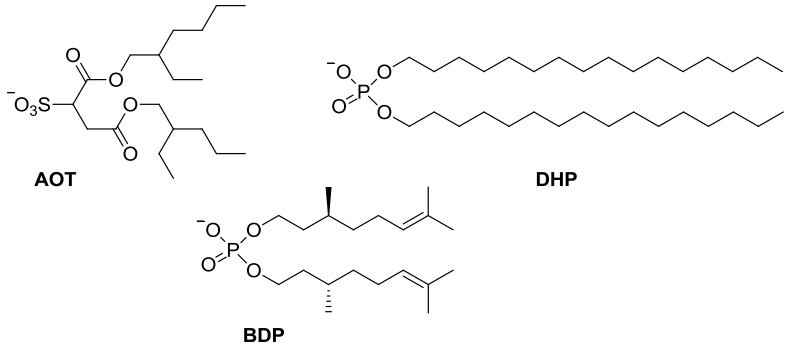

Figure 21. Counterions for PBI **7**, anions bis(2-ethylhexyl) sulfosuccinate (**AOT**), dihexadecyl phosphate (**DHP**), and bis[(3R)-3,7-dimethyloct-6-enyl]phosphate (**BDP**).

The complexation of **7** with a chiral phosphate surfactant bis[(3*R*)-3,7-dimethyloct-6-enyl]phosphate (**BDP**, Figure 21) was tested by the Faul group as well.[64] In poor solvents (for this mixture these are chloroform, 1,2-dichlorethane, and particularly THF) chiral supramolecular aggregates are formed which could be derived from the related CD spectra (Figure 22).

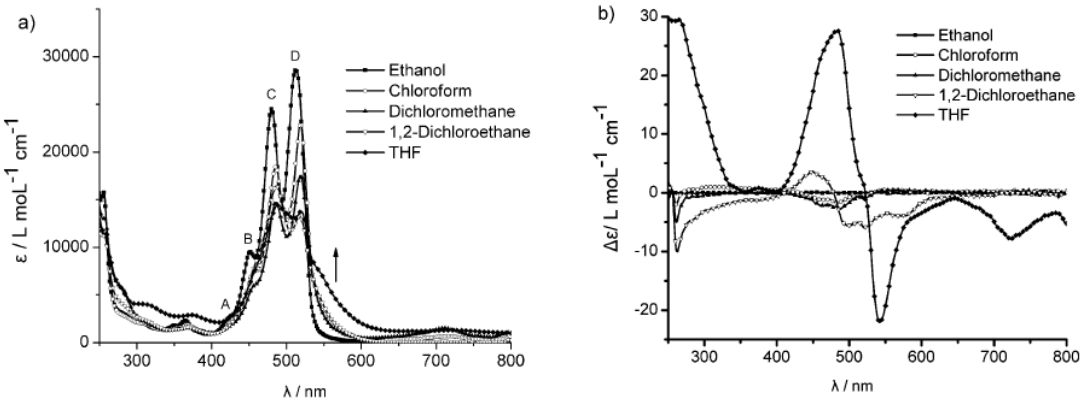

Figure 22. a) UV/Vis and b) CD spectra of **7** complex with chiral phosphate surfactant **BDP** in different solvents (c = 0.1 mg mL^{-1}). Reproduced from ref. [64] with permission of The Royal Society of Chemistry.

One PBI molecule is assumed to be attached ionically to two phosphate molecules which is called ionic self-assembly. The assembled complexes then form helical aggregates as chiral information from the alkyl chain of the phosphate surfactant is transferred to the perylene bisimide.

Chiral supramolecular structures can also be obtained by adding the bioanion adenosine triphosphate (ATP) to a solution of **8** in a DMSO-water mixture.[65] The effect can be controlled by the mixing ratio of the solvent, the concentration of the aromatic compound, and the temperature of the system as these variables strongly influence the extent of aggregation of **8** previous to the addition of chiral dopant. The maximum effect (means the strongest induced CD signal) can be achieved in DMSO/water mixture with 80 % DMSO and a concentration of 5.0×10^{-5} M of **8**, which can be derived from the corresponding CD spectra (Figure 23). The importance of the aggregation extent is emphasized by the fact that there is no chiral induction in pure DMSO (where **8** is dissolved monomerically) or in DMSO-water mixtures with a high percentage of water (where **8** is strongly aggregated in advance). Addition of adenosine monophosphate (AMP) or adenosine diphosphate (ADP) causes no chiral induction, as well. Hence, important influencing factors on the formation of chiral PBI aggregates seem to be the extent of aggregation (controlled by the solvent properties, concentration and temperature), and the number of phosphate groups respectively the valency of the dopant. Consideration must also be given to the ratio PBI/chiral dopant.

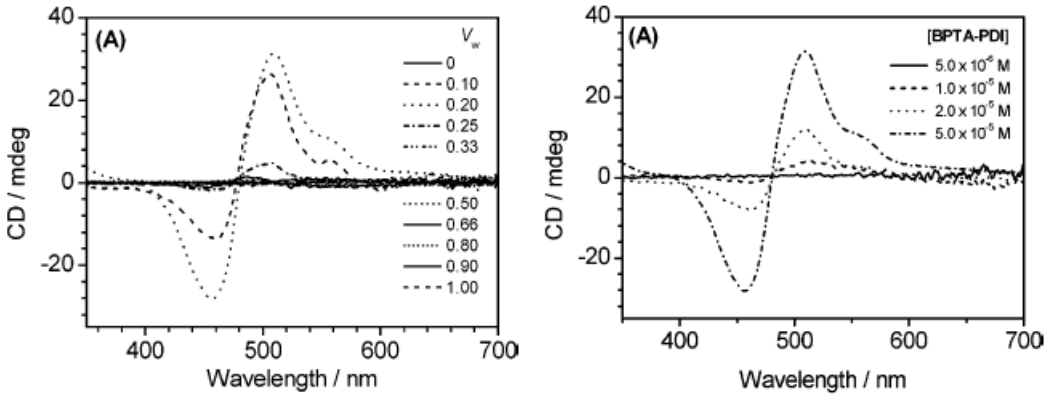

Figure 23. CD spectra of **8** (5.0×10^{-5} M) in the DMSO/water mixed solvents with various compositions in the presence of equimolar amount of ATP (left); Concentration-dependent CD spectra of **8** at various concentrations in the DMSO/water mixed solvent (DMSO 80 %) in the presence of equimolar amount of ATP (right). Reproduced with permission from ref. [65]. Copyright 2008, American Chemical Society.

Very interesting and comparable correlations have been observed for mixtures of PBI **32** (Figure 24, top left) and adenosine phosphates.[66] Pure **32** having dipicolyl ethylenediamine-zinc substituents in the imide positions is strongly H-aggregated in a solvent mixture of acetonitrile and aqueous buffer (HEPES buffer [= 4-(2-hydroxyethyl)-1-piperazineethanesulfonic acid], 1:9 v/v) at a concentration of 2×10^{-5} M and does not show a CD-signal in the perylene absorption region. The solution still stays CD silent up to an addition of 0.5 equivalents of the fourfold negatively charged ATP (Figure 24, left, H1 state). Further addition of ATP leads to an increasing bisignate CD signal which saturates beyond 0.8 equivalents ATP indicating P-helices (Figure 24, left, H2-state, homotopic allostery, arrow to the left). Addition of either chiral or achiral diphosphates to the CD-silent but pre-doped (by 0.5 equiv. ATP) solution of **32**, too, induces helical aggregates. While addition of achiral pyrophosphate ($P_2O_7^{4-}$) leads to the same helicity as addition of ATP (*P*-handed; Figure 24, left, H2 state, heterotopic allostery, arrow to the right), extra chiral ADP causes *M*-helicity (not shown). Monophosphates (like PO_4^{3-} and AMP) do not have this effect. This example for allosteric regulation of supramolecular chirality shows again the importance of the valency of the anionic partners, the ratio of PBI/anion, and the solvent quality, and it reveals the complexity of those systems.

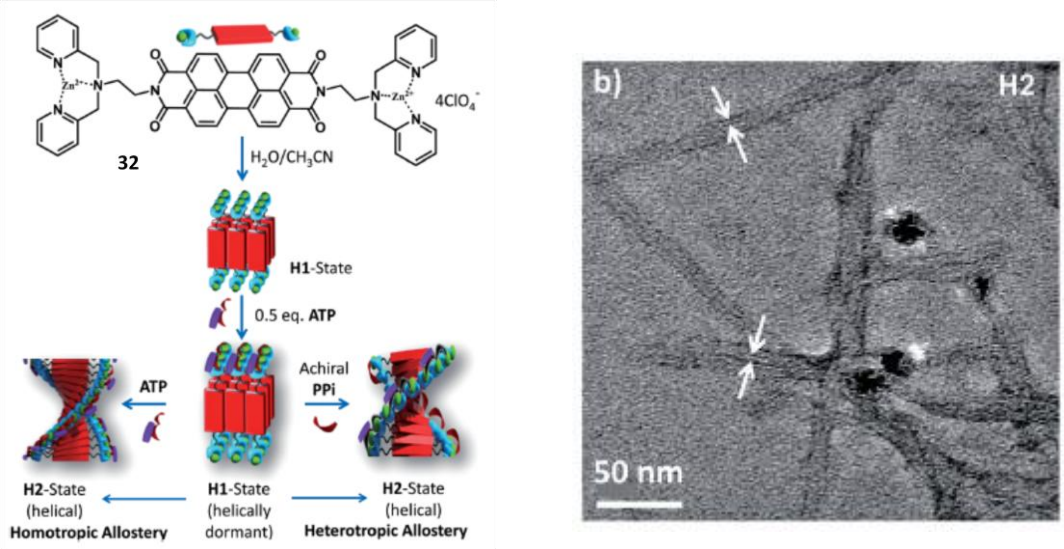

Figure 24. Chemical structure of **32** and schematic illustration of the guest-induced allosteric regulation of supramolecular chirality in the PBI assemblies (left); TEM image of nanostructures obtained from a 2.0 x 10^{-5} M solution of **32** (10 % acetonitrile in water) with one equivalent ATP (right). Reproduced from ref. [66] with permission of The Royal Society of Chemistry.

It is also worth mentioning that polymeric counterions can be applied for ionic self-assembly with PBIs as well. **7**, for example, forms nanofibrous films with polyacrylate counterions (Figure 25, right). These macroscopic alignments have been prepared by *Everett et al.*[67,68] by dip coating. The authors describe a mechanism where symmetrical **7** (Figure 25) forms small π-stacked aggregates in aqueous solution which grow on the surface after dip-coating as a function of the mass weight of the polyelectrolyte with high mass weight means more efficient deposition. They call this 'surface growth'. An unsymmetrically functionalized and less soluble PBI **33** (Figure 25), underlies the 'solution growth' mechanism. Preformed larger pi-stacked aggregates of **33** exist in the precursor solution and act as templates for the growth of the nanofibers on the surface. This mechanism is less dependent from the mass weight of the polyelectrolyte. Such materials are likely to play a role in the development of anisotropic organic thin films for use as one-dimensional conductors or polarized electroluminescent devices.

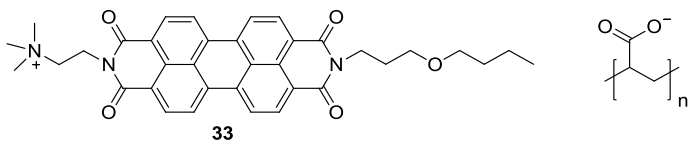

Figure 25. Unsymmetrical PBI **33** and schematic polyacrylate anion (right).

Aggregated **29Cl**$^-$, known from Tam-Changs work on liquid crystals, can be used as template for producing silica nanotubes which was shown in the work of *Rodríguez-Abreu et al.*[69] Cooperative interactions of **29Cl**$^-$ aggregates with silica species during a sol-gel reaction form tubes which precipitate from solution. Silica nanotubes of 1-5 µm length and an average diameter of around 300 nm with supermicroporous walls could be obtained upon calcinations (Figure 26). Such material can find applications in photovoltaics and in shape selective catalysis and absorption, as the authors state. The template size is tunable by varying the side chains of the PBI monomer, what is easily feasible.

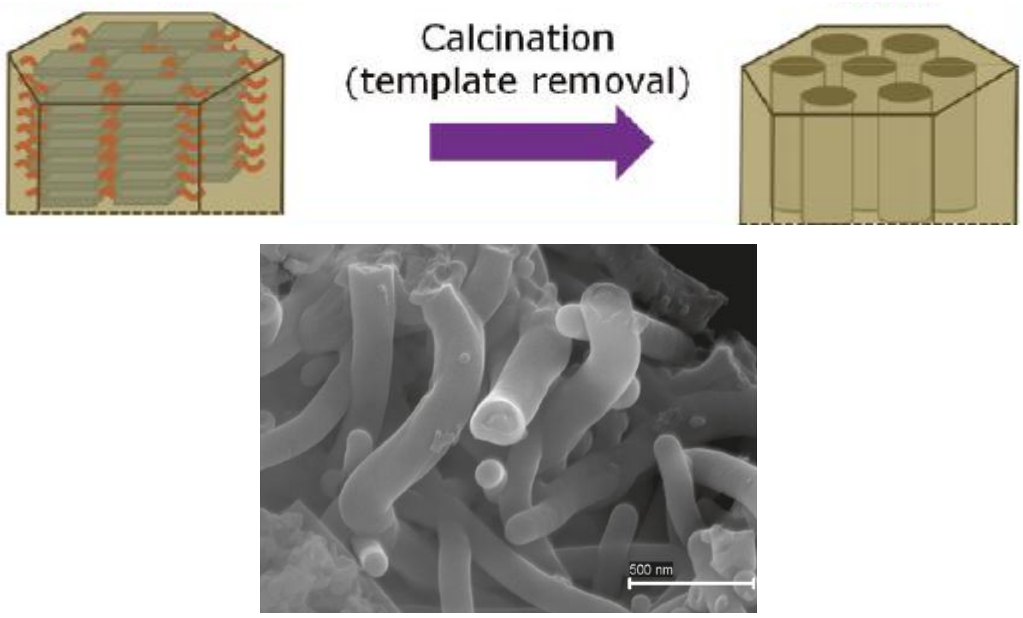

Figure 26. Schematic illustration of the preparation of nanoporous silica (top right) by calcination of a silica-dye nanocomposite (top left). SEM image of calcinated silica synthesized form PBI solution (bottom). Reproduced with permission from ref [69]. Copyright 2011, American Chemical Society.

2.2.4 Supramolecular Structures – Electronic Properties

Perylene bisimides are most electron deficient dyes which can easily be reduced. Due to their high electron affinity, PBIs can be used as n-type semiconductors in electronic devices.[2,11] This is also the reason for their susceptibility to photoinduced electron transfer described in section 2.2.1.

Electrostatic layer-by-layer self-assembly of **7** and an anionic polymer mixture for example results in composite films. *Chen et al.* described the fabrication of a hybrid film-coated electrode of this for inverted organic solar cells.[70] In addition to the n-type

semiconducting properties of the PBI core π-π-interactions and electrostatic interactions of the positively charged ammonium functionalities were utilized in this application.

George and Rao obtained hydrogels with excellent mechanical and conducting properties of **7** alternately co-assembled with an also amphiphilic oligo(phenylenevinylene) derivative with anionic side chains[71] (Figure 27, top) although one would perhaps expect phase-segregation of the two structurally different extended π-conjugated backbones. The efficient co-facial supramolecular assembly occurs possibly through synergistic π–π stacking, charge-transfer and electrostatic interactions. The perylene core acts as electron acceptor and the oligo(phenylenevinylene) as electron donor to give fibers with high conductivity which can be further investigated in the context of supramolecular electronics. Figure 27 (bottom) shows photographs of the gel exhibiting self-standing and viscous behaviors and a SEM image of the hydrogel on a glass substrate.

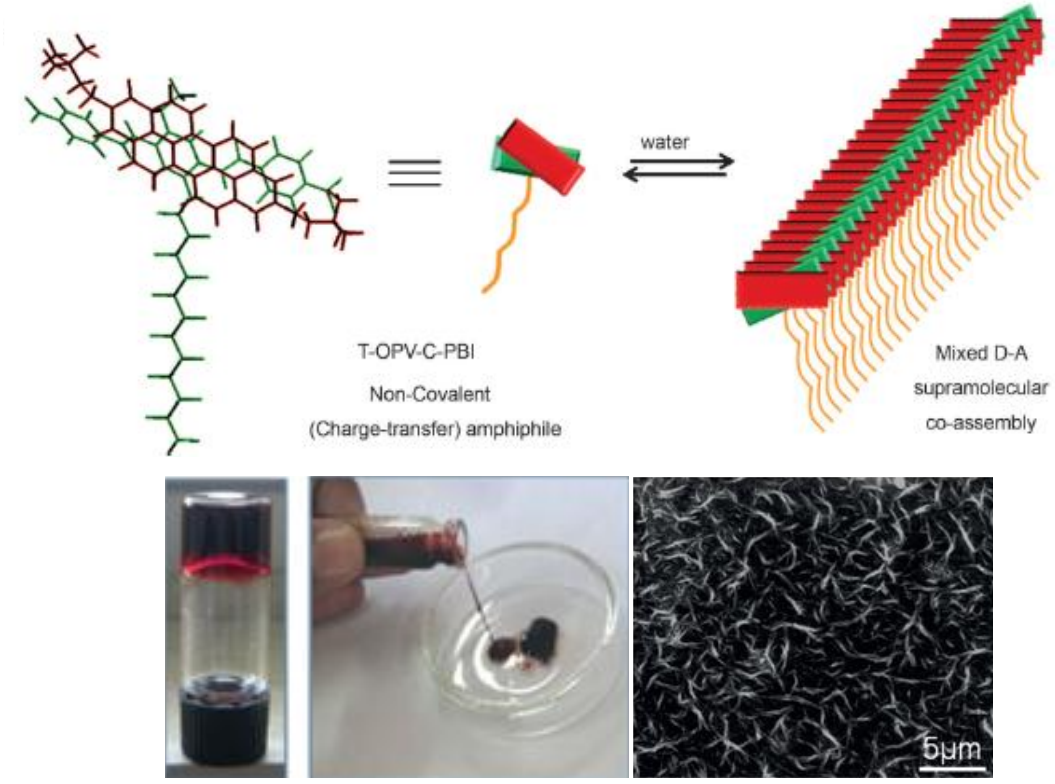

Figure 27. Schematic representation of the non-covalent PBI **7**-OPV amphiphile and its self-assembly into 1-D supramolecular structures (top). Photographs of the gel of co-self-assembled **7**-OPV exhibiting self-standing and viscous behaviors (bottom left). FE-SEM image of the hydrogel on a glass substrate (bottom right). Reproduced with permission from ref. [71]. Copyright 2012, John Wiley & Sons, Inc.

Fukuzumi's group also made attempts to co-assemble **7** with aromatic amphiphiles with anionic side chains.[72] The authors found that the π-extent of the co-assemblers influences the kind of interaction. Large π-extent (e.g. for a styryl biphenyl derivative) favors π-π-stacking of **7** and the anionic amphiphile (and hence electron coupling). Aromatic molecules with anionic side chains but with a relatively small π-extent (e.g. anthracene and naphthalene derivatives) interact with the positively charged side chains of **7** stacks via ionic interaction. This results in an enhanced distance between the PBI-π-planes which improves the extensive electron transport along the PBI-stacks after photoinduced electron transfer from electron donors.

Sulfonated porphyrins, aromatic molecules with anionic side chains as well, co-self-assemble with columnar **7** nanostructures at various ratios in water. Driving forces are strong π–π and ionic interactions, here too.[73] Compared to the co-assembling of **7** with oligo(phenylenevinylenes) this co-self-assembly is not alternating (Figure 28). Electron transport has been observed, owing to the probable π-delocalization mechanism along the electron deficient stacks of **7**. The authors found a high ratio of charge separation to charge recombination which is a fundamental parameter for organic photovoltaic applications targeting high efficiency.

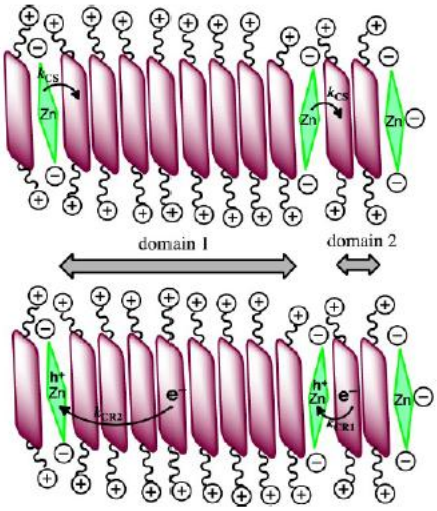

Figure 28. Representative illustration of the charge separation and charge recombination between the stacks of **7** and porphyrine. Reproduced with permission from ref. [73]. Copyright 2012, American Chemical Society.

PBI **7** and graphene oxide (functionalized with COOH groups) self-assemble in water via π-π- and electrostatic interactions forming gels. For these gels, too, fast charge separation and slow charge recombination has been observed (Figure 29).[74]

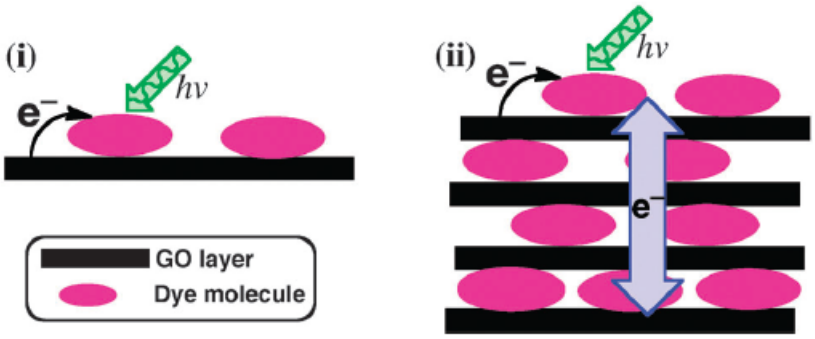

Figure 29. Photoinduced charge separation in single of a few layers of dye-graphite oxide hybrids examined (left). Proposed photoinduced charge separation and interlayer charge migration in ordered self-assemblies of PBI **7**-graphite oxide hybrid layers (right). Reproduced from ref. [74]. Published by The Royal Society of Chemistry.

Huang et al. reported on the formation of different nanostructures from **7** by evaporation.[75] Dependent on the solvent and evaporation speed either hollow nanotubes with outer diameters of 100 – 300 nm and length of several micrometers (out of water) or nanorods with diameters of 200 – 300 nm and lengths up to tens of micrometers (out of methanol) could be obtained (Figure 30).

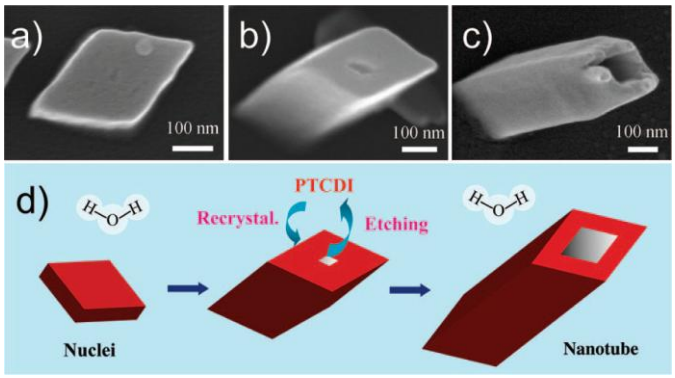

Figure 30. SEM images of **7**: (a) a short parallelogrammic nanoparticle; (b) a parallelogrammic nanocolumn with small defects on the top; (c) a parallelogrammic nanotube; and (d) a possible formation mechanism of the nanotubes from aqueous solution on silicon substrate (PTCDI = PBI **7**). Reproduced with permission from ref. [75]. Copyright 2009, American Chemical Society.

Resistance measurements on devices based on the nanotubes and nanorods with and without a dopant (e.g. hydrazine) reveal modulations upon doping which suggest **7** nanotubes and nanorods as building blocks for electronic devices and sensors.

Thin films of **7** and its two higher homologues with four and six methylene groups, **34** and **35** (Figure 31), are electrically conductive.

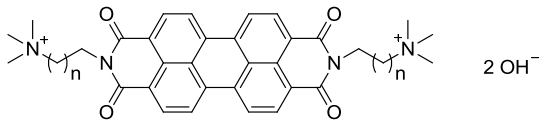

7: n = 1
34: n = 3
35: n = 5

Figure 31. Electrically conductive PBIs **7**, **34**, and **35**.

Russ et al.[76] recently reported that increasing the alkyl spacer length from two (**7**) to six methylene groups (**35**) increases the electrical conductivity one hundredfold (reaching 0.5 S cm^{-1}). The films also show thermoelectric properties (what means that an electric potential is created with a temperature difference in the material) with the highest n-type thermoelectric performance for solution processed small molecules known until then. In the polycrystalline thin films PBIs are stacked via π-π-interactions which has been attested by UV/Vis spectroscopy and X-ray diffraction. Three characteristic peaks in the visible-near-infrared region of the UV/Vis spectra (~730, 815, and 1000 nm, Figure 32) further indicate the presence of PBI radical anions (polarons), responsible for conductivity.

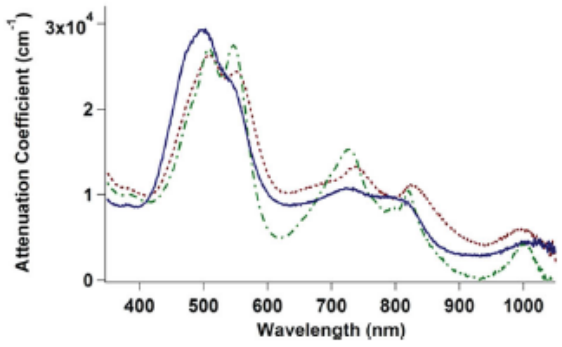

Figure 32. Self-doping in PBI derivatives **7**, **34**, and **35** leads to high polaron charge charier concentrations. Drop-cast films (~ 200 nm thick on glass) of **7**, **34**, and **35** indicate similar optoelectronic transitions regardless of spacer length. Spectra of all three materials (red dotted line = **7**; green dash-dotted line = **34**; blue solid line = **35**) display the characteristic peaks for PBI radical anions (polaron) charge carriers (~730, 815, and 1000 nm). The peak broadening seen in **35** is attributed to significant intermolecular interactions. Reproduced with permission from ref. [76]. Copyright 2014, Wiley-VCH.

PBIs **7**, **34**, and **35** can be called self-doped polymers as they own (positive) charges in their side chains and counterions (OH^-) for fast exchange. Hence electrical conductivity is modified by morphology-induced changes in mobility and remarkably not by changes in the electronic structure of the PBI.

PBI **36** (Figure 33) is, together with an oligo pyrene, suitable for layer-by-layer deposition as well. Multilayer films with rapid photocurrent response can be produced from these compounds by means of both electrostatic interactions and π-π stacking.[77]

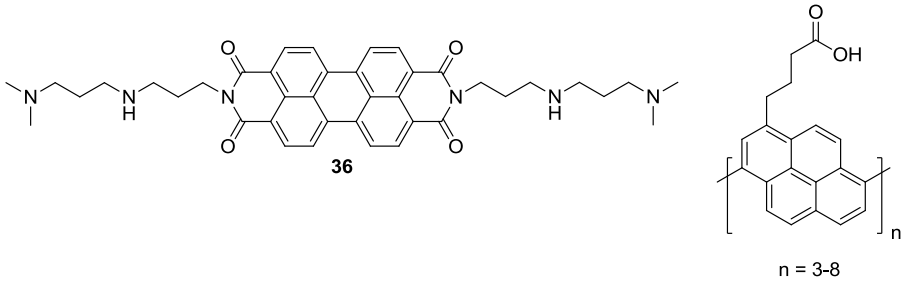

Figure 33. PBI **36** and an oligo pyrene for layer-by-layer deposition.

2.2.5 Interaction with Nucleic Acids

Nucleic acids are polymers consisting of monomers which combine a heterocyclic nitrogen base, a pentose sugar and a phosphate group.[78] As nucleic acids can also form secondary structures, there are, apart from non-specific electrostatic interactions, other modes of interaction with small molecules in general and with PBIs in particular. Double stranded DNA helices for example can interact with appropriate partners additionally by groove binding or intercalation (Figure 34).[78,79]

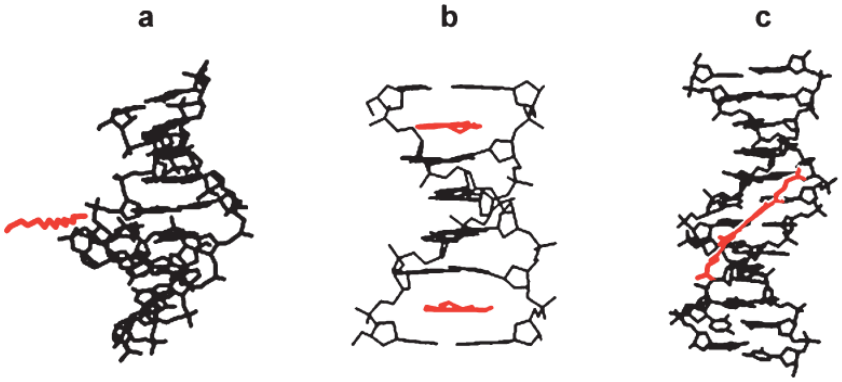

Figure 34. Schematic representations of the three primary binding models for ligand-duplex DNA binding. The ligand is shown in red and the DNA chains are in black: a) Outside edge binding; b) Intercalation; c) Groove binding. Reproduced with permission from ref. [78] Copyright 2006, The Royal Society of Chemistry.

Special secondary structures of nucleic acids are so called G-quadruplexes. These unusual four-stranded guanine-quadruplexes are formed by guanine-rich sequences of polynucleotides (Figure 35).[80]

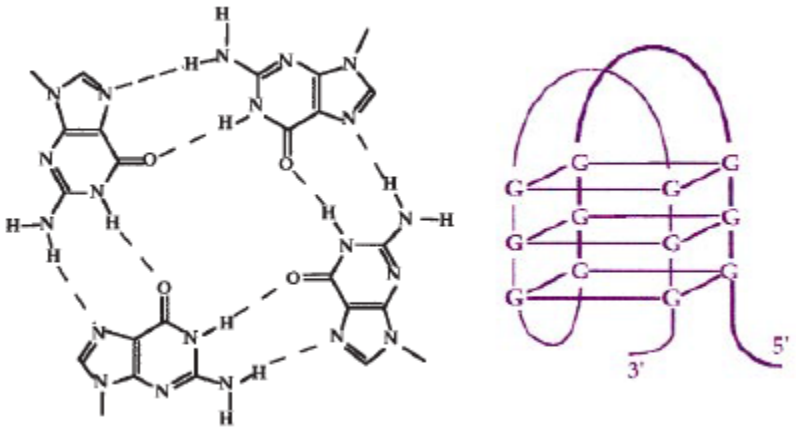

Figure 35. Guanine-rich telomeric DNA adopts several different conformations including G-quadruplexes, which interfere with the activity of the telomerase enzyme. The figure depicts G-quadruplex DNA (left) and intramolecular folding of a G-rich oligonucleotide into a tetraplex that includes three consecutive G-quadruplexes (right). Reproduced with permission from ref. [81], Copyright 1998, Macmillan Publishers Ltd.

The mode of interaction of **10** with double stranded DNA has been investigated by *Xu et al.* recently.[82] Water solubility of **10** is very high (> 8 mg/mL). Absorption and emission spectra in water (5×10^{-6} M) are broadened with maxima at 498 nm and 545 nm suggesting strong aggregation of **10** even at low concentrations. The fluorescence quantum yield is 0.23. High water solubility and a reasonable fluorescence quantum yield in water are good requirements for the utilization of PBIs in biological environment. The authors employed **10** for intercalation experiments with double stranded DNA (in phosphate buffer 10 mM, pH 7.4; c(**10**) = 5 µM). Hypochromicity (reduced absorption of light), a slight red shift and an isosbestic point in the UV/Vis spectrum indicate the intercalation of **10** into DNA double strand (Figure 36). CD and viscosity measurements of DNA without and with **10** have proven as well the intercalation model. Due to the strong interaction with dsDNA, **10** accumulates in the cell nuclei. It causes a decrease in tumor weight in experiments with mice *in vivo*. This suggests high potential of **10** as anti-cancer drug due to suppression of cancer cells.

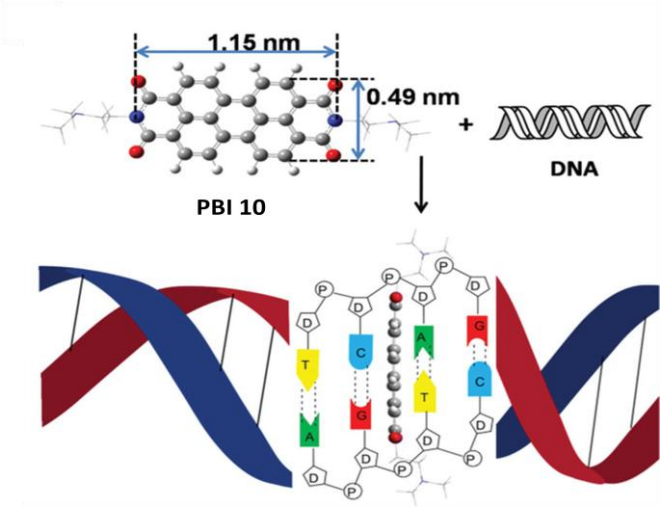

Figure 36. 3-D structure of **10** simulated by Gaussian 09w Program (top) and schematic diagram of **10** intercalating into double-stranded DNA base pairs (bottom). Reproduced with permission from ref. [82]. Copyright 2014, John Wiley & Sons, Inc.

The seeking for anti-cancer drugs is the main driving force for investigating the interaction of PBIs with G-quadruplexes, as well. Guanine-rich structures, the necessary prerequisite for G-quadruplex formation, appear in telomeres which are the ends of chromosomes. Telomeres, which are shortened with every cell division, are responsible for chromosome stability. When the telomere length drops below a critical minimum, the cell can no longer divide further. This often leads to programmed cell death or zero growth. But there is an enzyme called telomerase (RNA-protein complex) which synthesizes G-rich nucleotide sequences and thus leads to re-elongation of telomeres. This enzyme is repressed in most normal human cells but not in large parts of human cancer cells. It is known that telomerase activity strongly correlates with cancer as telomerase allows cancer cells to escape from this ageing process. Telomerase inhibition (direct or indirect) hence is a potential target for anti cancer drug design.[83,84] As telomerase needs single stranded DNA as a template, stabilizing G-quadruplex structures causes indirect inhibition of telomerase.[85] And interaction with PBIs (or other small organic molecules with π-surfaces of small organic molecules like porphyrins or diamido anthraquinones) stabilizes G-quadruplexes.[80,85] Therefore it is little surprising that perylene bisimide derivatives are under investigation as G-quadruplex binders. G-quadruplexes own four negatively charged grooves which allow additional electrostatic interactions with possible cationic residues of appropriate molecules. PBIs with ammonium side chains hence are ideal subjects for binding studies with G-quadruplex.

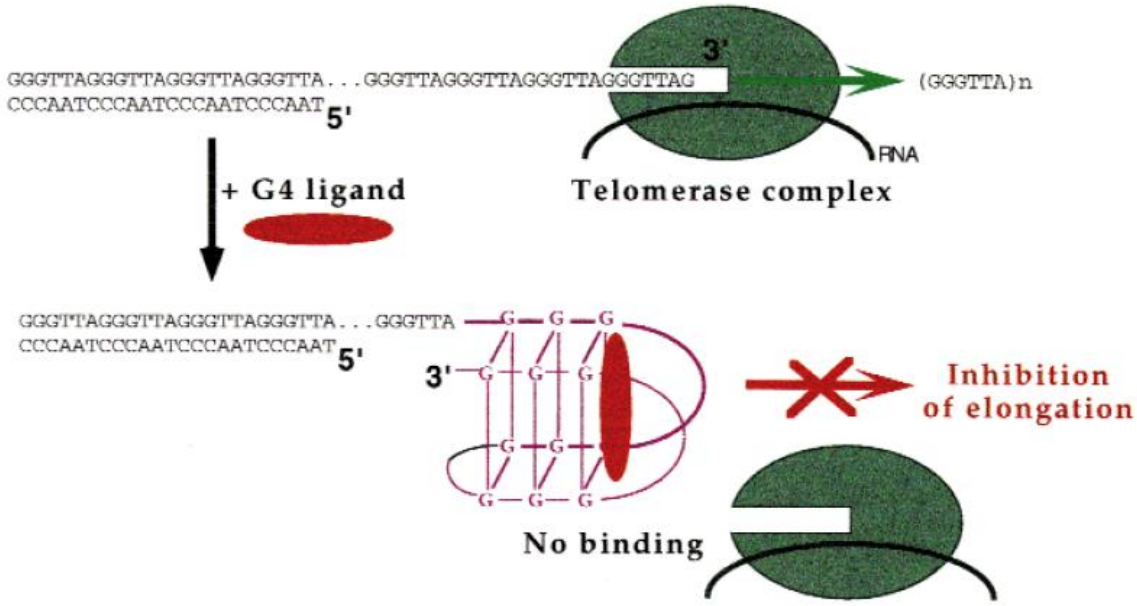

Figure 37. Schematic presentation of telomerase inhibition by G-quadruplex stabilization. Reproduced with permission from ref. [81]. Copyright 1998, Macmillan Publishers Ltd.

The G-quadruplex binding mode and selectivity of PBI derivatives **9** and **41** as well as of numerous other related structures with amino/ammonium containing side chains have been studied for around fifteen years. A selection of those PBIs is shown in Figure 38.

The two main points of interest here are the binding mode of PBIs to G-quadruplex DNA and the selectivity. Selectivity in this case means the ability of PBIs to distinguish between G-quadruplexes (binding desirable) and double stranded DNA (binding unwanted). An ideal G-quadruplex ligand should bind to the target but show little interaction with duplex DNA. Otherwise it leads to non specific cytotoxicity. The ability to bind selectively hence is critical for a possible application of PBIs as anti-cancer drugs.[80,81,85] The perylene core itself seems to have a binding preference for the G-quadruplex structure. Most likely the different side chains of perylene derivatives are responsible for induction and/or stabilization of certain G-quadruplex structures and therefore are responsible for selectivity.[86] It is found that PBIs that are less aggregated under certain conditions show much lower levels of G-quadruplex DNA selectivity.[87,88] Less availability of monomeric PBI (due to stronger aggregation) leads to higher selectivity to G-quadruplexes, most likely as interaction of PBIs with G-quadruplexes is possible from monomeric and aggregated dye whereas interaction with dsDNA affords

monomeric PBI for intercalation.[88] The extent of aggregation of PBI can be controlled by the pH of the solution as it dictates protonation/deprotonation of the according amino/ammonium groups and with that overall charge and charge density. For example, **37**, which is less aggregated at pH 6.4 than at pH 7, demonstrates only low G-quadruplex DNA binding selectivity at the lower pH 6.4. **38** is aggregated at pH 8.5 and shows high G-quadruplex DNA selectivity[87]

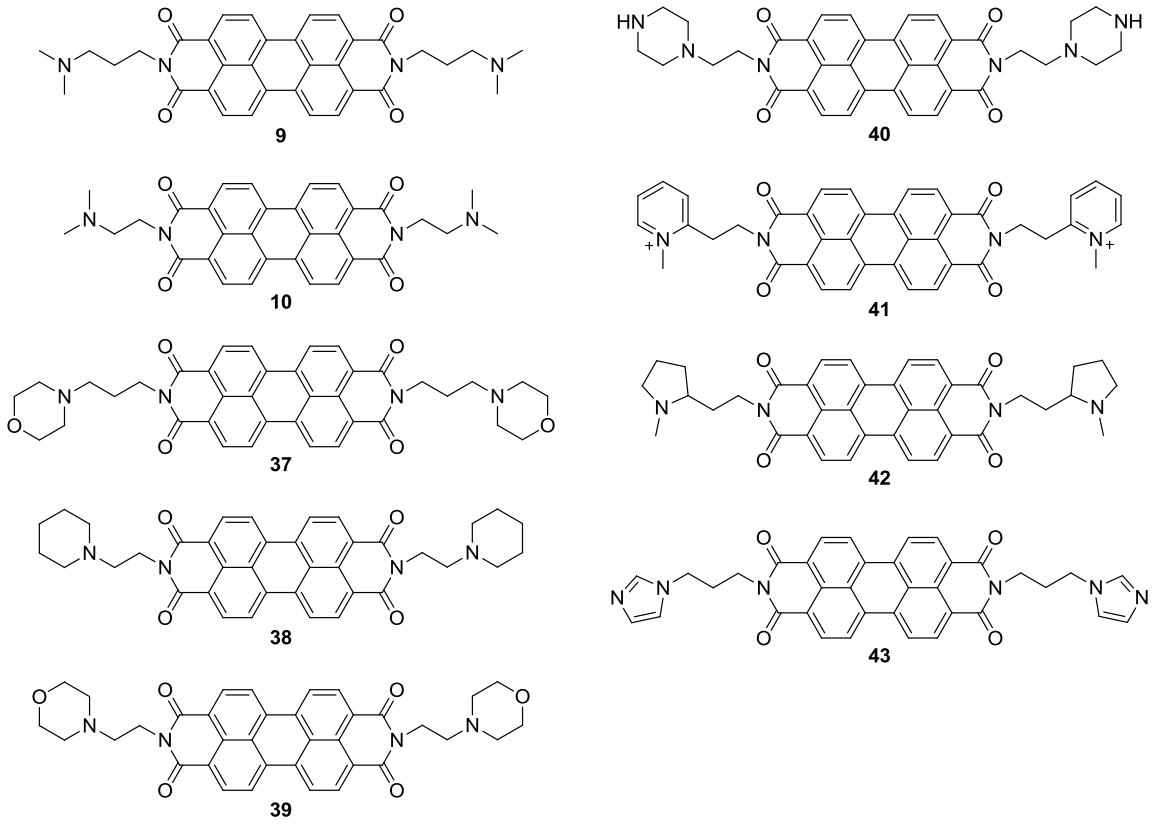

Figure 38. Examples for PBI G-quadruplex binders.

The distance between the PBI core and the (charged) nitrogen atoms in the side chains seem to play an important role for the mode of interaction with DNA.[89] Furthermore the number of basic sites in the imide substituents and their distance among themselves influences G-quadruplex binding formation and selectivity as well as their terminal groups.[90,91] The basicity of the side chains correlates with the potency of telomerase inhibition.[91] PBI compounds with high affinity to G-quadruplex structures do not display high selectivity automatically. For example **9** with two imide substituents is the most specific ligand for G-quadruplex DNA in a series studied but shows less

affinity than PBI derivatives with four ligands (two in the imide- and two in the bay-positions).[91]

Tuntiwechapikul and co-workers[86] found for **38** (Figure 38)and two other basic PBI derivatives, **44** and **45** (Figure 39, left) a solution behavior which is dependent not only on the pH of the utilized buffer solution but on the kind of buffer as well. The authors compared the solubility of the PBI compounds in TRIS buffer (TRIS = 2-Amino-2-hydroxymethyl-propane-1,3-diol), phosphate buffer and acetate buffer (Table 3).

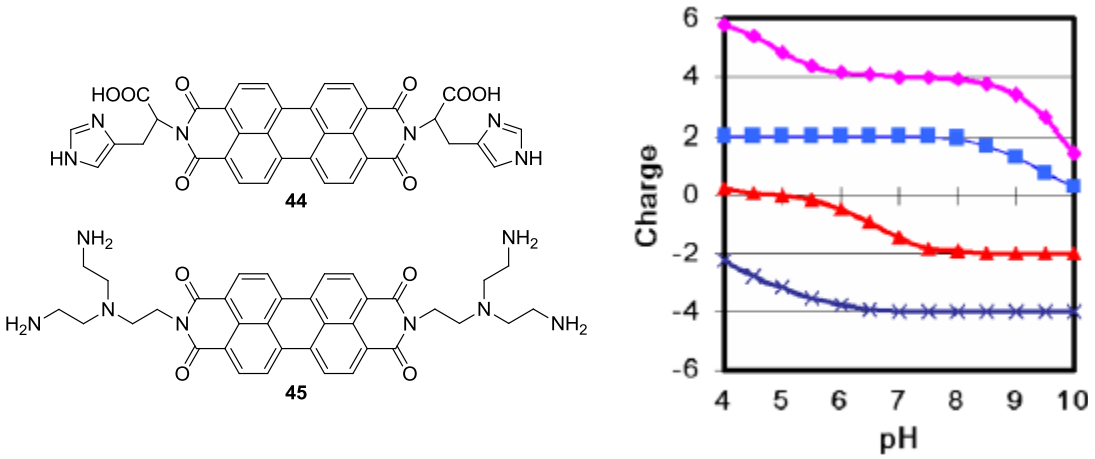

Figure 39. Structures of **44** and **45** (left) and calculated charges of **38** (blue), **44** (red), **45** (pink), and additionally of a PBI derivative with two carboxylic acid functionalities at each imide substituent (violet, structure not shown) Charges are calculated by ChemAxon Marvin. Reproduced with permission from ref. [86]. Copyright 2006, Elsevier.

For **38** and **44**, the authors found an expected solubility behavior in accordance with the corresponding (calculated) pK_a values of the PBI substituents (Figure 39, right) and with it the charge density. For **45** the situation is special. This sixfold amino compound is soluble in acetate buffer (pH 5) and TRIS-buffer (pH 7, 8 and 9) but not soluble in phosphate buffer (pH 6, 7 and 8) although that are partly the same pH values. The complexation of phosphate anions from the buffer by the amine groups possibly supports the formation of huge aggregates which precipitate. The nature of the buffer (and not only its pH) obviously influences the aggregation behavior and therewith the solubility of PBIs.

Table 3. Solubility of **38**, **44**, and **45** dependent on buffer and pH (sol = soluble, part. sol = partly soluble, ppt = precipitation). Produced with information from ref [86].

compound		buffer						
PBI	pK_a	TRIS pH 9	TRIS pH 8	phosphate pH 8	TRIS pH 7	phosphate pH 7	phosphate pH 6	acetate pH 5
38	9-10	ppt	ppt	ppt	ppt	ppt	sol	sol
44	4.75 6.95	sol	sol	sol	part. sol	part. sol	ppt	ppt
45	10-11	sol	**sol**	**ppt**	**sol**	**ppt**	ppt	sol

All the mentioned investigations regarding G-quadruplex binding of PBI derivatives have been performed in various buffer solutions. The nature of the ions of the buffer may strongly affect the behavior of the PBIs. For some of the measurements co-solvents like DMSO have been employed (for example for preparing stock solutions). This has to be taken into account for conclusions and evaluation, as well.

2.3 Spermine-functionalized Perylene Bisimide Dyes

Many of the amino functionalized PBIs presented in the prior Chapter 2.2 have only one or two amino group(s) at each imide substituent. Quaternization or protonation of these amino groups enhances the water solubility and the fluorescence quantum yield of the corresponding PBI as discussed before. However, those PBIs are strongly aggregated in water or even need organic co-solvents such as THF, DMF or DMSO to achieve a reasonable solubility at moderate concentration. Fluorescence quantum yields rarely exceed values of 0.6. In order to increase solubility, of both soluble aggregates and monomeric dye, substituents with more than one or two amino groups can be introduced. As mentioned in the introduction, spermine was utilized as hydrophilic part of the bolaamphiphilic target molecules that are discussed in the main part (Chapters 3 and 4) of this thesis. By using the tetraamine spermine as substituent, three amino groups at each imide substituent, six in all, are available to improve solubility as one of the four amino groups of spermine is necessary for covalent linkage.

2.3.1 Spermine-functionalization of the Bay Positions

PBI **46** (Figure 40) with four spermine substituents has been synthesized and investigated as part of my diploma thesis.[92] In this case spermine is linked via resorcin and butyric acid linker to the four bay positions of the perylene bisimide dye. Due to the steric hindrance of the substituents in the bay positions the perylene core is not planar but the two naphthalene units are twisted. Thus the (optical) properties of **46** differ significantly from those of all other PBIs discussed in Chapters 2–4. **46** is soluble in water and buffer (phosphate, pH 7) at least up to a concentration of 8 x 10^{-4} M. The solubility is supported by protonation of the twelve amino groups at neutral pH and the twisted PBI core. Aggregation, however, is not fully prevented as UV/Vis measurements suggest. Interaction of **46** with nucleic acid has been tested. Addition of calf thymus DNA to a solution of **46** in phosphate buffer leads to a red precipitate, at a certain point. Fluorescence spectroscopy and microscopy as well as AFM measurements strongly indicate the formation of a DNA-dye complex, most possibly due to electrostatic interactions between the spermine ammonium groups and the phosphate groups of nucleic acids. This is in accordance with the fact that spermine (like other polyamines and polycations respectively) is able to condensate nucleic acids.[93–95]

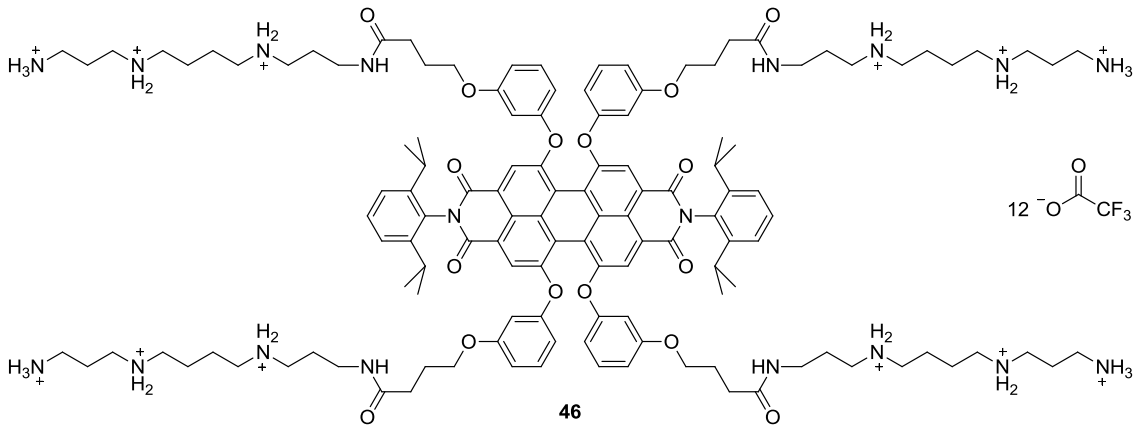

46

Figure 40. Bay-substituted PBI **46** was employed for cell staining.

Besides, **46** was employed for cell staining experiments. It could be shown that the dye is distributed predominantly in the cytoplasm of the cells but not in the nucleus.

2.3.2 Spermine in the Imide Positions

Perylene bisimides with substituents just in the imide positions are more easily to access by imidization with the corresponding amine. One of the target molecules of this thesis is PBI **2** where spermine is directly bound to the perylene bisimide. PBI **2** is also part of a series tested for G-quadruplex binding by *Franceschin et al.*[90] The authors investigated the influence of the number and position of positive charges in polyamine side chains of different PBIs on their ability to induce G-quadruplex structures and inhibit telomerase. PBI **2** as well as its acetylated relative **47** (Figure 41) in fact are unable to induce G-quadruplex structures under the given conditions. This disability is explained by the assumed 'low solubility' of the dyes which here does not mean precipitation but strong aggregation. UV/Vis spectra of **2** and the acetylated compound **47** suggest in deed strong aggregation in the utilized aqueous buffer (MES-KCl = 2-(N-morpholino)ethanesulfonic acid KCl, pH 6.5). The aggregation seems to be even stronger for the non-acetylated **2**. This is surprising. One would expect less aggregation of the non-acetylated compound as there is one more positive charge in each side chain. Apparently there is no easy correlation between the number of 'free' amino groups and aggregation behavior as the authors state. The complexity of the interactions with water respectively buffer with various ions has to be taken into account.

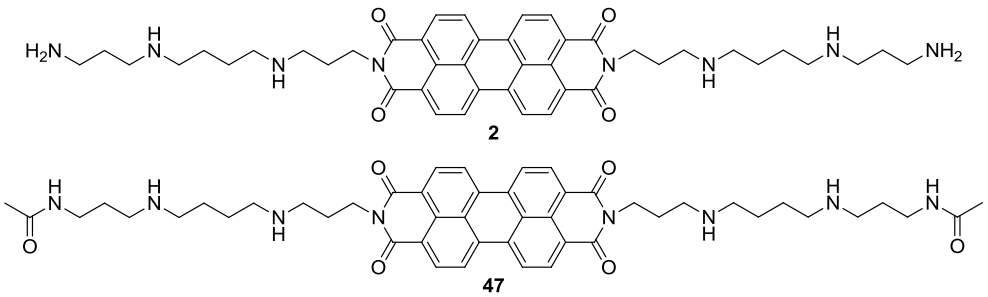

Figure 41. Target compound **2** and the twofold-acetylated **47** tested for G-quadruplex binding.

However, it should be mentioned that the concentration at which UV/Vis spectra have been measured is not clearly specified. As aggregation is dependent on concentration this information is important. Spectra possibly are not measured at the same concentration and hence are not comparable.

Amine functionalized PBIs interact with (poly)anions as illustrated above with numerous examples. PBI **48** with spermine substituents in the imide positions and additional two propyloxy amine substituents in the bay positions (Figure 42) has been applied to quantify heparin in human blood serum.[96,97]

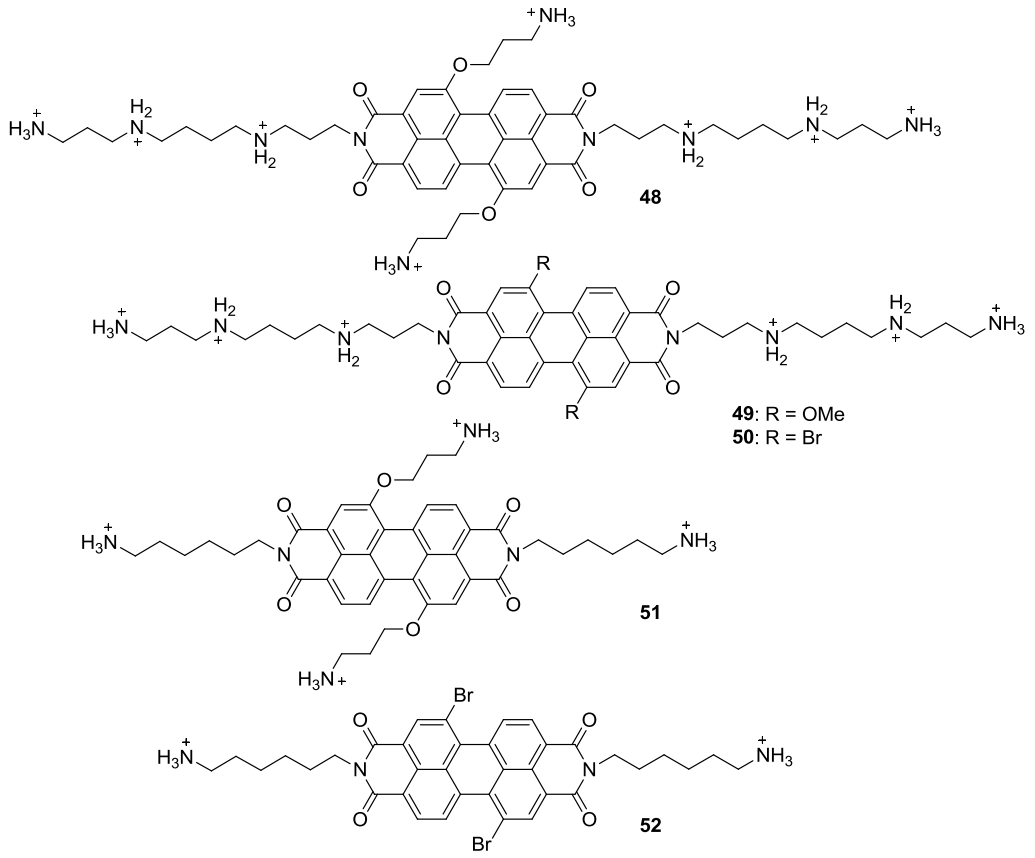

Figure 42. Cationic PBIs **48**–**52**, bearing eight, six, four or two positive charges, respectively, for quantifying negatively charged heparin.

Heparin is a highly sulfated glycosaminoglycan with a very high negative charge density and therefore ideally suited for interaction with up to eightfold positively charged **48**. The quantification of heparin in this case is based on changes in fluorescence intensity of the PBI. The interaction of cationic **48** with the polyanion heparin leads to an increased aggregation of the dye and hence decreased fluorescence intensity. The affinity of **48** with up to eight positive charges (six in the imide positions and two in the bay positions) to bind to heparin and neutralize its negative charges has been compared to the affinity of similar but less charged compounds **49**–**52** (Figure 42). Specific binding stochiometries ('loading') could be determined for each of the PBIs by

fluorescence titration experiments (Figure 43). The affinity of the positively charged PBI dyes to bind to heparin increases with increasing charge.

It should be mentioned that mixtures of 1,6 and 1,7 regioisomers (referred to the bay-positions) of the perylene bisimide dyes have been used in this study. Although the fluorescence responses of 1,6- and 1,7-propyloxy amino substituted PBIs do not seem to be discriminable,[97] this does not necessarily apply for other kind of bay substituents like bromine or methoxy groups.[98,99] Assumptions which emanate from a comparable behavior of other substituents are to be critically assessed. Here certainly a closer look on the (optical) properties of the regioisomers is needed.

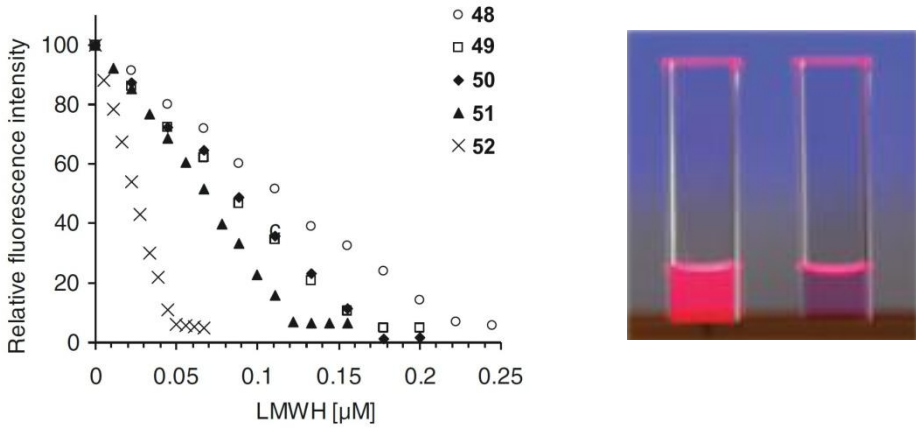

Figure 43. Fluorescence titration of probes **48**–**52** (0.1 µM) with low molecular weight heparins in aqueous solution at pH 7.0 (buffer 10 mM 3-(N-morpholino) propanesulfonic acid, T = 20 °C) (left). Red fluorescent and heparin quenched solutions of **48** (right). Reproduced with permission from ref. [96]. Copyright 2010, The Royal Society of Chemistry (right). Reproduced with permission from ref. [97]. Copyright 2010, Elsevier (left).

As mentioned earlier, perylene bisimide dyes can act as pH sensors. This ability is based on protonation/deprotonation processes which prevent or enable photo electron transfer and with that strongly influence the fluorescence extent of the dyes.[36] Vice versa the effect of fluorescence quenching by photoinduced electron transfer can be used to determine approximate pK_a values of **48**–**52**.[97] Fluorescence intensity has been measured dependent on the pH value (Figure 44). In the range of the corresponding pK_a values (around 8–10) the fluorescence intensity strongly decreases since the loss of protonation provides free electron pairs at the amino groups which can be involved in photoinduced electron transfer. In addition electrostatic repulsion decreases with increasing pH as the density of positive charges at the PBI substituents becomes less. This entails aggregation tendency as well. The determined pK_a values can at least serve

as rough guides. The pH-dependent fluorescence intensity measurements clearly demonstrate the constancy of the fluorescence intensity at pH values below the pK_a values for (poly)amino substituted perylene bisimide dyes. This suggests that the aggregation behavior is not affected by the pH in the range below the corresponding pK_a value.

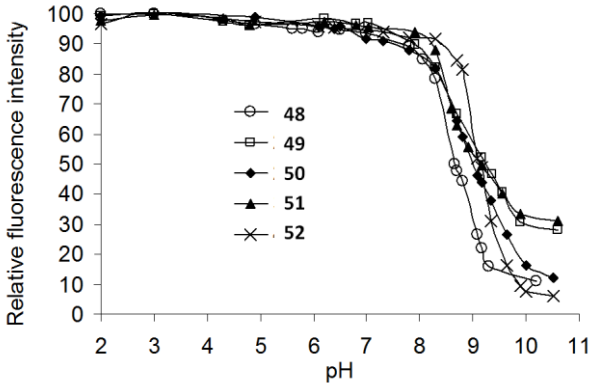

Figure 44. Fluorescence pH titration of probes **48–52** (0.1 µM). Decrease of fluorescence intensity was monitored with increasing pH. Reproduced with permission from ref. [97] (from the supplementary). Copyright 2010, Elsevier.

Interaction of target molecule **4a** (spermine functionalized PBI with chiral alanine linkers, see chapter 4) with nucleic acids has been successfully tested by our group in cooperation with Ivo Piantanida's group.[100] **4a** seems to bind as a dimer to DNA minor groove and RNA major groove. The grooves of the nucleic acids act as templates as the spacial conditions (groove structure and width) strongly influence the supramolecular arrangement of the PBI. The aggregate size is limited to dimeric units. Further the rotational and the longitudinal offset of PBI monomers is modulated by the grooves constitution and is directly reflected in the band structure of the CD spectra recorded for the appropriate DNA-PBI mixtures (Figure 45). This highly sensitive feedback from the DNA/RNA binding site on the mutual orientation of the PBI dimer is a very promising approach for probing of DNA and RNA secondary structures.

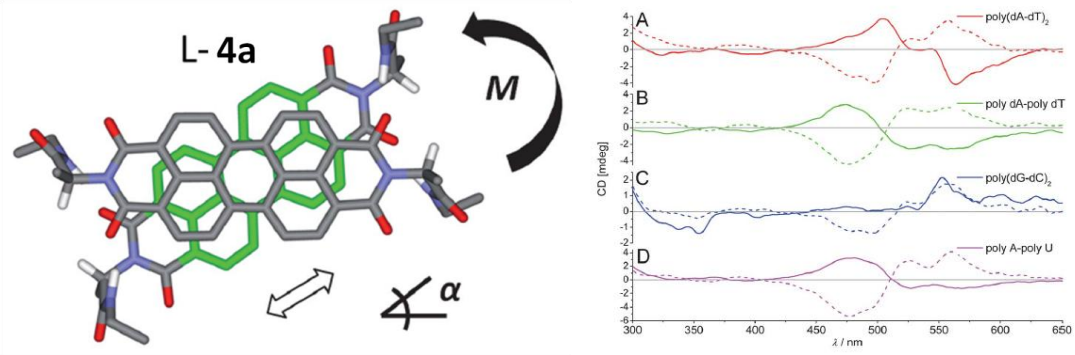

Figure 45. The preferential left- or right-handed offset (M or P) of PBI π-stacks is controlled by amino acid chiral centers; and the angle *α* depends on the steric and electronic parameters of PBI (left). CD spectra of PBIs **4a** (solid lines) and **4c** (dashed lines) upon interaction with (A) poly(dAdT)$_2$, (B) polydA-polydT, (C) poly(dG-dC)$_2$ and (D) polyA-polyU in a sodium cacodylate buffer with I = 50 mM at pH = 7; polynucleotide concentration: 4 x 10^{-5} M; r[PBI]/[polynucleotide] = 0.16 (right) Reproduced from ref. [100]**.** Copyright 2012, The Royal Society of Chemistry.

Further investigations have also been done with the PBIs carrying not only alanine linkers, but also chiral phenylalanine linkers (see Chapter 4). For getting deeper knowledge of the impact of the linker's positive charges, spermine was substituted by 4,9-dioxa-1,12-dodecanediamine. Here both secondary amino groups are replaced by oxygen atoms resulting in just two positively charged ammonium groups in the final PBI molecule. With these compounds it was possible to use the extended steric hindrance given by the phenyl group of the chiral linkers and the reduced number of charges to further investigate the sensing ability of PBI dimers in ds-DNA minor grooves and ds-RNA major grooves. In case of the dioxa PBI derivatives a lower DNA stabilization has been observed, but *vice versa* more specific differences can be observed upon interaction with polynucleotides. Even more important, compared to the smaller alanine linker the stronger steric hindrance of the phenylalanine linker allows the enantioselective sensing of DNA/RNA secondary structures. In this example *L*-phenylalanine-derived PBI dimers have a clear preference for poly(dA-dT)$_2$ and poly(dG-dC)$_2$ (Figure 46).

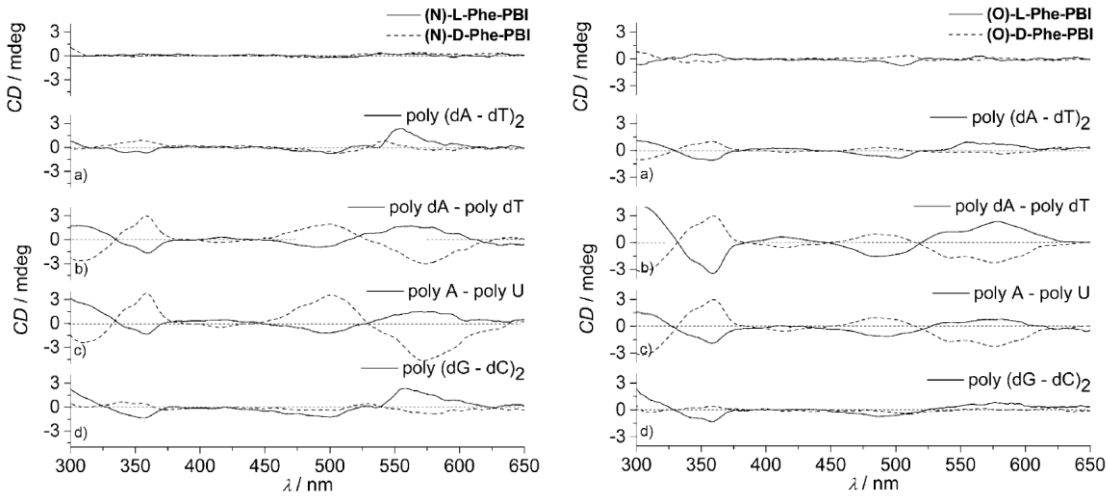

Figure 46. CD spectra of phenylalanine derived PBIs with spermine [(N)-*L*-Phe-PBI, **4b** and (N)-*D*-Phe-PBI, **4d**, left] and 4,9-dioxa-1,12-dodecanediamine [(O)-*L*-Phe-PBI and (O)-*D*-Phe-PBI, right] as positively charged groups. Reproduced with permission from ref. [101]. Copyright 2015, John Wiley & Sons.

2.4 Conclusion

Symmetrically amino-functionalized perylene bisimide dyes combine an outstanding dye with (potential) cations forming bolaamphiphiles. By combination of the characteristics of both, amines and perylene bisimide, numerous possibilities of interactions become possible and with it many applications can be derived, as shown in this chapter. The outstanding fluorescence properties of the PBI are in focus of the applications mostly. Minimal aggregation and the lack of free electron pairs in the side chains are good preconditions for high fluorescence quantum yields of perylene bisimide dyes. Aggregation and quaternization degree are influenced by many parameters like solvent, concentration of PBI, pH and counter ions. The complex supramolecular systems arising due to these external influences are currently poorly understood. Rational design of structure and function is accordingly impossible. This is why many more studies are required to come to a better understanding of these complex systems. In the meantime many findings happen by chance and acquired knowledge may apply only to a very specific set of parameters.

The investigations presented in chapters 3 and 4 contribute to better understand some of the influences on the aggregation behavior of PBIs in water.

Chapter 3

Spermine-functionalized Perylene Bisimide Dyes†

Abstract: A series of four spermine-functionalized perylene bisimide dyes without (**2**) and with linkers (**3a–c**) between the chromophore and the polyamine were synthesized. Protonation of the spermine moieties resulted in the formation of highly water soluble dyes with up to six positively charged ammonium ions. The aggregation behavior of these strongly fluorescent bola-amphiphiles was studied in pure water as solvent by UV/Vis and fluorescence spectroscopy, and an astonishingly high fluorescence quantum yield of up to Φ_{fl} = 0.90 for PBI **2** was observed. Atomic force microscopy and transmission electron microscopy were applied for the visualization of the aggregates on surfaces. Molecular modeling studies were performed by force field calculations to explore the aggregate morphologies which also provided valuable information on the influence of the additional alkyl carbonyl linkers. The detailed spectroscopic and microscopic investigations revealed that the excellent optical properties of perylene bisimide chromophores can be used even in pure water if their aggregation is efficiently suppressed.

† This chapter was published and is reproduced with permission from Wiley-VCH, Weinheim:
S. Rehm, V. Stepanenko, X. Zhang, T. H. Rehm, F. Würthner, *Chem. Eur. J.* **2010**, *16*, 3372–3382,
Spermine-functionalized perylene bisimide dyes – highly fluorescent bola-amphiphiles in water[102]
AFM studies were carried out by V. Stepanenko, electron microscopy by X. Zhang and molecular modeling by T.H. Rehm.

3.1 Introduction

In the past years, perylene tetracarboxylic acid bisimides evolved as one of the most intensively studied classes of functional dyes. Their outstanding optical and redox properties in combination with their thermal and light stability give rise to applications in different fields of current research. PBIs were initially used as high performance pigments on industrial scale due to their wide color range in the solid state and their extremely low solubility.[103,104] The latter property prevented the use of PBIs in solution and their targeted derivatization. Through the introduction of solubility enhancing groups like alkyl chains in the imide- and bay-position of the PBI it was possible to overcome their low solubility and investigate the optical properties of molecular dyes as strong fluorophores as well as their aggregation behavior as novel supramolecular building blocks.[2,105] As a result of this development, nowadays PBIs are widely used as fluorophores in organic media,[106,107] as organic semiconductors in solar cells,[108–111] light-emitting diodes[112–114] and field effect transistors,[115–117] as π-acidic anion receptors[118–121] or high-performance fluorophores for protein labeling[122–126] and DNA research[127–134].

However, upon changing the focus from common organic solvents to the biologically most relevant solvent water new strategies for the synthesis of PBI dyes have to be developed since the solubility of the chromophore decreases rapidly with the increasing polarity of the solvent.[8] Uncharged residues such as polyethylene glycol chains,[135–140] hydrophilic dendrimers,[141–146] crown ethers[147,148] and cyclodextrines[149] as well as peptide chains[150] were employed for the solubilization of the perylene core. These systems could be used, for instance, as biocompatible and biodegradable staining material of cells[151] or as e.g. guanine-quadruplex inducing DNA intercalator.[86,152–154] Nevertheless, most of these PBIs still lack of high solubility in pure water or exhibit unfavorable fluorescence properties due to aggregate formation.[3] To address these deficiencies charged groups, either permanent ions or reversible ionic groups via protonation and deprotonation were introduced. For anionic derivatives of water-soluble PBIs, carboxylate and sulfonate groups were most often incorporated via the phenoxy substituents in the bay region.[155] Also permanent positive charges were created in the imide position by alkylation of amino groups or nitrogen-containing

heterocycles.[7] The combination of the excellent optical properties of the PBI chromophore with the strongly enhanced water solubility was used for single-molecule spectroscopy of biological systems, e.g. for tracking experiments of bioparticles in living cells.[126]

Polyamines represent another class of highly hydrophilic compounds, which can be used as excellent solubility enhancing residues for investigations in water.[156] They also offer biological activity in many respects and play a major role in a huge variety of genetic processes, such as DNA replication, gene expression and gene delivery.[157–163] In an initial study, the biologically active polyamine spermine was introduced into the bay region of the perylene core.[92] It could be shown that the protonated polyamines act as solubilizing moieties in aqueous solutions as well as a fluorescent probe that interacts with the negatively charged sugar phosphate backbone of *calf thymus* DNA. At the same time, the groups of Savino and Franceschin reported on PBIs bearing several amines and polyamines in the imide position of the perylene bisimide dye. This mode of substitution sustains the planar structure of the perylene core which makes the system very interesting for intercalation experiments, in particular with guanine-rich DNA.[89,90,164–167]

Owing to their planarity, the formation of self-assembled nanostructures is also possible for core-unsubstituted PBIs by the pronounced π-π-stacking interactions of these chromophores in water.[3] Here the synthesis of a series of four highly water-soluble amphiphilic PBIs (**2, 3a–c**) is presented which incorporate spermine residues at the imide positions (Figure 47).

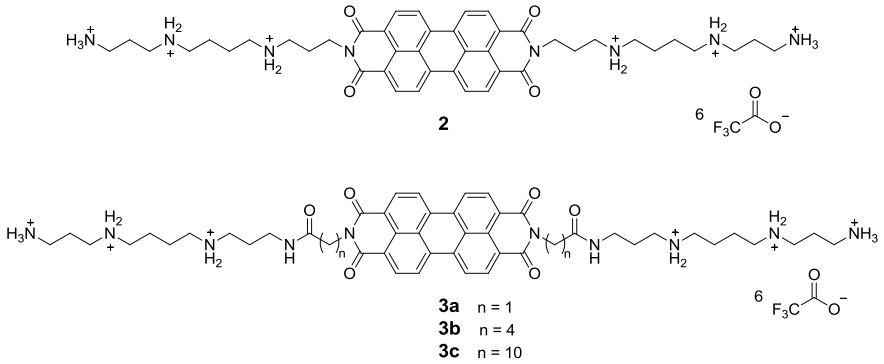

Figure 47. Structures of PBI **2** with directly attached spermine and PBIs **3a**-**d** with alkyl carbonyl spacer between the chromophore and the spermine residues.

Different spectroscopic studies in aqueous solution (UV/Vis and fluorescence spectroscopy) and on the solid surface (AFM, TEM) disclosed the aggregation behavior of these bola-amphiphilic systems[18,20,168] depending on the length of their alkyl chain interconnects.

3.2 Results and Discussion

3.2.1 Synthesis

The synthesis of compound **2**, where spermine is directly connected to the perylene bisimide, was achieved in two steps (Figure 48). Threefold ^{t}Boc-protected spermine **53** was synthesized according to literature procedures[169] and directly reacted with perylene tetracarboxylic bisanhydride (**54**) in DMF at 80 °C to give the fully protected precursor **55** in 36 % yield. The protecting groups were removed by adding trifluoroacetic acid to a solution of **55** in dichloromethane. The trifluoroacetate salt **2** was obtained as a dark red solid after removal of the solvent and lyophilization from water. PBI **2** was characterized by ^{1}H NMR, UV/Vis and fluorescence spectroscopy.

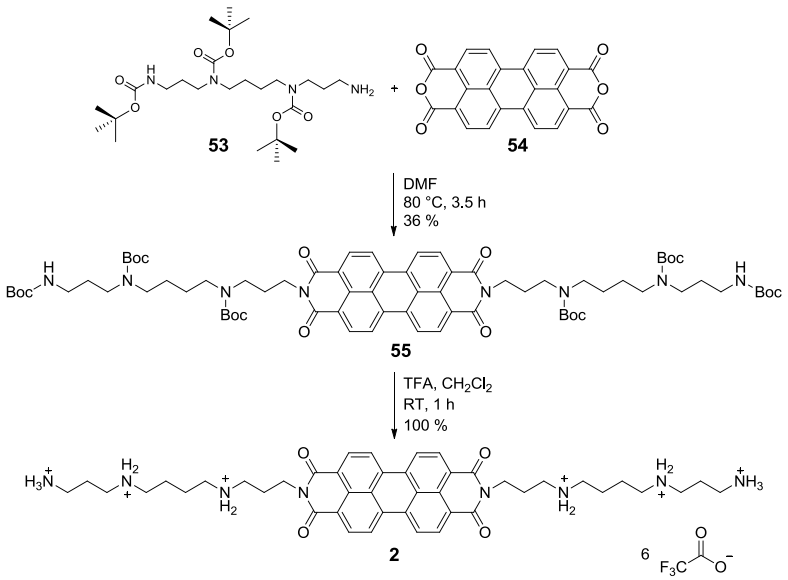

Figure 48. Synthesis of PBI **2**.

Compounds **3a–c** were synthesized in three steps according to the route depicted in Figure 49. The respective dicarboxylates **57a–c** were obtained according to literature procedures with some modifications in the workup.[37] A solution of the corresponding

ω-amino carboxylic acid (glycine (**56a**), n = 1; 5-amino valeric acid (**56b**), n = 4; 11-aminoundecanoic acid (**56c**), n = 10) with potassium hydroxide in water was added to a hot suspension of **54** in DMSO.

The mixture was vigorously stirred at 100 °C for 3 h. The reaction solution was cooled down to room temperature. After adjustment of the pH with aqueous hydrochloric acid to a value of 5 the resulting precipitate was collected by centrifugation. After several washing steps with water and methanol, the red solid was treated with hot aqueous hydrochloric acid (2 M) and filtrated. Compounds **57** were obtained in 82 % (**57a**), 77 % (**57b**) and 83 % (**57c**) yields based on starting compound **54**. Due to their low solubility, compounds **57a–c** were characterized only by FT-IR spectroscopy, melting point and high-resolution mass spectrometry (HRMS).

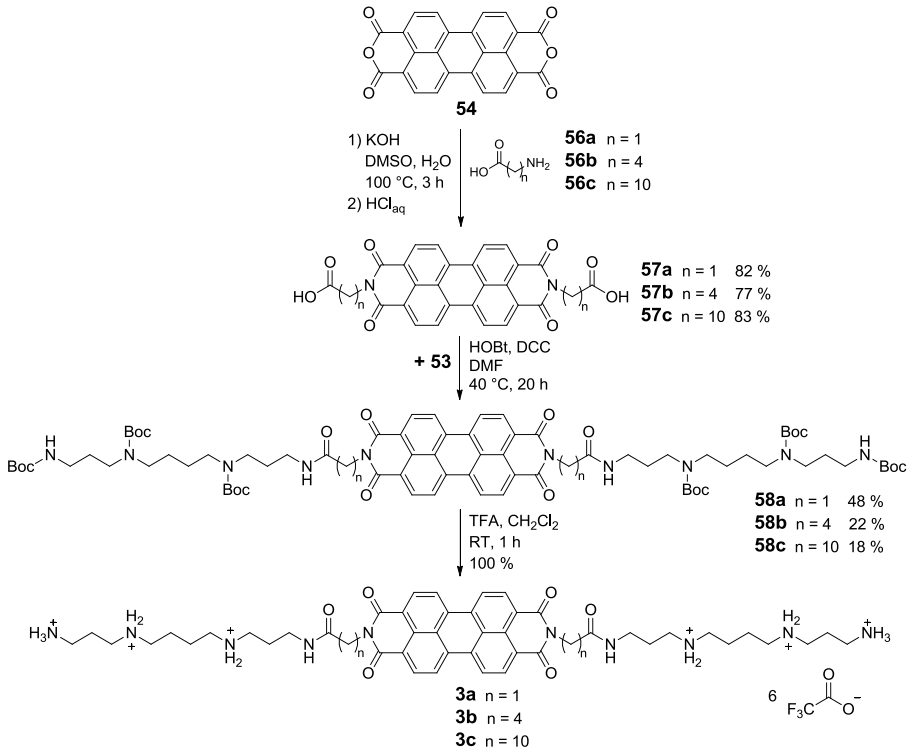

Figure 49. Synthesis of PBIs **3a–c** with alkyl carbonyl interconnectors of different length.

In the second step the corresponding dicarboxylic acids were activated by dicyclohexylcarbodiimide (DCC) and hydroxylbenzo-triazole (HOBt) in DMF. After addition of threefold ^{t}Boc-protected spermine **53**, the reaction solutions were stirred for up to 41 hours at 40 °C. After dilution with water and subsequent extraction with CH_2Cl_2,

the crude product was purified by standard column chromatography followed by HPLC. The ^{t}Boc-protected precursors **58a–c** could be isolated in yields of 48 %, 22 % and 18 %, respectively, and characterized by ^{1}H NMR and UV/Vis spectroscopy and HRMS. Removal of the protecting groups leads to the trifluoroacetate salts **3a–c** in quantitative yield. These compounds were lyophilized from water and characterized by ^{1}H NMR spectroscopy, UV/Vis and fluorescence spectroscopy, and high-resolution mass spectrometry.

3.2.2 Aggregation Studies by UV/Vis Spectroscopy

Owing to their good solubility even in pure water, the UV/Vis absorption properties of the trifluoroacetate salts of twofold spermine-functionalized perylene bisimide dyes **2** and **3a–c** is investigated in pure water over a wide concentration range. Figure 50A shows the absorption spectra of **2** in the concentration range of 4×10^{-3} to 7×10^{-7} M. All spectra display an absorption band between 400 and 625 nm related to the S_0-S_1 electronic transition of the PBI chromophore. At low concentrations, the well-resolved vibronic structure with the 0-0, 0-1, 0-2 transitions can be recognized with the two most intense bands at 533 nm (ε = 70100 $M^{-1}cm^{-1}$) and 497 nm (ε = 45500 $M^{-1}cm^{-1}$). Pronounced spectral changes could be observed with increasing concentration of PBI **2**. Concomitantly, the color of the solution changed from bright orange (owing to luminescence) in diluted samples to a deep red for the concentrated ones. The absorption maximum was shifted from 533 to 501 nm with a significant decrease of the absorption coefficient (ε = 36400 $M^{-1}cm^{-1}$). Furthermore an increase of absorption occurred in the range between 550 and 600 nm. Both phenomena indicate aggregation of the PBI dyes in a H-type manner with rotational displacement, similarly as observed for other core-unsubstituted PBI dyes in aliphatic solvents.[32,170,171] Considering the absorption spectra of, e.g., **2** only in the low concentration range between 2×10^{-4} and 7×10^{-7} M (red curves, Figure 1A), isosbestic points at 549 and 514 nm are evident. These crossover points indicate the existence of two species in equilibrium. At highest dilution ($c < 10^{-6}$ M) the two most intense bands have a ratio of 0.65, which points to the predominant existence of PBI **2** in its monomeric form.[172–174] Thus, the equilibrium most likely represents the transition from monomeric PBI **2** to its dimeric form. A

dimerization constant of approximate $10^4\ M^{-1}$ could be estimated.[1] At higher concentrations ($c > 2 \times 10^{-4}$ M) the growth toward extended oligomers of **2** seems to take place since the spectra at this concentration range do not cross through the isosbestic points anymore and get broadened (black curves, Figure 50A).

For PBI **3a** with a methylene carbonyl linker between the PBI and the spermine subunit, a similar absorption behavior was found (Figure 50B). In the concentration range from 5×10^{-3} to 5×10^{-7} M the absorption changed from a typical monomer spectrum of PBIs with the two most intense bands at 533 and 497 nm (ε = 70000 and 45300 $M^{-1}cm^{-1}$, respectively, ratio 0.65) to a broader spectrum with less resolved vibronic pattern. The absorption maximum shifted hypsochromically to 502 nm and the absorption coefficient dropped to 41200 $M^{-1}cm^{-1}$.

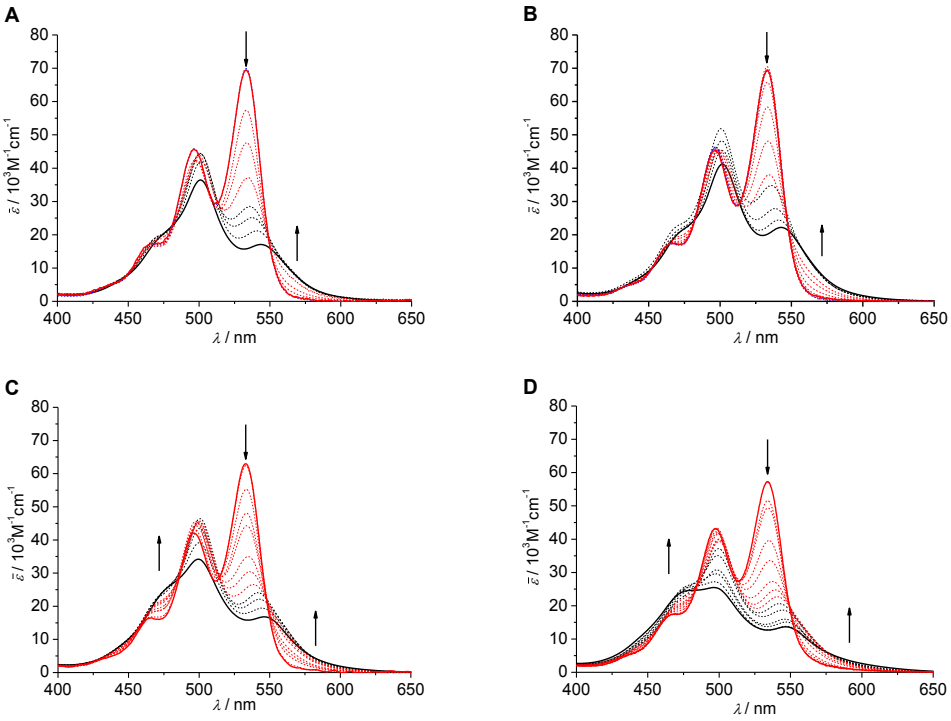

Figure 50. Absorption spectra of PBIs **2**, **3a–c** in water: A) **2**, c = 4×10^{-3} to 7×10^{-7} M; B) **3a**, c = 5×10^{-3} to 1×10^{-6} M; C) **3b**, c = 5×10^{-3} to 5×10^{-7} M; D) **3c**, c = 5×10^{-3} to 5×10^{-7} M. The red curves represent the low concentration range: A) **2**, $c_{low} = 2 \times 10^{-4}$ to 7×10^{-7} M; B) **3a**, $c_{low} = 3.5 \times 10^{-4}$ to 5×10^{-7} M; C) **3b**, $c_{low} = 2 \times 10^{-4}$ to 5×10^{-7} M; D) **3c**, $c_{low} = 1 \times 10^{-4}$ to 5×10^{-7} M.

[1] Reproducible dimerization constants for all systems could be only obtained for the lowest energy band of the $S_0 \rightarrow S_1$ transition (520 – 530 nm).

In comparison to PBI **2**, the monomeric form of PBI **3a** seems to be more favored since the decrease of the absorption coefficient is less pronounced for the latter one in the same concentration range. As for compound **2**, isosbestic points could be observed for the lower concentration range of the absorption spectra (3.5×10^{-4} to 5×10^{-7} M) of PBI **3a** at 546 and 514 nm. In higher concentrated solutions, the spectra also indicate the formation of larger oligomers as they do not fit to the isosbestic points anymore and appear broadened. Likewise PBI **3b**, possessing a butyl carbonyl linker, exhibits a very similar absorption behavior on increasing concentration (Figure 50C).

In contrast to PBI dyes **2, 3a** and **3b**, chromophore **3c** does not show the (typical) bright orange color of bay-unsubstituted PBIs in low concentrated aqueous solution. Already for the least concentrated solution (5×10^{-7} M), aggregated species seem to be present as indicated by the ratio of the two bands at 498 nm (ε = 43200 $M^{-1}cm^{-1}$) and 534 nm (ε = 57300 $M^{-1}cm^{-1}$) of 0.75 (Figure 50D) which is considerably higher than the ratios observed for PBIs **2** and **3a**,**b** at lowest concentration. Upon increasing the concentration a rather high absorption in bathochromic region of 550 to 600 nm and the formation of a distinct shoulder at *ca*. 475 nm are observed which indicate strong aggregation of PBI **3c** leading to a unique aggregate structure.

The absorption spectra of PBIs **2** and **3a–c** indicate that the degree of aggregation is dependent on the existence and on the length of the alkyl carbonyl spacers linking the perylene bisimide with the spermine moieties. PBI **3a**, which has only one CH_2 group between the building blocks, shows least aggregation in this series. Although the aggregation behavior of **3a** is very similar to that of PBI **2**, the latter possesses higher aggregation propensity, even though the spermine moiety is directly connected to the perylene bisimide. Apparently, the polar effect of the amide bond in **3a** prevails over the CH_2 group and hence leads to the most polar environment around the chromophore core within this series. For compound **3b** with four CH_2 groups, aggregation is more pronounced and initiates already at lower concentration compared to that of **2** and **3a**. The ten CH_2 groups of PBI **3c** have the strongest influence on the aggregation. The π-π-stacking of the chromophore in combination with the van-der-Waals interactions between the alkyl chains leads already at the lowest concentration to distinct aggregates of **3c** in water.

It is noteworthy that the pH values of aqueous solutions of PBIs **2** and **3a–c** were not constant over the concentration range applied here. The pH values varied between 4 for the most concentrated solutions to 7 for the most dilute ones. Obviously, this effect originates from the acidic character of the ammonium functional groups of the imide substituents. Presumably, upon aggregation of the monomers the positive charges of the spermine residues come in close contact to each other and form a cationic micro-environment around the chromophore. To prevent this destabilizing interaction between equally charged groups, protons are released to the bulk solvent leading to a decrease of the pH value. On the other hand, the existence of free amine groups facilitates the formation of hydrogen bonds between charged ammonium and neutral amine groups, resulting in a stabilized aggregate. But with increasing length of the aggregate the donation of protons results in a critical pH value which prohibits a further release of protons into the bulk solvent.[175,176] This equilibrium between deprotonation and reprotonation of the spermine moieties can be regarded as a self-regulating system and might be the reason that PBIs **2** and **3a–c** do not act as hydrogelators. Hence, pure aqueous solutions of PBIs **2** and **3a–c** are stable against precipitation over months. In contrast, attempts to measure the concentration-dependent aggregation behavior of PBIs **2** and **3a–c** in phosphate buffer solution (10 mM, pH 7, ionic strength 148 mM, 25 °C) were hampered by partial precipitation of the aggregates. According to literature, spermine is fully protonated at a physiological pH value of 7.4[177] and thus prevents the precipitation of the dyes. In basic solutions (pH ≥ 8) the spermine residues get deprotonated which results in the precipitation of the dyes due to a reduced solubility in water. Figure 51 shows the spectra of PBI **3b** in phosphate buffer within a concentration range from 5×10^{-4} M to 5×10^{-6} M (black lines). Already for the most dilute concentration (5×10^{-6} M), the absorption maximum is observed at lower wavelength of 497 nm (ε = 24600 $M^{-1}cm^{-1}$) pointing at the presence of extended aggregates. Upon increasing the concentration a further hypsochromic shift of the absorption maximum to 483 nm (ε = 22300 $M^{-1}cm^{-1}$) is observed. The second absorption band appears at 547 nm (ε = 11100 $M^{-1}cm^{-1}$) and shifts bathochromically to 552 nm (ε = 8700 $M^{-1}cm^{-1}$) in the most concentrated sample.

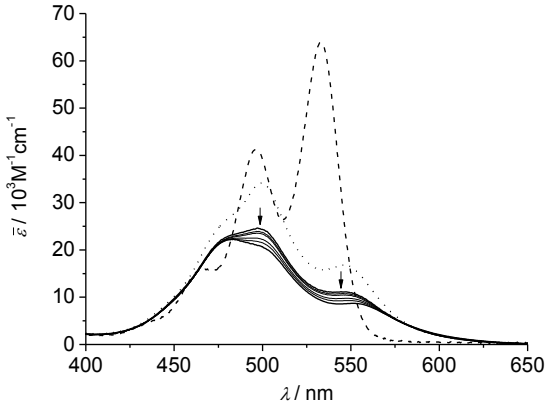

Figure 51. UV/Vis spectra of PBI **3b** in phosphate buffer (10 mM, pH 7, 25 °C) in the concentration range from 5×10^{-4} M to 5×10^{-6} M (black lines; arrows indicate the spectral changes upon increasing concentration); PBI **3b** in pure water at c = 5×10^{-4} M (dotted line) and 5×10^{-6} M (dashed line).

The position of these absorption maxima and the rather low absorption coefficients compared to those of PBI **3b** in pure water (dashed and dotted lines) are indicative for the formation of even larger aggregates. Two reasons might be responsible for this extended aggregation: first, the buffer absorbs the released protons upon increasing concentration and thus impedes the decrease of the solutions' pH value (contrary to the behavior in pure water) and second, the higher ionic strength of the solution might suppress the electrostatic self-repulsion within the cationic residues and favor stacking interactions.[178,179]

3.2.3 Fluorescence Spectroscopy

Fluorescence emission spectra of PBIs **2** and **3a–c**, measured in water solutions, are shown in Figure 52, together with their corresponding UV/Vis absorption spectra. The emission spectra of **2**, **3a** and **3b** in dilute solutions, which are supposed to contain predominantly monomeric dyes, are mirror images of the corresponding absorption spectra with Stokes shifts of around 13 nm. The fluorescence quantum yields range from 0.90 for **2** to 0.78 for **3a** and 0.72 for **3b**, which are appreciably high for perylene bisimide dyes in aqueous solution. The fluorescence emission spectrum of PBI **3c** (Figure 52D) was recorded at a concentration (5×10^{-7} M) where the dye molecules did not predominantly exist as monomers according to the absorption spectrum.

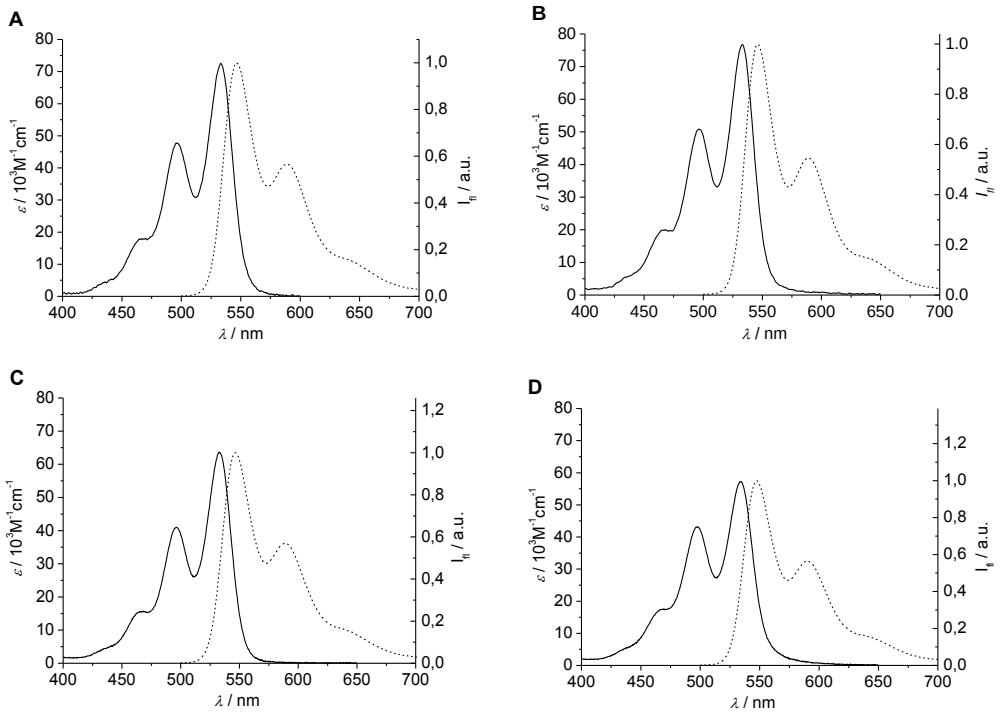

Figure 52. Absorption (solid lines) and emission (dotted lines) spectra of PBI **2** and **3a–c** in water: A) **2**, c = 7×10^{-7} M, Φ_{fl} = 0.90; B) **3a**, c = 5×10^{-7} M, Φ_{fl} = 0.78; C) **3b**, c = 5×10^{-7} M, Φ_{fl} = 0.72; D) **3c**, c = 5×10^{-7} M, Φ_{fl} = 0.39; excitation wavelength 475 nm; internal standard 0.1 N NaOH solution of fluorescein.

Nevertheless, the fluorescence emission spectrum of **3c** displays the typical shape of monomeric PBIs, whilst the fluorescence quantum yield is with 0.39 notably lower than those for PBIs **2** and **3a**,**b**. The obtained fluorescence quantum yields are not easy to interpret due to the concentration-dependent aggregation of the spermine-functionalized PBIs and the possibility for the formation of excited-state PBI aggregates (excimers).[180] Except for PBI **3c**, all emission spectra represent the mirror image of the respective monomer absorption spectra and thus corroborate the existence of monomeric PBIs in the excited state within the appropriate concentration range. Likewise, a single exponential fluorescence decay and a fluorescence lifetime of 4.0 ns was recorded for a 5×10^{-7} M solution of PBI **3a**, which is in agreement with the literature data found for monomers of bay-unsubstituted perylene bisimides (Figure 53).[32]

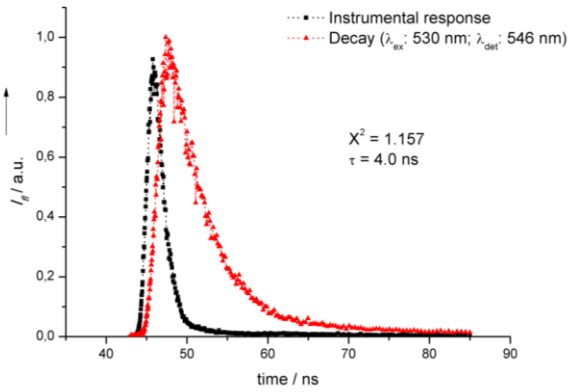

Figure 53. Fluorescence intensity decay curves for PBI **3a** monomer (water, 25 °C, c = 5×10^{-7} M). Detection wavelength λ_{det} = 546 nm and fitted with a single-exponential decay function.

However, with increasing spacer length and thus higher propensity for aggregation the fluorescence quantum yield is reduced from 0.90 (**2**) to 0.39 (**3c**). As the shape of the emission spectrum of **3c** is identical to those of **2**, **3a** and **3b** it may concluded that only (or rather predominantly) the excited monomers that are present in equilibrium contribute to emission, which are in the case of PBI **3c** around 40 %. Two important conclusions can be drawn from these studies: first, simple PBI dyes without any substituents in the bay area can become excellent fluorophores even in water, if their aggregation is prohibited and second, polycationic side chains in the imide positions are particularly suited to inhibit aggregation, because their repulsive forces sustain in the dyes' excited state.

3.2.4 AFM and TEM Experiments

To obtain better insights into the aggregate structure of PBIs **2** and **3a–c** tapping mode AFM (atomic force microscopy) images were recorded at a concentration of 1×10^{-3} M in water. The samples were spin-coated from freshly prepared water solutions on mica and after aging the solution for one month in order to investigate the time-dependent growth of supramolecular structures.

Figure 54A – D depict the topography images of thin films spin-coated from freshly prepared solution of PBIs **2** and **3a–c** onto mica. The height image of compound **2** shows small globular structures with a mean diameter of 3–6 nm (Figure 54A). Within a time period of one month, the shape and size of the structures did not change (Figure 55A).

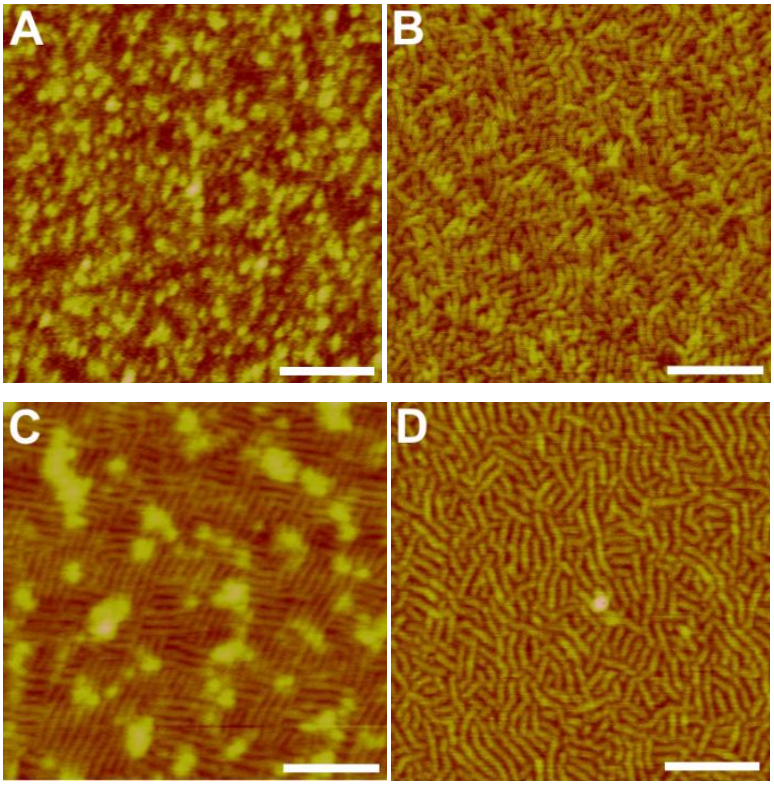

Figure 54. AFM tapping mode images (height) of films prepared from fresh aqueous solutions of **2** (A), **3a** (B), **3b** (C) and **3c** (D) spin-coated onto mica (c = 1 × 10^{-3} M). The scale bar corresponds to 50 nm and the z-scale is 1 nm.

Compared to this result, PBI **3a** reveals a completely different morphology on the mica surface. Rod-like structures with a mean diameter of 3.9 ± 0.3 nm and lengths of up to 40 nm cover the whole surface, hence circumventing a height measurement (Figure 54B). The aged solution of **3a** shows even longer structures indicating a slow growth process of the nanorods in solution (Figure 55B). Figure 54C displays the results for the freshly prepared solution of compound **3b**. Long, straight rods of *ca*. 4.8 nm in diameter form lamellae-like networks both for the freshly prepared solution and for the aged sample (Figure 55C). In this case a cross-section analysis was possible and a mean height of 1.3 nm could be determined (Figure 56). The rather low value might result both from the strong ionic interaction of the positively charged spermines with the predominantly negative charged mica surface as well as from the deformation of such a soft surface by the tip during the measurement in tapping mode.[181,182]

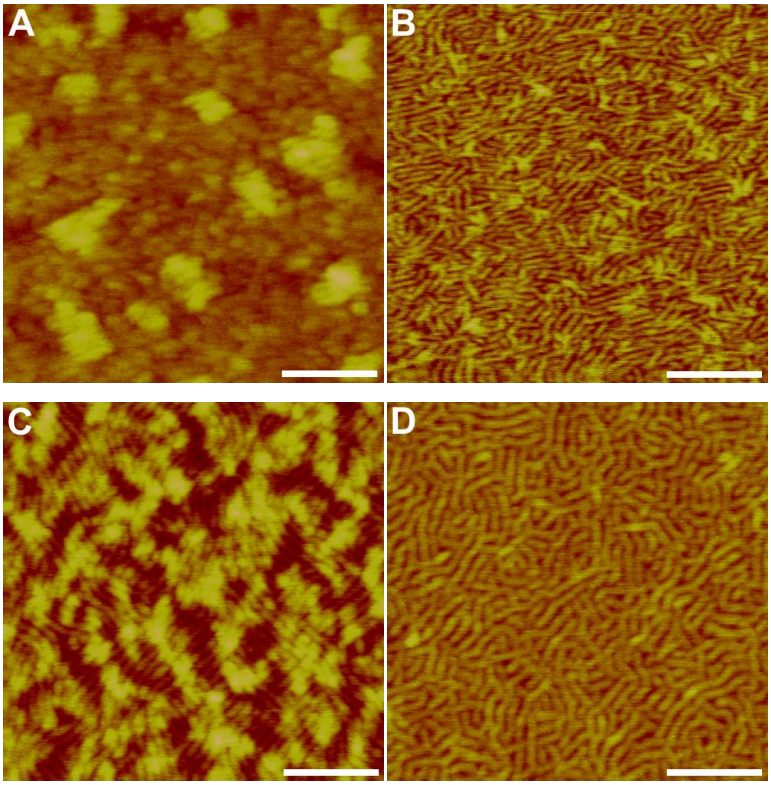

Figure 55. AFM tapping mode images (height) of films aged for one month of **2** (A), **3a** (B), **3b** (C) and **3c** (D) spin-coated onto mica (c = 1 × 10^{-3} M). The scale bar corresponds to 50 nm and the z-scale is 1 nm.

The rods of PBI **3b** align more in parallel than those of compound **3a** and show a woven network. For compound **3c**, the images of the fresh and aged samples cannot be distinguished (Figure 54D and Figure 55D). Very long worm-like structures with 5.5 ± 0.5 nm in diameter cover the whole surface. The lengths of the rods cannot be determined with high accuracy due to the interwoven pattern on the surface. However, a rough estimation reveals lengths up to 200 nm.

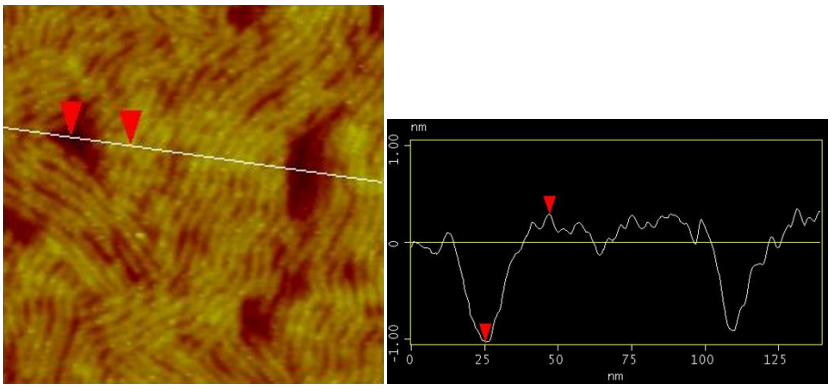

Figure 56. Cross-section plot of a thin film prepared from a solution of PBI **3b** onto mica (c = 1 × 10^{-3} M in water).

Although a precise size analysis of the rod aggregates is not possible due to a close packing on the surface, some conclusions can be reasonably drawn based on the AFM observations. With increasing length of the imide substituents the growth of nanorods is favored, both in diameter (minimum 3.6 nm for PBI **3a** and maximum 6.0 nm for PBI **3c**) and in length (minimum 20 nm for PBI **3a** and ~ 200 nm for PBI **3c**). This diameter can be related to the dimension of the longitudinal axis of the monomers, whereas the length of the worm-like objects depends on the number of monomers forming the aggregates by π-π-stacking interactions. As the increase in diameter is caused by an increase of the spacer length, aggregation is promoted by the more hydrophobic character of the molecules in aqueous solution. Moreover, the time-dependent growth within one month is also influenced by the length of the imide substituents since aggregates of PBI **2** do not grow at all within one month, while the length of PBI **3a** aggregates extend up to 100 %.

Furthermore, the aggregation behavior of PBI **3c** was investigated by TEM. Figure 57A shows the TEM image of a film from the freshly prepared solution of **3c** in water, drop-casted on the carbon-coated copper grid and stained with uranyl acetate solution. There are numerous short rods and only few are of extended lengths. The diameter of these rods is about 6–9 nm.

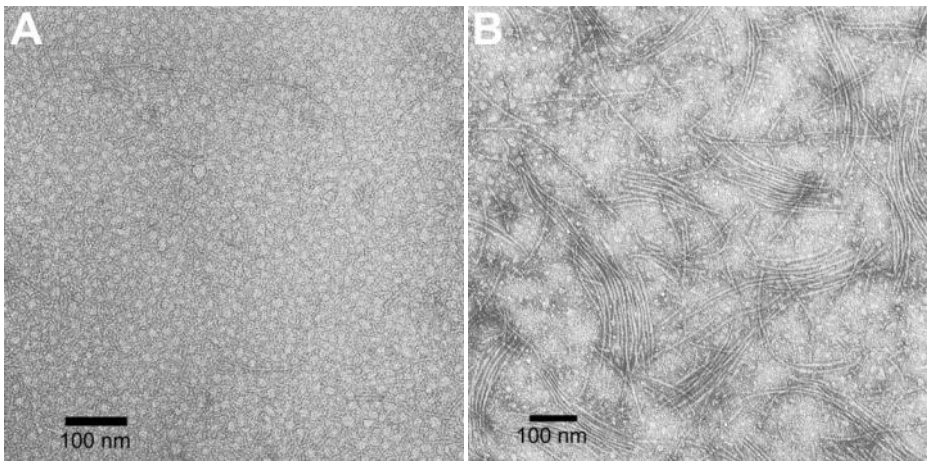

Figure 57. TEM images of films prepared from solution of **3c** in water ($c = 1 \times 10^{-3}$ M) casted on a carbon-coated copper grid: A) from a freshly prepared solution; B) from a solution aged for one month.

Compared to the diameter obtained from AFM data (5.5 ± 0.5 nm), this value is slightly increased, which is most likely resulted from the swollen hydrophilic shell of the

bola-amphiphile upon staining. The white interior represents the less polar and thus almost unstained perylene core and the black outer area occurs due to the well-stained ionic spermine substituents. This contrast pattern underlines again the amphiphilic character of the PBIs presented here. After aging the solution for one month (Figure 57B) the long rods can be recognized more precisely and they are the dominant species on the carbon-coated copper grid. The length of the rods was increased, while the diameter remained unchanged, suggesting that no morphology change took place.

3.2.5 Molecular Modeling

Towards a structure model for the self-aggregated PBIs **2** and **3a–c** force-field calculations were performed. Molecular dynamics studies were used to simulate the stacking of six molecules of PBI **2** and PBI **3c**, respectively, in a time slot of 500 ps at 300 K (snapshots of the appropriate arrangement were taken every 50 ps). Figure 58A shows the superimposed structures of six stacked molecules of PBI **2**. The top view reveals clearly the separation of the rather stiff and unpolar perylene core and the far more flexible shell of hydrophilic spermine residues. The oxygen atoms of the bisimide groups mark the border between the hydrophilic outer shell based on spermine residues and the inner cylinder of hydrophobic perylene cores. The overall diameter is about *ca*. 4.3 nm whereas the interior hydrophobic core has a dimension of *ca*. 1.5 nm in diameter. Figure 58B presents the overlay of six molecules of PBI **3c** under the same conditions as for PBI **2**. Again the π-π-stacked inner core is the central element. Compared to the shell of the PBI **2** stack the introduction of the alkyl carbonyl linkers led to an apportionment of the shell (overall diameter: *ca*. 6.2 nm). Hydrophobic interactions force the alkyl chains to a surface less accessible to solvent, underlining the stronger overall interaction between the bola-amphiphiles. At the outer rim of the PBI **3c** stack the spermine residues behave in the same manner as in the case of PBI **2** since the protonated polyamines form brush-like structures under intensive interaction with the polar solvent. Hence the calculations corroborate the importance of the alkyl linkers for the enhanced aggregation of the PBI **3c**.

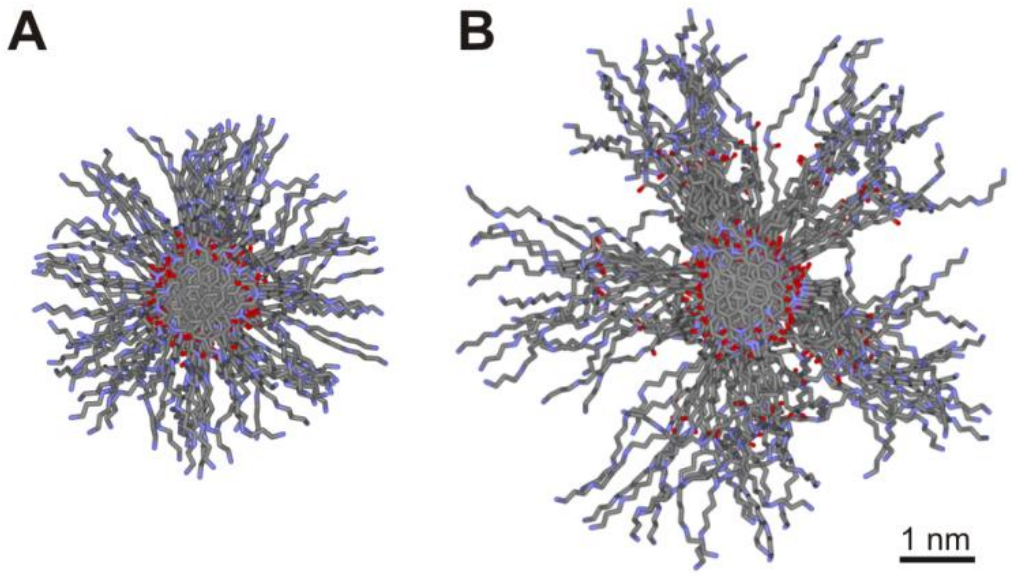

Figure 58. Top view on ten superimposed structures of six stacked molecules (60 molecules in total) of A) PBI **2** and B) PBI **3c** (grey = carbon, red = oxygen, blue = amine; hydrogens are omitted for clarity).

3.3 Conclusion

In summary, the synthesis of four twofold spermine-functionalized and core-unsubstituted perylene bisimides was accomplished. Three of them incorporate alkyl carbonyl linkers of different length between the chromophore and the polyamine spermine (PBI **3a–c**) whereas in PBI **2** a terminal amino group of spermine provides the imide nitrogen of the perylene bisimide dye. These PBI derivatives are highly water soluble owing to protonation of the amine groups of the spermine residues. At high dilution, the PBIs presented here exhibit a very high fluorescence quantum yield (Φ_{fl}) of up to 0.90 for PBI **2** in water. With increasing linker length the Φ_{fl} value decreases to 0.39 for PBI **3c**. Both UV/Vis and fluorescence spectra confirm the formation of H-type aggregates at higher concentration by efficient stacking of the planar π-system of the chromophores. AFM and TEM studies reveal the formation of large rod-like aggregates that grow both in length and diameter with increasing linker length. Finally, force-field calculations illustrate the dynamic behavior of the PBI-based bola-amphiphiles with a rather stiff inner core and a flexible outer shell. These results demonstrate that perylene bisimides can be outstanding fluorophores also in aqueous media if their aggregation is efficiently suppressed. This observation might open a new research avenue for this popular class of functional dyes.

Chapter 4

Chiral Bola-Amphiphiles in Water†

Abstract: A series of chiral perylene bisimide dyes were synthesized which incorporate alanine and phenylalanine in combination with spermine or dodecyl alkyl chains in the imide positions. Their aggregation behavior in water and chloroform, respectively, is investigated by UV/Vis-, fluorescence and CD spectroscopy. Besides AFM and TEM experiments additional computational studies were performed for the elucidation of the spectral data. The spectroscopic investigations show that the chiral substituents direct self-assemble into π-stacks with preferential helicity. However, due to the lack of long-range order and preferential growth into globular nanostructures, no helicity is observed on the macroscopic level by microscopy investigations.

† This chapter was included in
T. H. Rehm, M. Radić Stojković, S. Rehm, M. Škugor, I. Piantanida, F. Würthner, *Chem. Sci.* **2012**, *3*, 3393–3397, Interaction of spermine-alanine functionalized perylene bisimide dye aggregates with ds-DNA/RNA secondary structure (ref. [100]) and
J. Gershberg, M. R. Stoiković, M. Škugor, S. Tomić, T. H. Rehm, S. Rehm, C. R. Saha-Möller, I. Piantanida, F. Würthner, Chem. Eur. J. **2015**, *21*, 7886–7895, Sensing of double-stranded DNA/RNA secondary structures by water soluble homochiral perylene bisimide dyes (ref. [101])
and is reproduced in part with permission from The Royal Society of Chemistry, London (for ref. [100]) and Wiley-VCH, Weinheim (for ref. [101]).
AFM studies were carried out by V. Stepanenko, electron microscopy by X. Zhang and molecular modeling by T.H. Rehm.

4.1 Introduction

Helicity is a widely observed phenomenon in biological macromolecules. The double helix of DNA permits safe information storage on the smallest natural size scale. Here the self-assembly process relies on the interplay of hydrogen bonds and π-stacking interactions of the nucleobases.[183] Another example is the formation of the tobacco mosaic virus via the self-assembly of a RNA fragment together with identical protein subunits.[184,185] Their highly ordered helical structure is directed by chiral elements within the subunits, e.g. the carbohydrates in the backbone of the RNA or the amino acids in the protein subunits of the TMV.[186] These systems serve as inspiration for the design of synthetic functional supramolecules, whose helical structures are based on the combination of a series of non-covalent interactions (hydrogen bonding, π-π-stacking, hydrophobic, ionic interactions ...)[187–189] together with a structuring force like chiral centers of amino acids or carbohydrates (*ex chiral pool synthesis*). The high number of possible combinations between building blocks from a natural source and artificial precursors permits the engineering of tailor-made functional materials. π-Conjugated molecules (e.g. triphenylene,[190] hexabenzocoronene[191] or phthalocyanine[192]) are used for the design of stacked supramolecules controlling their packing mode with and without chiral components. The rylene chromophore class offers beside naphthalene bisimides (NBI)[193–196] the family of perylene bisimides dyes, which exhibit very high chemical and thermal stability and offer interesting optical and electrochemical properties.[2,105] In earlier works *Würthner et al.* introduced chirality into PBIs either via bridging the bay substituents by ether chains,[197–200] attaching stereocenters in the alkyl chains of the imide substituents[201–204] or by co-self-aggregation with a chiral compound[205]. Only the last two methods were useful for the formation of larger stacked structures with a defined helical arrangement. In order to use perylene bisimides in highly polar solvents, e.g. water, it was necessary to increase their solubility by attaching hydrophilic residues at the imide positions.[7,8,86,126,135–145,147–155] Polyamines like spermine serve best for this intention since they are perfectly water-soluble by protonation of the amino groups. Additionally, these polyamines play a major role in a huge variety of genetic processes, such as DNA replication and gene expression, making them interesting for potential applications in the life sciences.[92,156–163] This chapter

presents the synthesis and self-assembly of water-soluble perylene bisimide dyes (**4a–d**) which form helical stacks whose stereochemistry is controlled by the side chains of *α*-amino acids (*L*/*D*-alanine and *L*/*D*-phenylalanine, Figure 59). Additionally, uncharged derivatives with dodecyl alkyl chains (**5a**, **5b**) were synthesized in order to analyze their self-aggregation process in chloroform (Figure 59). Comparison of the data obtained allowed a deeper insight into the mechanism of self-aggregation under the appropriate conditions.

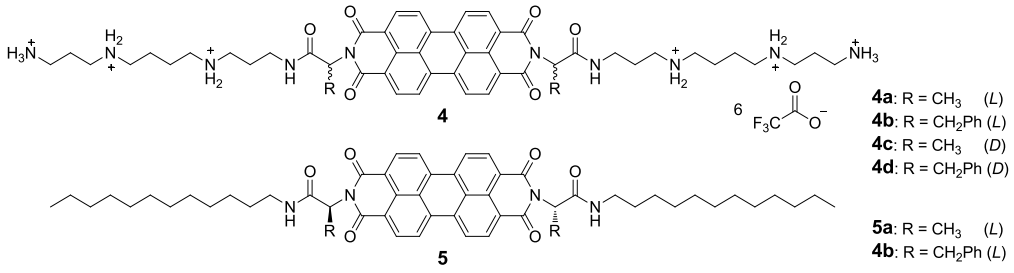

Figure 59. Chiral perylene bisimide dyes **4a–d** for studies in water and **5a**,**b** for studies in chloroform.

4.2 Results and Discussion

4.2.1 Synthesis

The synthesis of the target compounds **4a–d** was achieved in three steps. Perylene tetracarboxylic acid bisanhydride (**54**) was reacted with the appropriate *α*-amino acid **59a–d** in molten imidazole at 140 °C to give the free dicarboxylic acids after acidic workup in 97 – 100 % yield.[37,206,207] Threefold ^{t}Boc-protected spermine (**53**) was synthesized according to literature procedures[169] and coupled to **60a–d** with dicyclohexylcarbodiimide (DCC) and hydroxybenzotriazole (HOBt) as coupling reagents in dimethylformamide (DMF) as solvent and diispropylethylamine (DIPEA) as base. The fully protected PBIs could be obtained with yields of 44 % (**61a**), 29 % (**61b**), 61 % (**61c**), and 75 % (**61d**). The protecting groups were removed by stirring the precursors **61a–d** in TFA to give the target compounds **4a–d** in quantitative yield after lyophilization from water (Figure 60A). The uncharged derivatives of chiral PBIs (**5a**, **5b**) were synthesized by twofold imidization of **3** with dodecylamine-functionalized *L*-alanine **64a** and *L*-phenylalanine **64b**, respectively (Figure 60B).

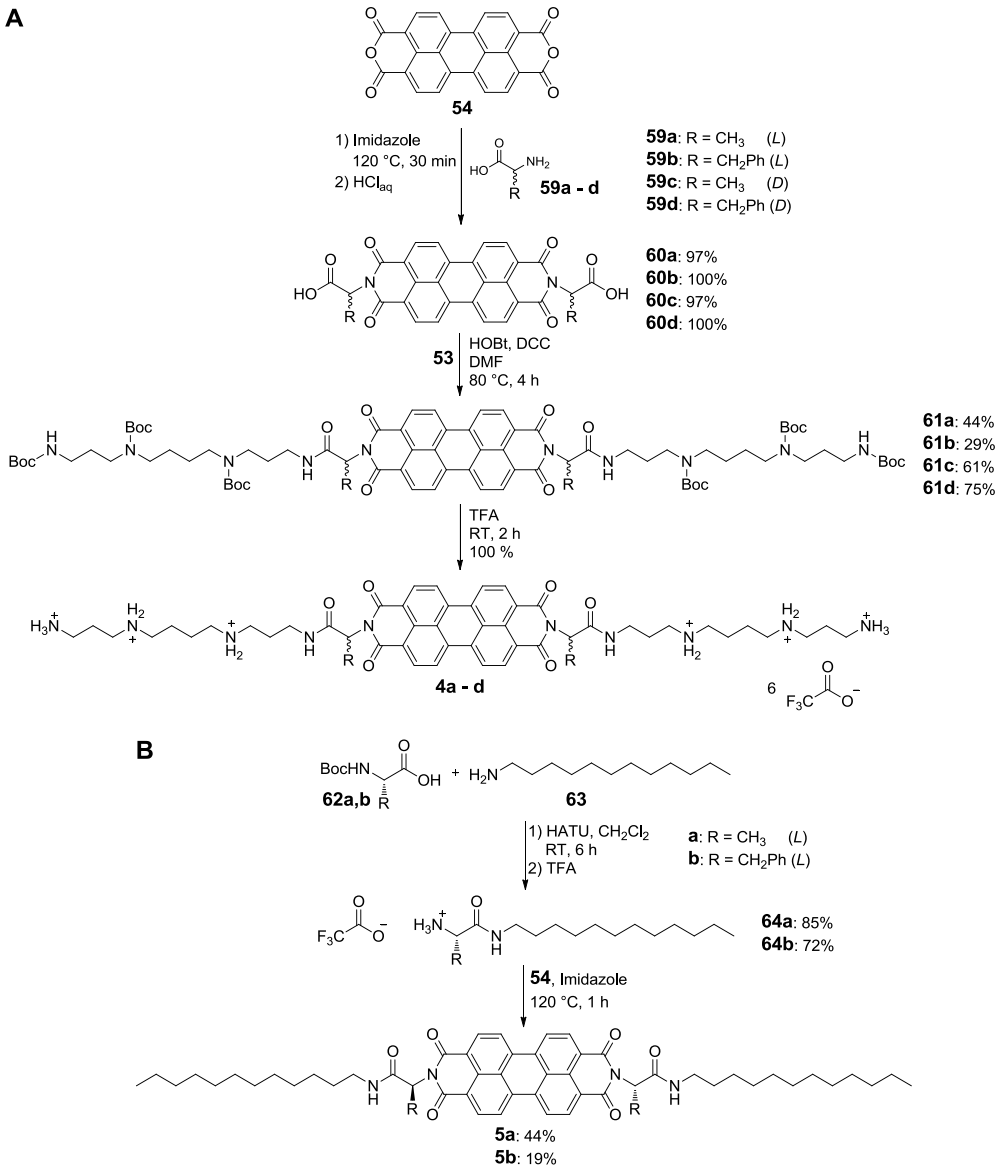

Figure 60. Synthesis of A) spermine-functionalized PBIs **4a–d** and B) dodecyl-functionalized PBIs **5a** and **5b**.

4.2.2 Aggregation studies by UV/Vis and Fluorescence Spectroscopy

Perylene bisimides **4a** and **4b** were first subjected to UV/Vis experiments in order to get an insight into the concentration dependent aggregation behavior in water. At low concentration (5×10^{-6} M) a typical monomer spectrum of bay-unsubstituted PBIs can be found for **4a** (Figure 61A). The absorption band between 400 nm and 600 nm is related to the S_0-S_1 electronic transition of the PBI chromophore and shows a well resolved vibronic fine structure with the 0-0, 0-1 and 0-2 transitions at 534 nm (ε = 77200 $M^{-1}cm^{-1}$), 497 nm (ε = 48500 $M^{-1}cm^{-1}$) and 466 nm (ε = 18000 $M^{-1}cm^{-1}$). The ratio of the two most intense bands is ε(534 nm)/ε(497 nm) = 1.6 again hinting to the

monomer state of **4a** in dilute solutions (Figure 61A).[172–174] The high concentration spectrum (5×10^{-3} M) is broader due to electronic coupling between the perylene bisimide cores with maxima at 542 nm (ε = 23000 $M^{-1}cm^{-1}$) and 502 nm (ε = 36200 $M^{-1}cm^{-1}$). Isosbestic points at 548 nm, 515 nm, 501 nm and 482 nm suggest a monomer – dimer equilibrium in the concentration range up to 5×10^{-4} M. Most likely higher oligomers appear above this concentration as the spectrum at 5×10^{-3} M differs obviously according to wavelength and extinction coefficient. The overall bathochromic shift of the absorption maximum and the rise of absorption in the region from 550 nm to 625 nm in the concentrated solution suggests H-type aggregation with rotational displacement of the PBI chromophores.[32,170,171] The emission of PBI **4a** presents a Stokes shift of 13 nm and appears at 547 nm with a high fluorescence quantum yield to 0.72 for the solvent water.

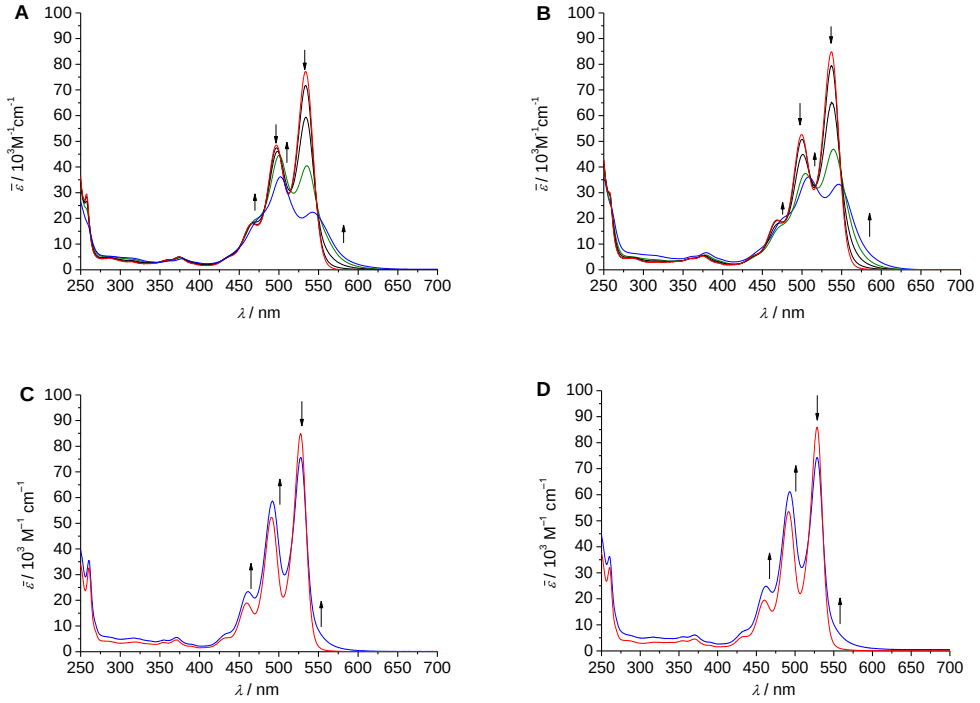

Figure 61. Top: UV/Vis spectra of A) *L*-alanine **4a** and B) *L*-phenylalanine **4b** in water at 25 °C in a concentration range from 5×10^{-6} M (red) to 5×10^{-4} M (green); the spectrum at 5×10^{-3} M is plotted in blue; bottom: UV/Vis spectra of C) *L*-alanine **5a** and D) *L*-phenylalanine **5b** in chloroform at 25 °C at 5×10^{-5} M (red) and 1×10^{-3} M (blue); the arrows indicate spectral changes upon increasing concentration.

PBI **4b** also shows strong concentration dependent aggregation in water (Figure 61B) which is in analogy to **4a**, at least in dilute solution. All absorption maxima of **4b** are shifted bathochromically compared to **4a**, in dilute solution up to 3 nm and in

concentrated solution up to 14 nm, respectively. The extinction maximum of **4b** at 508 nm is *ca*. 10000 $M^{-1}cm^{-1}$ lower compared to the corresponding maximum of **4a** at 500 nm. This difference hints to a less strong aggregation for **4b** in concentrated solution.

Table 4. Spectral properties of **4b** in water.

c/M	λ_{abs}/nm	ε/$M^{-1}cm^{-1}$	λ_{em}/nm	Φ_f
5×10^{-6}	537	84900	549	0.79[a]
	500	52600		
	469	19400		
5×10^{-3}	546	24600		
	508	26100		

[a] A 0.1 N NaOH solution of fluorescein has been used as standard for this measurement (excitation wavelength: 475 nm).

In Chapter 3 the aggregation behavior of the glycine derivative **3a** (Figure 49) was described which is not chiral due to two protons at the α-carbon atom resulting in less steric hindrance.[102] By comparing the absorption spectra of **4a** and **4b** with the achiral system the clear structural influence of the amino acid side chains on the aggregation propensity is demonstrated (Figure 62A). Achiral **3a**, without any steric hindrance at the α-carbon atom of the amino acid linker, shows the strongest degree of aggregation as seen by the highest extinction coefficient at the absorption maximum (ε = 41000 $M^{-1}cm^{-1}$). Using the spectral data of the dilution row a dimerization constant of approximate 10^3 M^{-1} could be estimated for **3a**.[102] However, the chiral PBIs show a lower degree of aggregation since the absorption maximum at 502 nm and 508 nm, respectively, are reduced by approx. 5000 $M^{-1}cm^{-1}$. For both chiral PBIs a dimerization constant of about 10^2 M^{-1} could be estimated. Although having the same aggregation propensity the UV/Vis spectrum of phenylalanine-derived PBI **4b** shows a variance from **4a**.

The absorption at 546 nm has an extinction coefficient of 33000 $M^{-1}cm^{-1}$ which is much higher compared to 23000 $M^{-1}cm^{-1}$ at 542 nm for **4a**. Most likely the steric impact of the benzyl groups forces the chromophores of aggregated **4b** to a greater rotational

displacement compared to **3a** and **4a**. The resulting alignment of the transition dipole moments permits formerly forbidden transitions resulting in two strong bands.

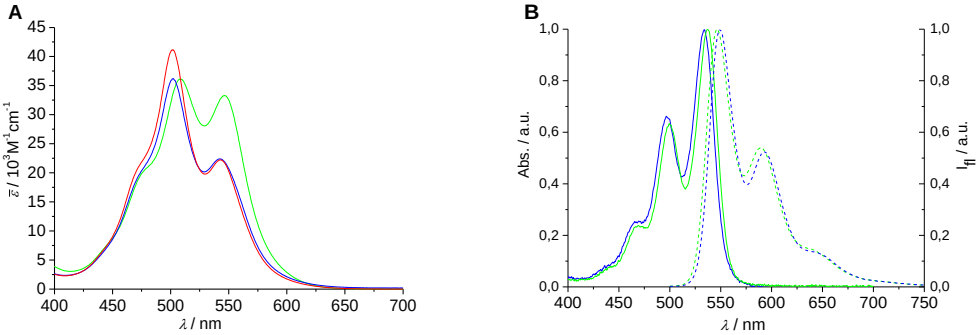

Figure 62. A) UV/Vis spectra of **4a** (blue), **4b** (green) and **3a** (red) at 5×10^{-3} M in water at 25 °C; B) UV/Vis (solid) and fluorescence (dotted) spectra of **4a** (blue) and **4b** (green) at 1×10^{-6} M in water at 25 °C.

However, the fluorescence quantum yield of **4b** has a value of 0.79 (which is 10 % higher compared to **4a**) hinting in contrary to a reduced degree of aggregation of **4b** and a higher amount of monomeric dyes in solution. Concentration dependent UV/Vis studies of **5a** and **5b** in chloroform show similar results as seen for **4a** and **4b** in water although the propensity for aggregation does not seem to be as strong as for the water-soluble systems (Figure 61C for **5a** and Figure 61D for **5b**).

4.2.3 Aggregation studies by CD Spectroscopy

Temperature dependent CD measurements of both chiral PBIs give a strong bisignate signal between 400 nm and 625 nm covering the whole PBI chromophore visible absorption range of strongly aggregated **4a** and **4b**. The zero-crossing of the bisignate signals is located at approx. 515 nm which is close to the UV/Vis absorption maximum at this concentration (Figure 63A and B). The bisignate signal is caused by excitonic coupling of rotational distorted perylene bisimide transition dipole moments arranged in such a helical stack aggregate with only one or at least one preferential direction, either clockwise (*P*-configured) or counter-clockwise (*M*-configured).The CD signal of **4a** gives a positive Cotton effect with a maxima at 494 nm ($\Delta\varepsilon$ = +12.2 $M^{-1}cm^{-1}$) and a negative Cotton effect with two maxima at 522 nm ($\Delta\varepsilon$ = -6.9 $M^{-1}cm^{-1}$) and 552 nm ($\Delta\varepsilon$ = -11.8 $M^{-1}cm^{-1}$). The signature sequence from positive to negative (+/-) points to a *M*-configured helicity of the PBI stack of **4a**.[129,130,132] The signal itself is most intense at

5 °C and decreases with increasing temperature as expected for an enthalpy-driven self-assembly process.

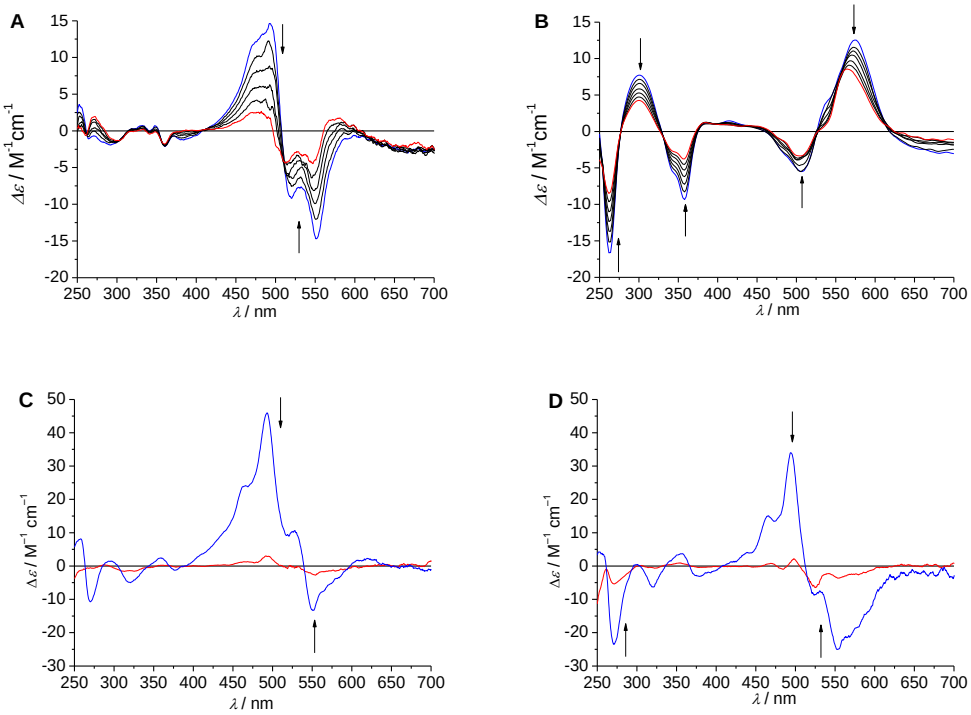

Figure 63. A) Temperature-dependent CD spectra of **4a** in water at 5×10^{-3} M from 10 °C (blue) to 70 °C (red); B) temperature-dependent CD spectra of **4b** in water at 5×10^{-3} M in water from 10 °C (blue) to 70 °C (red); C) CD spectra of **5a** at 1×10^{-3} M (blue) and 5×10^{-5} M (red) in $CHCl_3$ at 25 °C; D) CD spectra of **5b** at 1×10^{-3} M (blue) and 5×10^{-5} M (red) in $CHCl_3$ at 25 °C.

In contrary the CD signal of **4b** differs clearly from the *L*-alanine derived PBI. Here, the first Cotton effect has a negative signature with a maximum at 506 nm ($\Delta\varepsilon$ = -5.5 $M^{-1}cm^{-1}$) whereas the second Cotton effect has a positive signature and with a single maximum located at 574 nm ($\Delta\varepsilon$ = +12.5 $M^{-1}cm^{-1}$). The reversed signature sequence (-/+) hints to a contrary helicity (*P*-configuration) in the aggregate of **4b** compared to the *L*-alanine derivative. Most likely the greater steric hindrance of the benzyl side chain in **4b** induces the switch of helicity. Interestingly, aggregated **4b** shows additional and strong CD signals. Two of them are located at 358 nm ($\Delta\varepsilon$ = -9.1 $M^{-1}cm^{-1}$) and 414 nm ($\Delta\varepsilon$ = +1.5 $M^{-1}cm^{-1}$). With a zero-crossing at approximate 374 nm this couplet can be attributed to the S_0-S_2 electronic transition of bay-unsubstituted PBI dyes, having also the same Cotton effect sequence as the first electronic transition (-/+ for *P*-configuration). The other signal set at 263 nm ($\Delta\varepsilon$ = -16.9 $M^{-1}cm^{-1}$) and 300 nm ($\Delta\varepsilon$ = +7.5 $M^{-1}cm^{-1}$) resemble with a zero-crossing at 277 nm the signal shape of naphthalene

imide units in a core-twisted perylene bisimide chromophore. In this case excitonic coupling of two such subunits results in a bisignate signal as seen in the CD spectra of **4b**.[197–200] Applying the exciton chirality method[208] the configuration of the rotational twist in aggregated **4b** is clockwise (*P*-configured). As shown here the steric influence of the benzyl group at the imide position of the PBI has a surprisingly high impact on the supramolecular structure of aggregated **4b**.

CD experiments of **5a** and **5b** in chloroform (Figure 63C and D) show for both *L*-alanine and *L*-phenylalanine derivatives the same Cotton signal sequence at 551 nm (negative signature) and 493 nm (positive signature) pointing at a *M*-configured helicity as seen for **4a** in water.

4.2.4 AFM and TEM experiments

In analogy to the investigations of the achiral bola-amphiphiles tapping mode AFM images were recorded for the chiral perylene bisimides. Freshly prepared solutions of **4a** (2.5×10^{-4} M in water) and **4b** (4×10^{-3} M in water) were spin-coated on freshly cleaved mica. The height images of both PBIs show small globular structures with a mean diameter of 6 nm for **4a** and 8 nm for **4b** (Figure 64). The measured height is about 0.4 nm. Both findings differ significantly from the AFM data collected for the achiral PBIs with amino acid linkers, as they form long worm-like structures with a length of up to 200 nm for and a height of *ca*. 1.3 nm (see Chapter 3.2.4). The chiral PBIs **4a** and **4b** resemble more PBI **2** which also forms small globular particles. In both cases the hindrance between the interacting monomers is based on structural characteristics of the imide substituents. For the achiral PBI **2** the repulsive interactions between the cationic ammonium groups in close proximity to the chromophore core results in the low degree of aggregation. In case of the chiral PBIs the amino acid side chains (a methyl group for **4a** and a benzyl group for **4b**) disturb the efficient interaction between the aromatic surfaces of the perylene bisimide core. In contrast to the PBIs with achiral amino acids no defined aggregates are formed, which might be also the reason for the rather low height value for the aggregates of **4a** and **4b**. The strong ionic interaction of the positively charged spermines with the predominantly negative charged mica surface

prevails the ineffective stacking interactions of the chromophore cores and results in such flat structures. Beside this fact the low height might be also caused by the deformation of such a soft surface by the AFM tip used in tapping mode.[181,182]

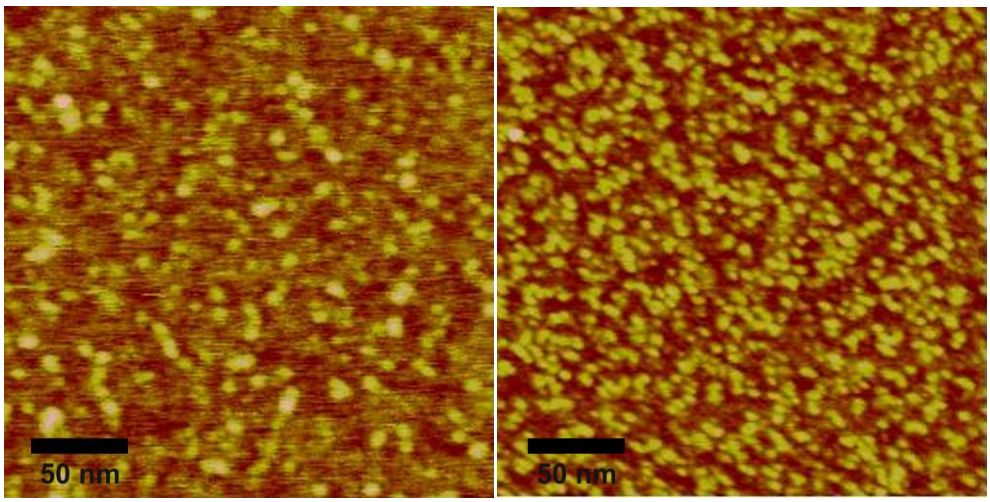

Figure 64. AFM tapping mode images (height) of films prepared from fresh aqueous solutions of **4a** (left, c = 2.5 × 10^{-4} M, z = 1 nm), and **4b** (right, c =4 × 10^{-3} M, z = 1.5 nm) spin-coated onto mica.

In case of PBI **4a** the aggregation behavior was also investigated by TEM. Figure 65 shows the TEM image of a film from a freshly prepared solution of **4a** in water, drop-casted on the carbon-coated copper grid and stained with uranyl acetate. The picture shows many particles on the scale of 4 to 7 nm that are not spherical but more of rectangle or cylindrical shape.

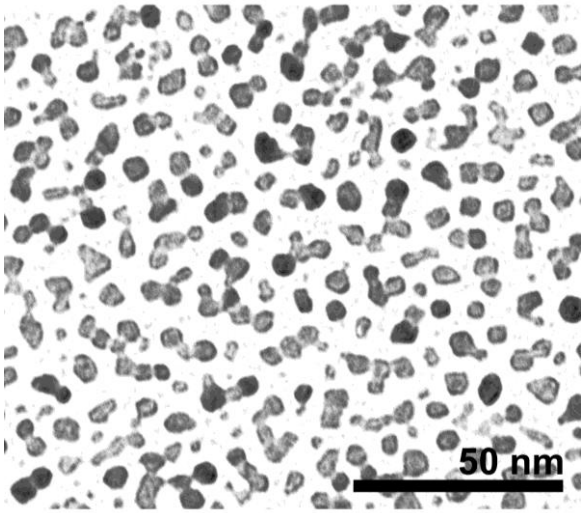

Figure 65. TEM images of films prepared from solution of **4a** in water (c = 5 × 10^{-3} M) casted on a carbon-coated copper grid.

Some dumbbell like structures could also be seen which consist of two conjoined smaller particles. These small particles strongly resemble the TEM picture of micelles found for wedge shaped PBIs.[135] However, these PBIs were unsymmetrical, amphiphilic molecules and not such a symmetrical and charged PBI like **4a**. Therefore formation of micelles is unlikely. Most likely the appearance of these structures is based on the formation of short rod-like aggregates. In conclusion AFM and TEM studies delivered information on the size and shape of aggregates of PBIs **4a** and **4b** but the assumed helicity of the aggregates could not be resolved.

4.2.5 Molecular modeling

L-configured alanine-derived PBI **4a** favors a pronounced aggregate helicity with *M*-configuration as seen in the CD spectra in water. Molecular modeling studies suggest also defined helical arrangement of the chromophores with *M*-configuration of the helix (Figure 66). Here, the distance between the sterically competing elements, the methyl group, the chromophore core and the spermine residue, is the largest. The *M*-configuration for stacked **4a** is also in agreement with literature data for the sequence of the Cotton signal signature found.[129,130,132]

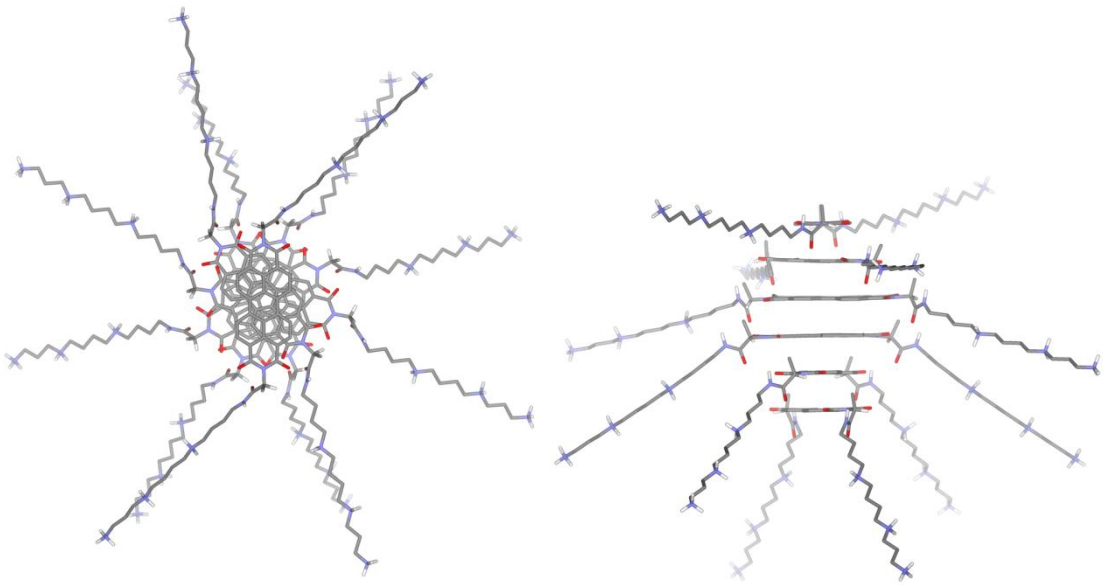

Figure 66. Top and side view on the minimized structure of helically stacked **4a** with M-configuration.

In case of *L*-configured phenylalanine-derived PBI **4b** a pronounced helicity with *P*-configuration is favored as seen in the CD spectra in water (Figure 63). This is

encouraged by molecular modeling which suggest defined helical arrangement of the chromophores with *P*-configuration of the helix (Figure 67) Two scenarios for the inversion of the helicity can be assumed. In earlier works the introduction of chiral elements with increased steric hindrance but with the same configuration of the chiral centers resulted also in inversion of the helical arrangement of the stack. Here the aggregate rearranged due to steric repulsion between the structural elements of the imide substituents. The inversed helicity provided a local order between the monomers with maximum distance between the interacting substituent residues, namely the benzyl group, the spermine residue and the perylene bisimide core.

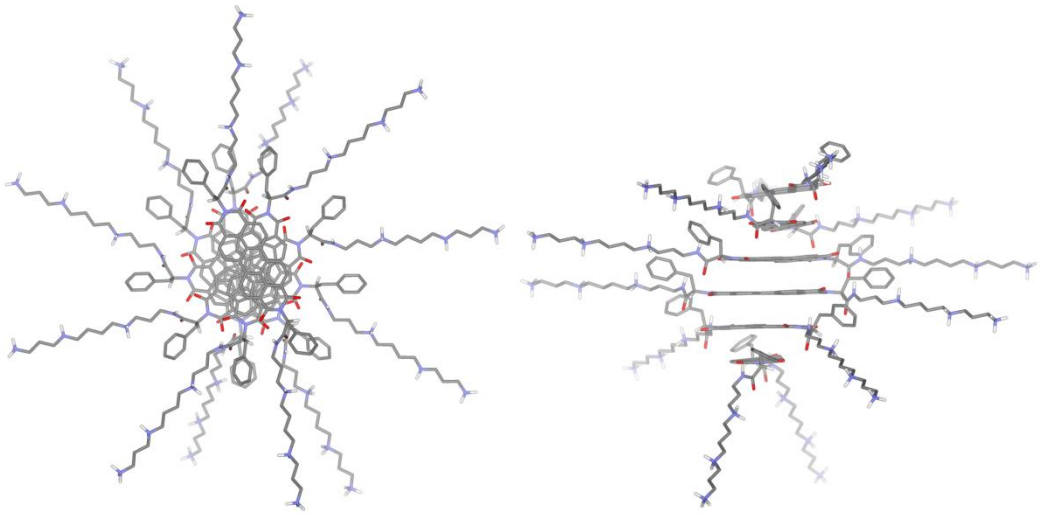

Figure 67. Top and side view on the minimized structure of helically stacked **4b** with *P*-configuration.

Further analysis of **4a** and **4b** by NMR spectroscopy with NOE correlation experiments might give deeper insights into the structure of the stacked PBIs. Beside further analysis also the synthesis of other PBI-spermine derivatives with amino acid side chains of alkyl residues with greater steric hindrance or extended aromatic residues might deliver information on the impact of these structural elements on the formation of such chiral perylene bisimide aggregates. Especially for the latter ones the introduction of other chromophores (e.g. pyrene) might deliver interesting systems for light harvesting or energy transfer and transport, respectively.

4.3 Conclusion

In summary, the synthesis of perylene bisimide dyes was presented which feature stereogenic centers at the imide substituents based on α-amino acids. Solubility was achieved by the incorporation of either spermine for water (**4a–d**) or dodecyl alkyl chains for chloroform (**5a**, **b**) over peptide couplings with the amino acids. Spectroscopic UV/Vis, fluorescence and CD studies disclosed a high fluorescence quantum yield in water (Φ_{fl} = 0.79 for **4b**) and the influences on the helicity control of the PBI stacks. It could be shown that not only the chiral centers must be regarded for stereochemical control, but also the size of the adjunct group (methyl *vs.* benzyl). Nevertheless, these findings present a possibility for the stereochemical control of the stacking behavior of perylene bisimide dyes which could be used in biological applications by utilization of the perylene bisimide dyes as chiroptical fluorescent probes.

Chapter 5

A symmetric Acridine-Perylene Bisimide Multichromophore

Abstract: A novel multichromophoric system was synthesized possessing two acridine units which are connected to the imide positions of a bay-unsubstituted perylene bisimide dye via flexible linkers. The aggregation behavior in chloroform was investigated by UV/Vis- and fluorescence spectroscopy. Dilution and diffusion studies were performed using ^{1}H NMR spectroscopy. Additional computational studies were executed for the elucidation of the spectral data. UV/Vis and NMR experiments suggest a concentration-dependent aggregation process indicating H-type aggregation via strong π-π-stacking interactions between perylene bisimide units at lower concentration. At highest concentration, NMR results suggest a pronounced interaction of the acridine units by π-π-stacking and by hydrogen bonding. These modes of interaction are also supported by molecular modeling studies, which show π-stacking interactions between the acridine units and the perylene chromophore in the monomer state. With increasing concentration, dimer structures were formed showing a nucleobase-like arrangement of the acridine units along the surface of the π-stacked perylene chromophores.

5.1 Introduction

The spermine functionalized PBI derivatives presented and discussed in Chapters 3 and 4 interact with nucleic acids unspecifically or via groove binding.[100,101] Acridine derivatives are known to bind to nucleic acids more specific, compared to spermine, by groove binding or by intercalation.[209] Acridine and its derivatives form planar, aromatic π-systems which can interact with themselves and other aromatic systems (e.g perylene, nucleobases). Molecules with the general structure shown in Figure 68 with two acridine moieties which are connected to the perylene core by flexible linkers are able to form intra- and intermolecular interactions. Theses interactions are supposed to be different in presence or absence of DNA due to possible interactions of acridine residues with DNA. This might be applied for probing DNA or RNA sequences.

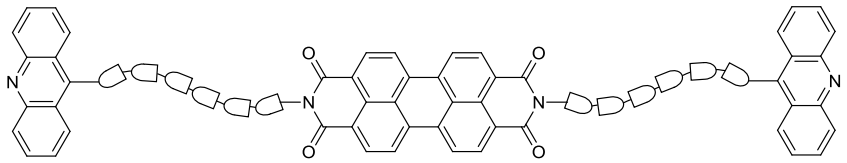

Figure 68. General structure of PBI with two acridine moieties, connected by flexible linkers.

Target molecule **6** with perylene and acridine linked by ethylene glycol linkers (Figure 69) was synthesized towards this goal. Spectroscopic measurements have been performed in order to get an insight into the aggregation behavior of pure PBI **6**. Investigation of the interaction of **6** with DNA or other nucleic acids was not possible in the context of this thesis.

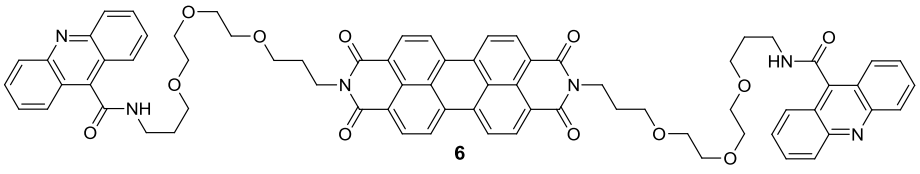

Figure 69. Acridine-perylene bisimide multichromophore **6**.

5.2 Results and Discussion

5.2.1 Synthesis

Target molecule **6** has been synthesized by an imidization reaction of perylene tetracarboxylic bisanhydride (**54**) with mono-boc-protected diamino-trioxatridecane **66** in DMF at 80 °C to give the boc-protected precursor **67** in 70 % yield.

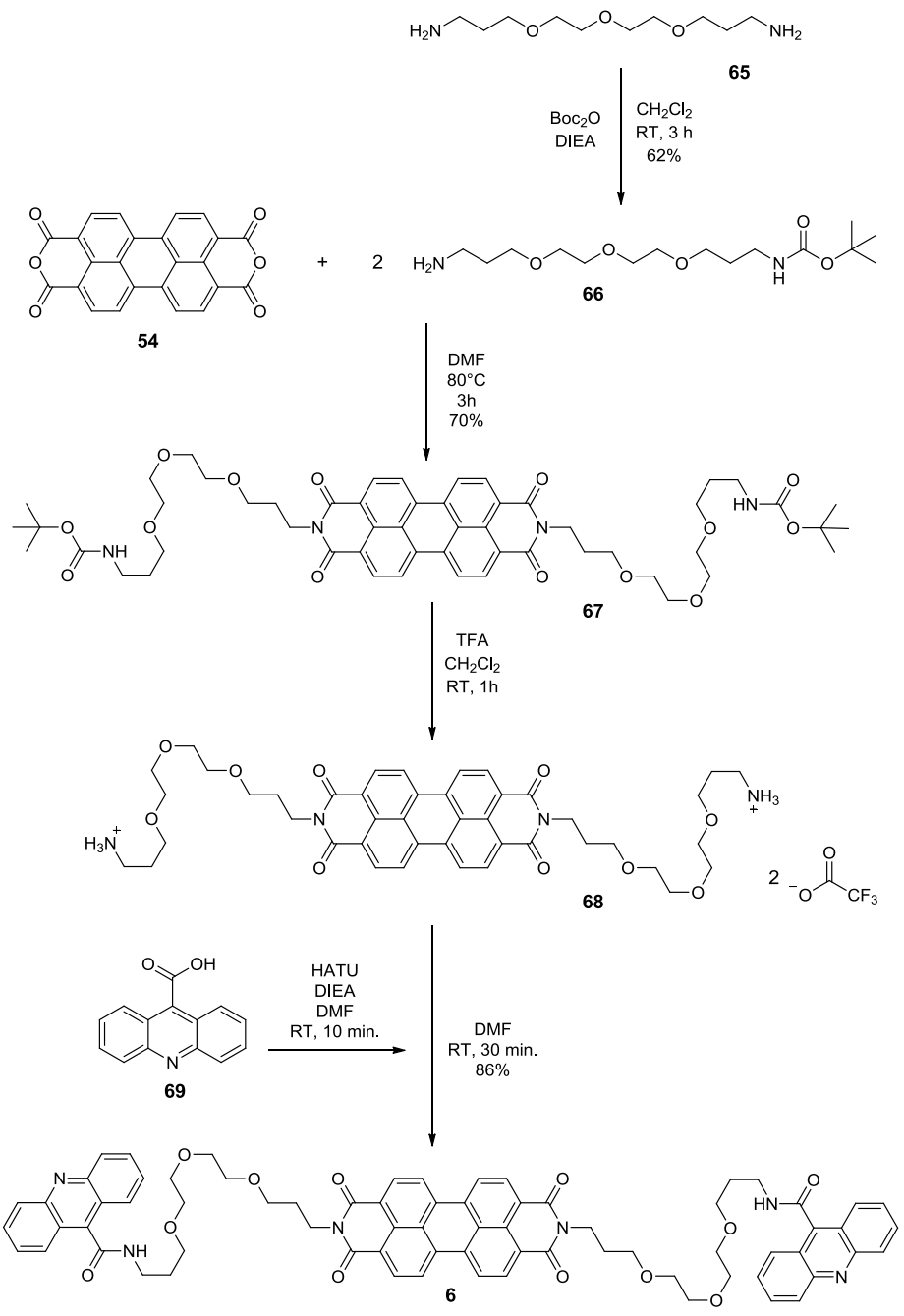

Figure 70. Synthesis of acridine-functionalized PBI **6**.

The protecting groups were removed by adding trifluoroacetic acid to a solution of **67** in dichloromethane. The trifluoroacetate salt **68** was obtained as a red solid after removal of the solvent and lyophylization from water. It was used without purification in a coupling reaction with activated acridine-9-carboxylic acid (**69**) to give target molecule **6** as a red solid in 86 % yield. PBI **6** was characterized by ^{1}H NMR, UV/Vis, fluorescence, mass spectroscopy, and elemental analysis.

5.2.2 Spectroscopic Studies

UV/Vis Spectroscopy

PBI **6** is not soluble in water which is attributed to the presence of three hydrophobic aromatic moieties and a relatively small polar ethylene glycol part. UV/Vis studies therefore have been performed in chloroform. Figure 71 shows the absorption spectra of **6** in the concentration range of 5×10^{-2} to 6×10^{-7} M. The spectra are displayed in the range between 250 and 600 nm where the perylene chromophore absorbs in the region between 400 and 600 nm and the acridine dye in the region 300 to 400 nm.

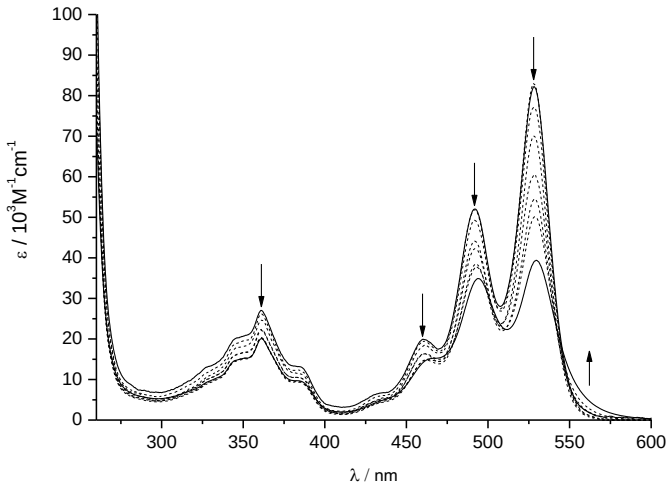

Figure 71. Absorption spectra of **6** in chloroform in the concentration range 10^{-2} to 10^{-7} M at 293 K. Arrows indicate increasing concentration.

At the lowest concentration, the spectrum shows a well resolved vibronic structure of the 400–600 nm region with the 0-0, 0-1, and 0-2 transitions of the perylene chromophore. The extinction coefficients of the two most intense bands at 528 nm and

492 nm have a ratio of 1.54 which suggests that monomeric PBIs prevail at low concentration. With increasing concentration of **6**, pronounced spectral changes could be observed particularly for the perylene absorption region. At the highest concentration all three bands exhibit a slight bathochromic shift of 2 nm. Here, the decrease of the extinction coefficient is largest for the band at 528 nm with $\Delta\varepsilon$ = 43650 $M^{-1}cm^{-1}$ followed by the second vibronic transition at 492 nm with $\Delta\varepsilon$ = 17127 $M^{-1}cm^{-1}$. The band at 462 nm decreases to a minor level with $\Delta\varepsilon$ = 5219 $M^{-1}cm^{-1}$. Now the extinction coefficients of the bands at 530 nm and 494 nm have a ratio of 1.12. This data and the small increase of the extinction coefficient between 545 nm and 600 nm point to a concentration-dependent self-assembly of the perylene chromophore into H-type aggregates.[32,170,171] In case of the acridine moiety the spectral changes are different and less pronounced. The absorption band between 300 nm and 400 nm decreases gradually with increasing concentration and the ratio of the extinction coefficients of the bands at 361 nm and 350 nm prevails at 1.3 over the complete concentration range.

Fluorescence Spectroscopy

The fluorescence emission of the acridine units has an overlap with the absorption of the perylene bisimide. In order to get more insight into the aggregation behavior of PBI **6** and a possible energy transfer between chromophores, absorption and fluorescence emission spectra have been recorded (Figure 72). First the emission spectrum was recorded using an excitation wavelength of λ_{ex} = 500 nm for the perylene (black broken line in Figure 72). As expected no emission for the acridine was observed, but, the appearance of the emission band is not typical for a bay-unsubstituted perylene bisimide. The first band at 536 nm corresponds to the emission from the vibronic ground state of the S_1 state of the perylene with a *Stokes* shift of 8 nm. The second much more intense band at 605 nm could not be assigned, but might be attributed to an acridine-PBI exciplex which has been formed by folding of the excited molecule. A second fluorescence emission spectrum was recorded after excitation of the acridine at λ_{ex} = 350 nm. Beside the emission bands at 536 nm and 605 nm a very weak band at 392 nm was observed as well, which might be assigned to the residual fluorescence emission of

the acridine. This is a first evidence for an efficient energy transfer from the acridine to the perylene chromophore. Interestingly, with an excitation at 350 nm the emission band at 605 nm is weaker. This might result from a less strong population of the proposed exciplex. The fluorescence quantum yield of **6** was determined against perylene standard and has a high value of 0.66 ± 0.15.

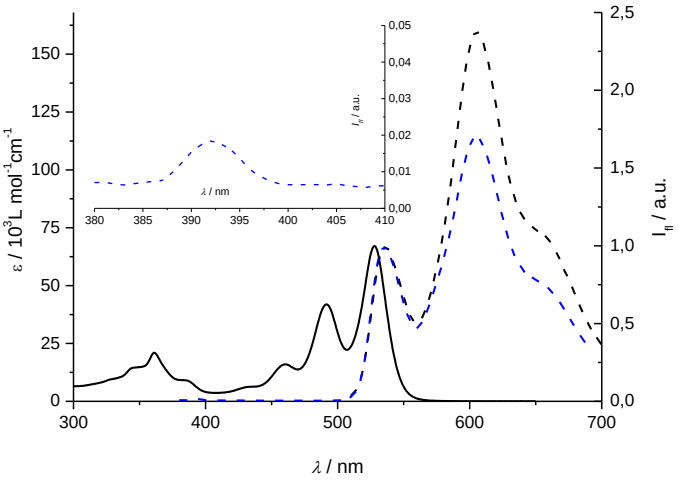

Figure 72. Absorption and fluorescence emission spectra (λ_{ex} = 350 nm, blue broken line; λ_{ex} = 500 nm black broken line) of PBI **6** in $CHCl_3$. Insert: Magnification of fluorescence emission (λ_{ex} = 350 nm) between 380 and 410 nm.

Fluorescence life times have been measured for λ_{ex} = 340 nm (Table 5) and λ_{ex} = 500 nm (Table 6) at different concentrations. In general the life times measured for the emission band at 536 nm is shorter than for the emission band at 605 nm. With increasing concentration nearly all life times get longer, except for the emission at 536 nm with λ_{ex} = 340 nm at concentrations of 1 x 10^{-5} M and 1 x 10^{-4} M. Here a slight decrease was observed.

Table 5. Fluorescence lifetimes τ of **6** at different concentrations in $CHCl_3$ in ns. Excitation wavelength 340 nm. [a] no signal.

c/M	λ_{em} = 392 nm	λ_{em} = 536 nm	λ_{em} = 605 nm
1 x 10^{-6}	[a]	[a]	[a]
1 x 10^{-5}	[a]	4.3	7.4
1 x 10^{-4}	[a]	4.1	8.6
2 x 10^{-3}	[a]	[a]	[a]

Table 6. Fluorescence lifetimes τ of **6** at different concentrations in $CHCl_3$ in ns. Excitation wavelength 500 nm. [a] no signal.

c/M	λ_{em} = 536 nm	λ_{em} = 605 nm
1×10^{-6}	4.4	5.3
1×10^{-5}	4.8	6.2
1×10^{-4}	7.6	8.8
2×10^{-3}	[a]	[a]

The emission at 392 nm does not show sufficient intensity to resolve its decay which might indicate an efficient energy transfer from the acridine to the perylene. In case of the highest concentration at 2×10^{-3} M all experiments at both excitation wavelengths failed, since fluorescence is most likely reabsorbed again by the dyes.

^{1}H-NMR Spectroscopy

The aggregation of **6** was further investigated by NMR spectroscopy. A dilution series was performed in $CDCl_3$ analyzing a concentration range from 1×10^{-4} M to 5×10^{-2} M. In Figure 73 the aromatic ^{1}H signals of both perylene bisimide (a,b) and acridine (c-f) as well as the amide proton (g) are shown in a concentration range from 9×10^{-4} M to 5×10^{-2} M. No spectral changes were observed below this range. At the lowest concentration all eight PBI protons show a singlet at δ = 8.44 ppm, which splits into two doublets upon increasing concentration (8.04 ppm and 7.90 ppm). At the highest concentration both doublets are distinctly broadened. In case of the doublet at 7.90 ppm a full overlap with the acridine proton signals c and d is observed as well. In the concentration range from 9×10^{-4} M und 2×10^{-2} M the chemical shift of all acridine proton signals change only a little to smaller delta values, whereas at the highest concentration the signals broaden as well. The signal for the amide proton g shows no changes from 9×10^{-4} M und 1×10^{-2} M, but undergoes a down-field shift from 7.35 ppm to 7.42 ppm upon increasing concentration to 5×10^{-2} M. These data point at a concentration-dependent intermolecular aggregation, whose driving force is based on π-π stacking interactions between perylene chromophores as the proton signals of these moieties change over the given concentration range.

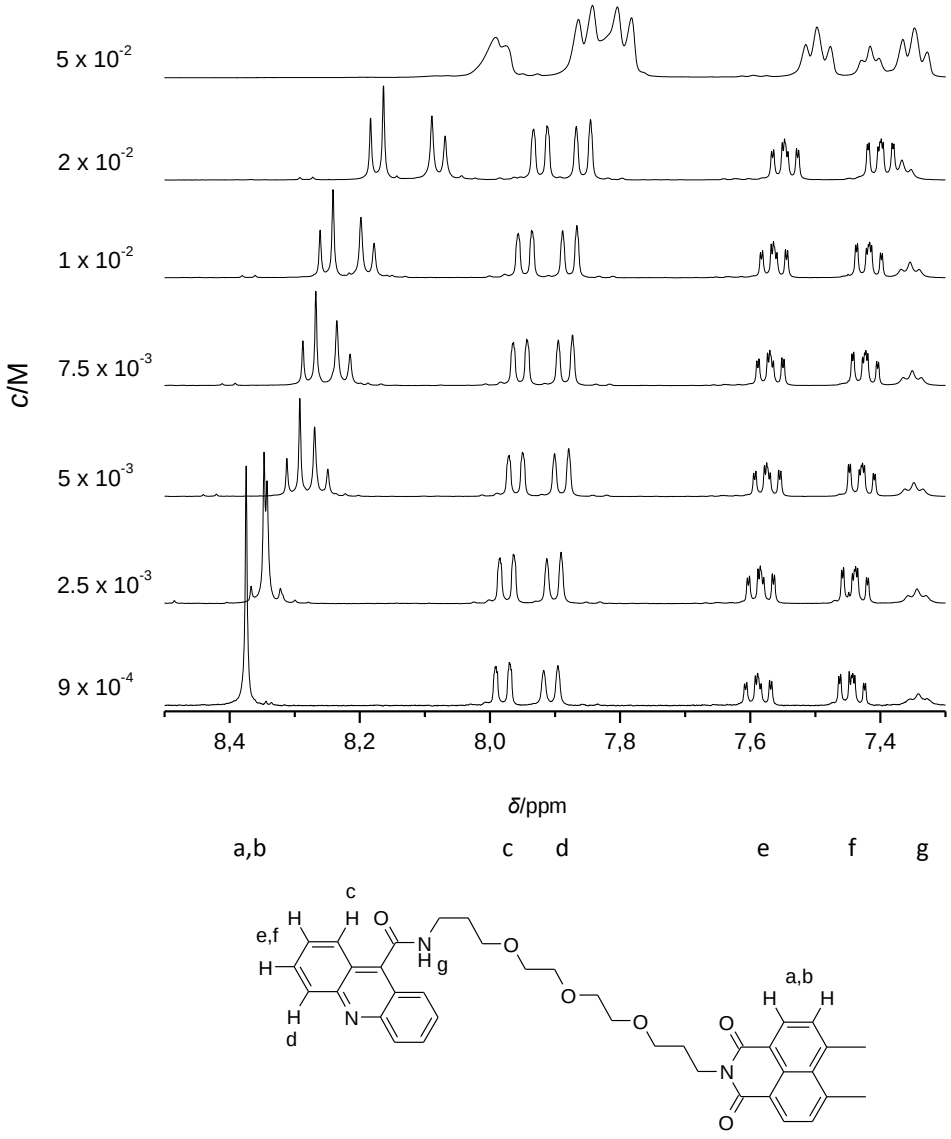

Figure 73. Changes of the chemical shift of PBI **6** in concentration dependent ^{1}H NMR spectra in $CDCl_3$.at 298 K.

At the highest measured concentration, most likely, further π-π stacking interactions also involve acridine units which interact with themselves or with the perylene bisimides. Beside these rather unspecific interactions, the down-field shift of the amide proton points at a certain degree of H-bonding between the amide groups of the acridines and most likely the oxygens of the bisimide units.

^{1}H-DOSY-NMR Spectroscopy

For further determination of the aggregate architecture diffusion ordered ^{1}H spectroscopy has been performed with **6** at three different concentrations (Table 7).

With increasing concentrations the diffusion coefficients decrease, which is indicative for an increase in size of the particle. By using the *Stokes-Einstein* equation (Eq. 1) one can calculate the hydrodynamic radius *r* of the aggregates:

$$D = \frac{k_B \cdot T}{6\pi\eta \cdot r} \qquad (1)$$

with k_B = 1.38066·10^{-23} JK^{-1} (*Boltzmann* constant), T = 298.2 K, and $\eta_{solvent}$ = 0.542 mPa·s. For Equation 1 it is assumed that the observed particles have a spherical architecture. As this is obviously not the case for PBI **6**, the values of the hydrodynamic radii are just mean values for most likely ellipsoidal structures of monomeric **6** and its higher aggregates.

Table 7. Diffusion coefficients and hydrodynamic radii for **6** at different concentrations in $CDCl_3$ at T = 298 K.

c/M	Diffusion coefficient *D*/m^{2}s^{-1}	Hydrodynamic radius *r*/10^{-9} m
1 x 10^{-3}	4.06 x 10^{-10}	0.99
1 x 10^{-2}	3.49 x 10^{-10}	1.16
5 x 10^{-2}	2.46 x 10^{-10}	1.64

5.2.3 Molecular modeling

At first, the possible structures of PBI **6** monomer have been investigated. These monomers can be differentiated by the arrangement of the acridine units, either both units are co-planar to one side of the PBI surface (M1 in Figure 74) or the acridine units cover both surfaces of the perylene chromophore (M2). In the course of the force field calculation, M1 converts into M2 showing that shielding both π-surfaces of the large chromophore is energetically more favored (relative energy -246 kJ·mol^{-1}). This process could be confirmed by energy calculations for a stretched monomer with both acridine units far away from the perylene core. In the next step two different dimers were calculated. The first dimer, D1, is based on two monomers M1 which are preorganized by co-planar arrangement of the free PBI surface. The other dimer, D2, is based on two

monomers M2, which were stacked upon each other with an offset of the interior acridines allowing a sandwich-like structure with two acridine units between the perylene chromophores.

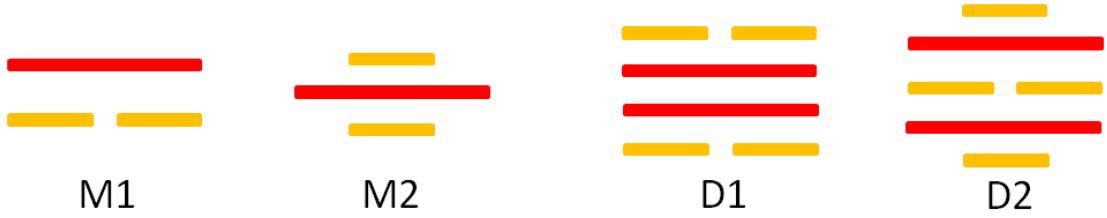

Figure 74. Monomer and dimer arrangements used for Amber* force field calculations (red: perylene chromophore; orange: acridine).

The calculations show that dimer D1 is energetically more favored exhibiting a direct interaction of the perylene chromophores (relative energy -580 kJ·mol^{-1}). Sandwich-like D2 gives a relative energy of only -562 kJ·mol^{-1}. With these data it can be assumed that the acridine units rearrange during the transition from monomeric PBI **6** into its dimeric form (Figure 75) as such a process is necessary for getting one free side of the perylene chromophore. In addition to the π-π-stacking interaction between the perylene chromophores in D1, four hydrogen bonding events occur between the acridine amide NHs and the bisimide oxygen atoms. This interaction is not possible in M2 and only to a lower degree in D2 (two hydrogen bonds). In D1 the acridine units exhibit an arrangement, which resembles the interaction of nucleobases. Although the distance is slightly too far, the central acridine nitrogen atoms seem to interact with the carbon-bound hydrogen atoms of the opposing acridine unit next to the nitrogen.

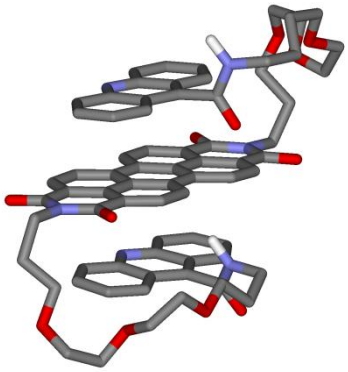

M2 (-246 kJ·mol^{-1})

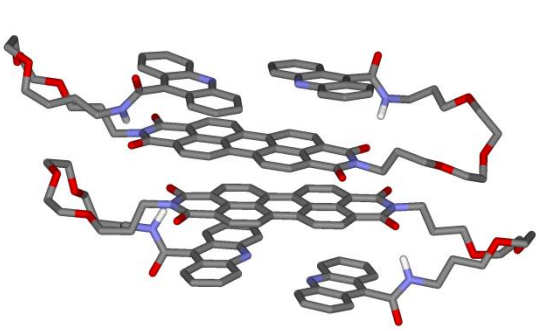

D1 (-580 kJ·mol^{-1})

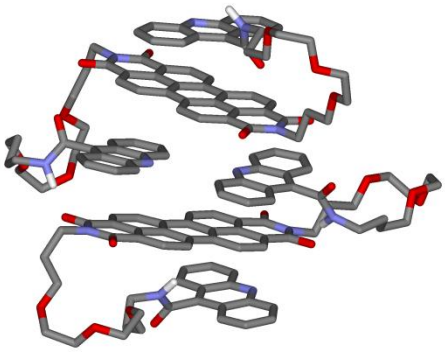

D2 (-562 kJ·mol^{-1})

Figure 75. Monomer and dimer arrangements of **6** as obtained by Amber* force field calculations (non-polar hydrogens omitted for clarity).

5.3 Conclusion

A symmetric acridine – perylene bisimide – acridine chromophore system (**6**) was successfully synthesized and subjected to several spectroscopic analytical methods for elucidating the aggregation behavior of this polyaromatic molecule. Both UV/Vis and ^{1}H NMR experiments suggest a concentration-dependent aggregation process starting with a monomer at lowest concentration. UV/Vis studies indicate H-type aggregation via strong π-π-stacking interactions between perylene bisimide units. NMR studies support the assumed interactions between the perylene chromophores and also show a pronounced interaction of the acridine units by π-π-stacking and, more important, by hydrogen bonding at highest concentration. These modes of interaction are also supported by molecular modeling studies which suggest π-stacking interactions between the acridine units with both surfaces of the perylene chromophore. With increasing

concentration, these monomers interact with each other resulting in a dimer having intense π-π-stacking of two perylene chromophores and four hydrogen bonds between the acridine units and the bisimide oxygens. Dimerization is also supposed by DOSY-NMR which reveals a modest decrease of the diffusion coefficient upon increasing concentration. Evidence for such nucleobase-like arrangement of the acridines in the dimers is provided by the hypochromic shift of the acridine absorption band between 300 and 400 nm with increasing concentration. This behavior is known from the UV/Vis absorption of nucleobases in single stranded DNA during annealing with complementary single strand to form a DNA double strand by hydrogen bonding and π-π-stacking.[210,211]

In summary, these data suggest a monomer-dimer equilibrium that involves multiple supramolecular forces. The energy transfer and proposed exciplex formation remain interesting topics for time-resolved spectroscopy investigations.

Chapter 6

Summary

The results discussed in the foregoing chapters of this thesis are a contribution to the chemistry of water-soluble perylene bisimide dyes. The idea for this work originates from the biological concept of bola-amphiphilic building blocks. The combination of a hydrophobic core element surrounded by hydrophilic residues offers the possibility to build defined architectures in polar solutions like water as the most biocompatible solvent. A multichromophore consisting of perylene bisimide and acridine moieties with an interesting aggregation behavior in chloroform was introduced, additionally.

The main objective of this thesis was the design and synthesis of perylene bisimide dyes with sufficient water-solubility for the construction of self-assembled architectures in aqueous solutions. Beside these tasks another goal of this project was the control over the self-assembly process in terms of aggregate size and helicity, respectively. Within this thesis an appropriate synthesis for the desired molecules was developed and conducted successfully. The characterization of these building blocks and their course of self-assembly were investigated by NMR, UV/Vis and fluorescence spectroscopy as well as by atomic force and transmission electron microscopy. For the better understanding of the experimental results theoretical calculations were performed.

The introductory **Chapter 2** gives a general survey on perylene bisimides with amine containing side chains in the imide positions. Those PBIs show a pronounced aggregation behavior in water and, but less pronounced, in many organic solvents. Under neutral to

basic conditions the amino groups of a large number of the described PBIs disposes free electron pairs. These may act as electron donors in photoinduced electron transfer reactions that constitute an efficient and rapid fluorescence quenching pathway. This process is particularly favored as perylene bisimides are electron deficient and hence good electron acceptors. Fluorescence quantum yield is significantly influenced by the two effects, aggregation and photoinduced electron transfer. PBIs with amino side chains can act as pH probes or probes for metal ions. The overall positive charge in neutral to acidic environment enables the interaction with negatively charged (macro)molecules leading to liquid crystalline systems or supramolecular complexes with exciting characteristics. Parameters like concentration, solvent, pH, temperature, and counterions play an essential role for the formation of those supramolecular systems. PBIs with amine containing side chains can also interact with different secondary structures of nucleic acids due to electrostatic and π-π-interactions and are therefore strong candidates for anti-cancer agents and for sensing DNA and RNA for example.

In **Chapter 3** the synthesis of a series of water-soluble perylene bisimide dyes is presented. For enhanced water solubility the biologically relevant oligoamine spermine was attached to the chromophore at the imide position. This functional residue was incorporated either directly as part of the imide function or via alkyl carbonyl spacers of different lengths. Upon acidification all free amino groups become protonated. In sum each molecule carries six positive charges which results in strong enhanced water solubility and an overall bola-amphiphilic character of the building blocks (Figure 76).

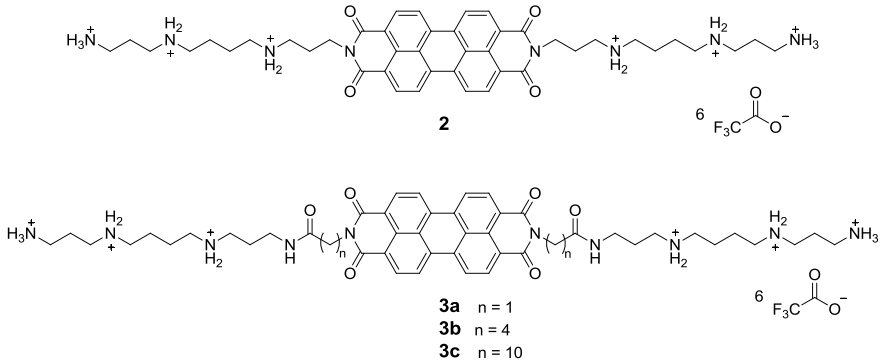

Figure 76. Structures of PBI **2** with directly attached spermine and PBIs **3a–c** with alkyl carbonyl spacer between the chromophore and the spermine residues.

The aggregation process of the PBIs was monitored with UV/Vis spectroscopy during dilution experiments in pure water. At lowest concentrations (10^{-7} M) the well-resolved vibronic structure of the S_0-S_1 electronic transition can be observed for PBIs **2**, **3a** and **3b** with the two most intense bands at 533 nm and 497 nm. With increasing concentrations pronounced spectral changes could be observed whereby the color of the solution changed from bright orange to deep red. The absorption maxima shifted hypsochromically to *ca.* 502 nm and decreased in extinction, whereas a weak absorption increase could be observed in a spectral range between 550 and 600 nm. Both phenomena indicate aggregation of the PBI dyes in a H-type manner with rotational displacement of the chromophore core. In the lower concentration range up to 10^{-4} M isosbestic points could be observed for PBIs **2**, **3a** and **3b** indicating the existence of two species in equilibrium, most likely a monomer-dimer transition. At even higher concentrations the spectral data do not fit anymore to the isosbestic points indicating the formation of higher oligomers. In contrast to the first three bola-amphiphiles, PBI **3c** already exists in an aggregated state at lowest concentration as indicated by the significant spectral data comparable with those of PBIs **2**, **3a** and **3b** at high concentrations. The stronger tendency of PBI **3c** to aggregate is based on the additional strong hydrophobic interactions between the long C10-spacers, most likely. Fluorescence spectroscopy and quantum yield measurements are in full agreement with the pronounced differences in aggregation depending on the spacer length. PBI **2** has a quantum yield of 0.90 which decreases to 0.39 for PBI **3c** upon stronger aggregation at the same concentration. The latter aspect leads to a lower number of free monomeric **3c**, which is the only species whose fluorescence is not quenched by H-type stacking interactions. The strong influence of the spacer length was also visualized by AFM experiments. PBI **2** just gives small globular particles on the surface, whereas the other PBIs give worm-like structures with a length up to 200 nm for PBI **3c**. Additional TEM experiments for this bola-amphiphile prove the time-dependent growth of such worm-like structures as well. Figure 77 shows concentration dependent UV/Vis and AFM results for PBI **2** without linker and PBI **3c** with the longest linker.

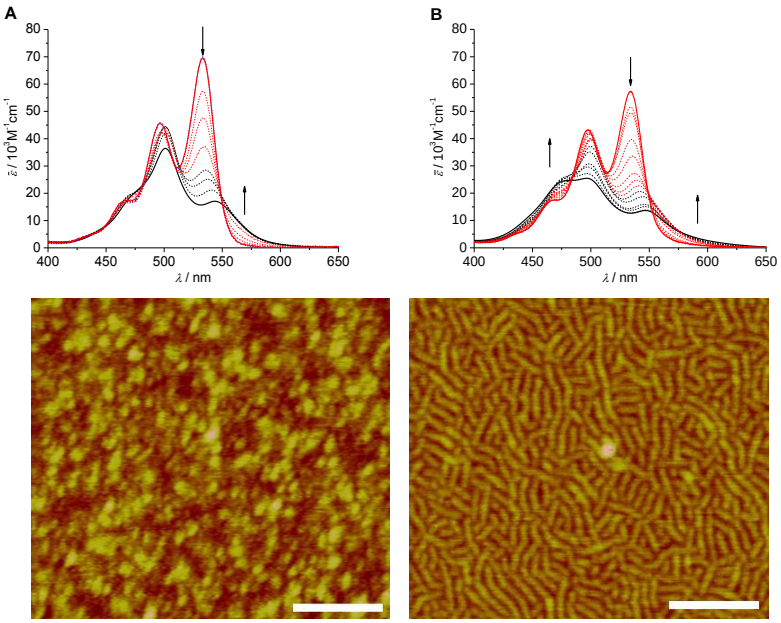

Figure 77. Comparing the absence of a spacer (PBI **2**, left) with the influence of the longest spacer between the chromophore and the spermine residue (PBI **3c**, right) on the aggregation of the bola-amphiphiles by UV/Vis spectroscopy and AFM.

Beside the control of the aggregates' size, the introduction of pronounced helicity within the PBI stack was a second goal of this thesis. In **Chapter 4** the synthesis of chiral PBI building blocks **4a–c** (Figure 78 top) is reported as well as the analysis of the resulting aggregates, especially with CD spectroscopy. In order to have a maximum impact on the PBI aggregate regarding chirality induction and helicity control, the chiral centers were attached as close as possible to the planar chromophore. To accomplish this task, *α*-amino acids, namely both enantiomers of alanine and phenylalanine, were used as spacers between the dye and the charged oligoamine. These amino acids were chosen due to their different steric hindrance (methyl *versus* benzyl). For parallel investigations in organic solvents like chloroform, neutral analogues with dodecyl alkyl chains instead of spermine were synthesized as well (Figure 78 bottom).

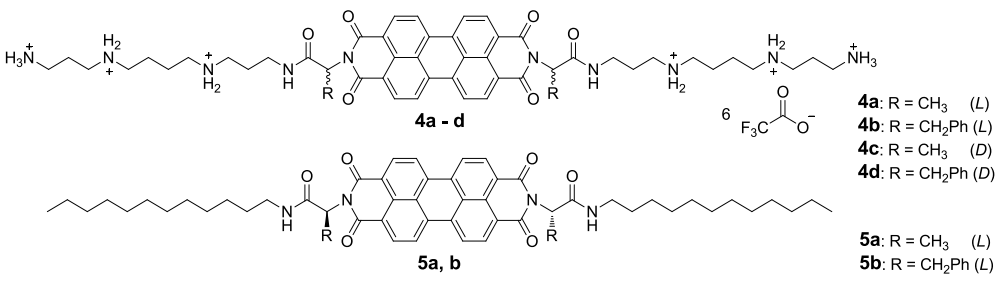

Figure 78. Chiral perylene bisimide dyes **4a–d** for studies in water and **5a**,**b** for studies in chloroform.

The aggregation process of the charged species was investigated first by UV/Vis spectroscopy during dilution experiments in pure water. A quite similar behavior was observed for **4a–d** compared to achiral PBIs **2**, **3a** and **3b**. At highest dilution (5×10^{-6} M) the vibronic fine structure of the S_0-S_1 electronic transition can be observed with the two most intense bands at 534 nm and 497 nm. With increasing concentration the spectrum gets broadened and the maximum is shifted hypsochromically to 492 nm. Again an increased extinction in the absorption range between 550 nm and 600 nm occurs and points to H-type stacking with rotational displacement in analogy to the achiral PBIs. Isosbestic points at 548 nm and 515 nm suggest a monomer – dimer equilibrium in the concentration range up to 5×10^{-4} M. Most likely, higher oligomers appear above this concentration since the absorption spectrum at a concentration 5×10^{-3} M does not cross the isosbestic points (Figure 61A and B). Comparing the UV/Vis spectra of **4a** and **4b** with the achiral glycine-based system **3a** at the same concentration shows that the degree of aggregation depends directly on the size of the α-amino acid side chain: the larger the substituent the lower the degree of aggregation (Figure 62A). The results of fluorescence spectroscopy experiments are in agreement with this trend. Compared to PBI **4a** with a fluorescence quantum yield of 0.72, PBI **4b** has a quantum yield of 0.79 pointing to higher amount of monomeric species due to less favored aggregation (Figure 62B). Subsequently the PBI aggregates obtained in pure water were investigated by CD spectroscopy. Temperature-dependent measurements of **4a** reveal a bisignate signal with first a negative Cotton effect including two maxima at 552 nm and 522 nm, and second a positive Cotton effect with a maximum at 494 nm (Figure 63A). The signal is caused by excitonic coupling of rotational distorted perylene bisimide transition dipole moments arranged in a helical aggregate with a preferential direction (*M*-configuration). In contrast to this result the temperature dependent CD spectra for **4b** differ in sequence signature and shape (Figure 63B). The peak maximum of the first Cotton effect (positive signature) is found at 574 nm, the second one (negative signature) at 506 nm. The reversal of the signature sequence hints to a contrary helicity in the aggregate of **4b** (*P*-configuration) compared to those of **4a**. CD experiments on **5a** and **5b** in chloroform show for both *L*-alanine and *L*-phenylalanine derivatives the same Cotton signal sequence at 551 nm (negative signature) and 493 nm (positive signature) pointing to a

M-configured helicity as seen for **4a** in water (Figure 63C and D). This is in clear contrast to the water-soluble bola-amphiphiles. For the direct visualization of the helical aggregates AFM and TEM images were taken from the chiral PBIs (Figure 64, left, and Figure 65). In obvious contrast to the aggregation behavior of the achiral PBIs **2** and **3a–c** the chiral bola-amphiphiles do not build worm-like structures, but small and flat globular particles. Thus, a strong influence of the amino acid side chains on the aggregation behavior of the PBIs is observed.

Multichromophore **6** (Figure 79) presented in **Chapter 5** contains a planar perylene bisimide and two acridine moieties, connected by flexible ethylene glycol linkers. The spectral changes recorded at UV/Vis measurements with increasing concentration from 10^{-7} to 10^{-2} M in chloroform point to self-assembly of the perylene chromophore into H-type aggregates. During fluorescence measurements two emission bands at 536 and 605 nm could be detected both for excitation of the acridine chromophores (excitation wavelength 340 nm) as well as for excitation of the perylene chromophore (excitation wavelength 500 nm). While the band at 536 nm is caused by the emission from the vibronic ground state of the S_1 state of the perylene, the more intense band at 605 nm might be caused by the emission of an acridine – perylene exciplex which has been formed by folding of the excited molecule. The acridine emission at 392 nm, in contrast, is only very weak after excitation of **6** in the acridine absorption region at 340 nm. These results indicate an efficient energy transfer from the acridine to the perylene chromophore.

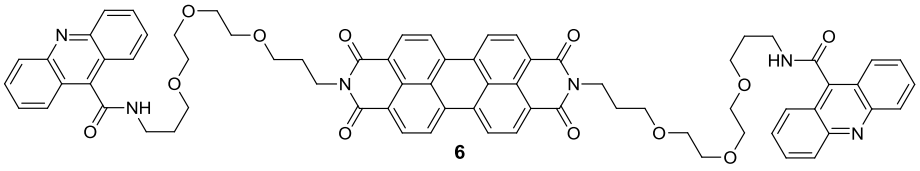

6

Figure 79. PBI **6** containing three chromophores.

NMR dilution experiments point at intermolecular π-π stacking between perylene chromophores as the signals of the perylene protons show major changes over the measured concentration range. The protons attributed to the acridine moieties are significantly affected only at the highest concentration which suggests a participation of

the acridine chromophores both in π-π stacking interactions and in H-bond interactions. Calculations of monomers and dimers of **6** are in accordance with the spectroscopic studies and suggest a transition from M2 to D1 arrangement, where two perylene moieties directly interact with each other and the acridine units show a nucleobase-like arrangement (Figure 80).

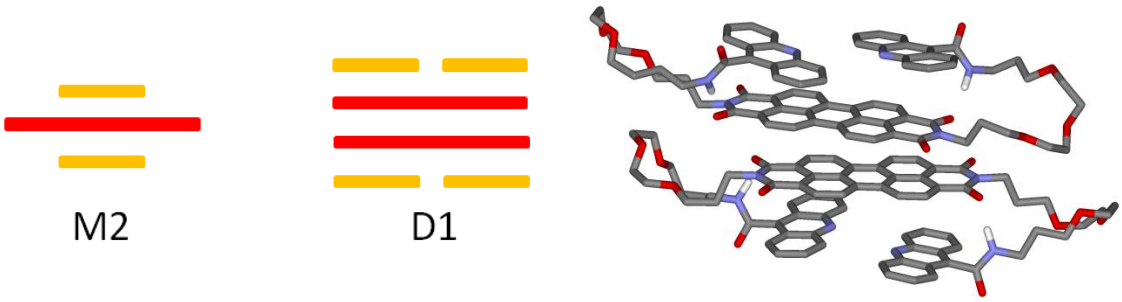

Figure 80. Schematic presentation of the favored monomer (M2) and dimer (D1) arrangements (left) and calculated dimer arrangement D1 of multichromophore **6** (right).

In conclusion, this thesis described an approach to solubilize highly hydrophobic perylene bisimide chromophores for self-assembly processes in aqueous solutions. The concept of bola-amphiphilic architecture was used to construct π-stacked PBI aggregates with a hydrophobic core and a positively charged shell for solubilization in pure water. It was possible to control the aggregate size and quality by the kind of the spacers between the chromophore and the charged spermine residues. Studies on a multichromophore with perylene bisimide and acridine moieties, which is less hydrophilic by comparison, gave first insights into its very interesting aggregation behavior in organic solvent.

Chapter 7

Zusammenfassung

Die Ergebnisse dieser Dissertation, die in den vorherigen Kapiteln diskutiert wurden, sind ein Beitrag zu der Chemie der wasserlöslichen Perylenbisimide (PBI). Die Idee für diese Arbeit ist an das biologisch-inspirierte Konzept der Bola-Amphiphile angelehnt. Die Kombination eines hydrophoben Kernbausteins mit ihn umgebenden hydrophilen Resten ermöglicht den Aufbau von definierten Strukturen in polaren Lösungen, z. B. in Wasser als dem kompatibelsten Lösungsmittel für biologische Systeme.

Das Ziel dieser Dissertation war das Design und die Synthese von Perylenbisimiden mit hinreichender Wasserlöslichkeit, die für den Aufbau von selbständig assemblierten Strukturen in wässrigen Lösungen verwendet werden sollen. Ein weiteres Ziel dieses Projektes war die Kontrolle über den Prozess der Selbstanordnung hinsichtlich der Aggregatsgröße beziehungsweise deren Helizität. Im Rahmen dieser Doktorarbeit wurde eine entsprechende Synthese für die gewünschten Moleküle entworfen und erfolgreich durchgeführt. Die Charakterisierung dieser Bausteine und der Prozess deren Selbstanordnung wurde einerseits mit Hilfe von NMR-, UV/Vis- und Fluoreszenz-Spektroskopie aber auch mit Rasterkraft- und Elektronentransmissionsmikroskopie durchgeführt. Für das bessere Verständnis der experimentellen Ergebnisse wurden theoretische Berechnungen durchgeführt.

Das einleitende **Kapitel 2** liefert einen allgemeinen Abriss über Perylenbisimide mit Amino-Funktionen in den Seitenketten der Imid-Positionen. Solche PBIs zeigen eine sehr

ausgeprägte Aggregationsneigung in Wasser und, wenngleich weniger stark, in vielen organischen Lösungsmitteln. In neutraler bis basischer Umgebung steht den Amino-Gruppen der meisten vorgestellten PBIs das freie Elektronenpaar zur Verfügung. Dieses kann als Elektronen-Donor bei photoinduzierten Elektronentransferprozessen fungieren, welche einen effizienten und schnellen Weg der Fluoreszenzlöschung darstellen. Dieser Prozess wird noch verstärkt durch die Elektronenarmut des Perylenebisimids. Die Fluoreszenzquantenausbeute wird maßgeblich von zwei Effekten beeinflusst, dem Aggregationsgrad und der Möglichkeit eines photoinduzierten Elektronentransfers. PBIs mit Alkyl-Amino-Seitenketten können als pH-Sensoren oder Sensoren für Metallionen eingesetzt werden. In neutraler bis saurer Umgebung ermöglichen die dann vorhandenen positiven Ladungen die Wechselwirkung mit negativ geladenen (Makro)Molekülen, was zum Beispiel zur Bildung von flüssigkristallinen Systemen oder supramolekularen Komplexen mit spannenden Eigenschaften führt. Parameter wie die Konzentration, die Lösungsmitteleigenschaften, der pH-Wert, die Temperatur und die Gegenionen spielen eine entscheidende Rolle bei der Entstehung solcher supramolekularen Systeme. PBIs mit Amino-Funktionen in den Seitenketten können auch über elektrostatische und π-π-Wechselwirkungen mit verschiedenen Sekundärstrukturen von Nukleinsäuren in Interaktion treten, was diese PBIs zum Beispiel zu potentiellen Kandidaten für Anti-Krebs-Mittel und DNA/RNA-Detektoren macht.

In **Kapitel 3** dieser Dissertation wird die Synthese einer Reihe von wasserlöslichen Perylenbisimiden präsentiert, die das biologisch relevante Oligoamin Spermin an der Imidposition des Chromophores tragen, um eine ausreichende Wasserlöslichkeit zu erlangen. Diese funktionale Gruppe ist entweder ein direkter Teil der Imideinheit oder wurde über einen Alkylcarbonyl-Linker mit dem Chromophor verbunden. In deutlich saurem Milieu werden die Aminogruppen protoniert. Auf diese trägt jedes dieser Moleküle nun insgesamt sechs positive Ladungen, die zu einer deutlichen Verbesserung der Wasserlöslichkeit führen und dem Baustein einen bola-amphiphilen Charakter verleihen (Abbildung 1).

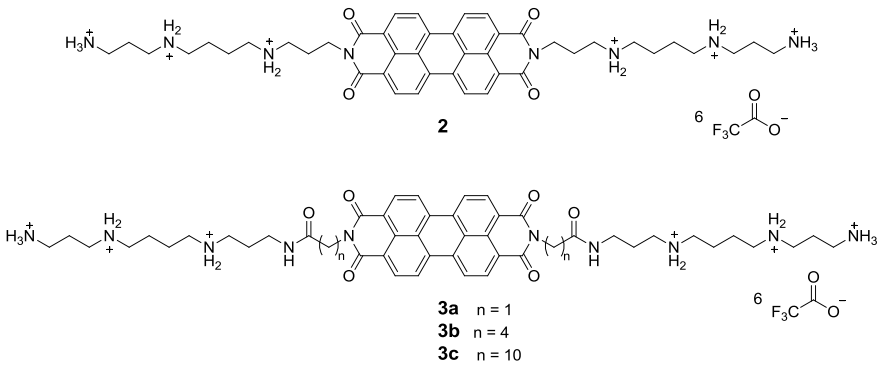

Abbildung 1. Die Struktur von PBI **2** ohne Linker zwischen Spermin und Chromophor und die PBIs **3a–c** mit unterschiedlich langen Alkycarbonyl-Linkern zwischen dem Chromophor und den Spermin-Einheiten.

Der Aggregationsprozess der Perylenbisimide wurde im Zuge von Verdünnungsreihen in reinem Wasser mit UV/Vis-Spektroskopie verfolgt. Im Falle von **2** und **3a–c** konnte bei niedrigster Konzentration (10^{-7} M) der elektronische S_0-S_1 Übergang mit einer sehr gut aufgelösten vibronischen Feinstruktur detektiert werden, wobei die intensivsten Absorptionsbanden bei 533 nm und 497 nm lagen. Mit zunehmender Konzentration veränderte sich das Absorptionsspektrum sehr stark. Die Farbe der Probelösungen wies zu Beginn eine orange Farbe auf, die sich nun in ein tiefes Rot wandelte. Das Absorptionsmaximum verschob sich hypsochrom auf 502 nm und verlor zudem an Extinktion, wobei eine weitere schwache Absorption zwischen 550 nm und 600 nm auftrat (Abbildung 2 oben). Beide Phänomene deuten auf eine Aggregation der Perylenbisimide hin, die einem *H*-Aggregat mit einem rotatorischen Versatz der Chromophore entspricht. In dem Konzentrationsbereich kleiner gleich 10^{-4} M konnten für **2** und **3a**,**b** isosbestische Punkte in der Verdünnungsreihe nachgewiesen werden, die auf ein Gleichgewicht zwischen zwei Spezies in Lösung hinweisen. Aller Wahrscheinlichkeit handelt es sich dabei um den Übergang von einem Monomer zu einem Dimer. Mit zunehmender Konzentration schneiden die Absorptionsspektren nicht mehr diese Punkte, was auf die Bildung höherer Oligomere schließen lässt. Im Gegensatz zu den ersten drei bola-amphiphilen Perylenbisimiden liegt das PBI **3c** bereits bei der niedrigsten Konzentration im aggregierten Zustand vor, da die Absorptionsspektren dieser Lösungen sehr stark den Spektren von **2** und **3a–c** bei hoher Konzentration ähneln. Die Tendenz von **3c** zu einer stärkeren Aggregation basiert aller Wahrscheinlichkeit nach auf zusätzlichen hydrophoben Wechselwirkungen zwischen den langen C10-Linkern. Fluoreszenz-Spektroskopie und Messungen der Quantenausbeute

stimmen mit den ausgeprägten Unterschieden in der Aggregation in Abhängigkeit von der Linker-Länge überein. PBI **2** hat eine Fluoreszenzquantenausbeute von 0.90, die bei gleicher Konzentration durch stärkere Aggregation auf einen Wert von 0.39 für PBI **3c** sinkt. Die zunehmende Aggregation führt zu einer geringeren Anzahl freier Monomere von **3c**, deren Fluoreszenz nicht durch Aggregation gelöscht wird. Der starke Einfluss der Linker-Länge auf die Aggregation konnte auch durch AFM-Experimente nachgewiesen werden. PBI **2** bildet dabei auf der mica-Oberfläche kleine kugelförmige Partikel, wohingegen die anderen drei Perylenbisimide relativ lange wurmartige Strukturen mit einer Länge von bis zu 200 nm (PBI **3c**) ausbilden (Abbildung 2 unten). TEM-Aufnahmen zeigten zudem, dass im Falle des stärksten Bola-Amphiphils **3c** ein zeitabhängiges Wachstum der Wurmstrukturen vorlag.

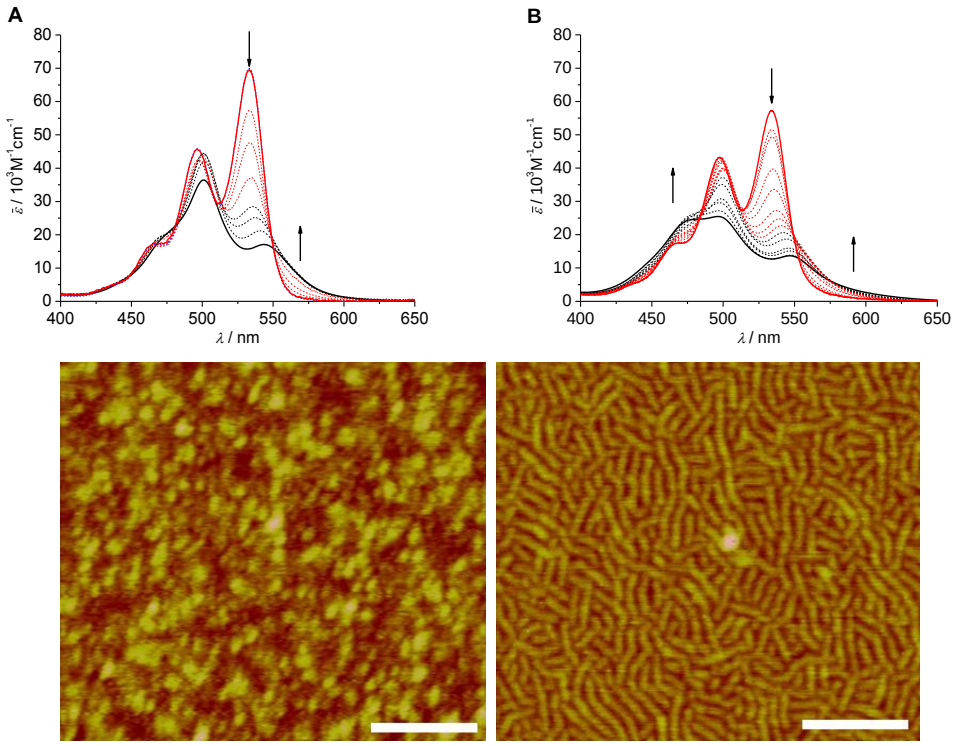

Abbildung 2. Einfluss der Linker-Länge zwischen dem Chromophor und dem Oligoamin Spermin auf die Aggregation dargestellt an Hand der UV/Vis-Spektren und AFM-Aufnahmen von PBI **2** (links, ohne Linker) und PBI **3c** (rechts, mit langem Linker).

Neben der Kontrolle über die Aggregatsgröße war ein zweites Ziel dieser Dissertation die Einführung einer nachweisbaren Drehrichtung (Helizität) in den Perylenbisimid-Aggregaten. Im **Kapitel 4** wurde die Synthese chiraler PBI-Bausteine präsentiert und die Analyse, vor allem mit CD-Spektroskopie, diskutiert. Um einen

maximalen Einfluss auf die Drehrichtung der PBI-Aggregate und deren Kontrolle zu erhalten, sollten sich die stereogenen Zentren möglichst nahe am planaren Chromophor befinden. Um diese Voraussetzung zu erreichen, wurden *α*-Aminosäuren, in diesem Fall beide Enantiomere von Alanin und Phenylalanin, als Linker zwischen dem Farbstoff und dem geladenen Oligoamin eingesetzt. Diese Aminosäuren wurden auf Grund ihres unterschiedlichen sterischen Anspruchs ausgewählt (Methyl *vs.* Benzyl). Für Untersuchungen in rein organischen Lösungsmitteln wurden ungeladene (neutrale) Analoga mit Dodecyl-Alkylketten synthetisiert (Abbildung 3).

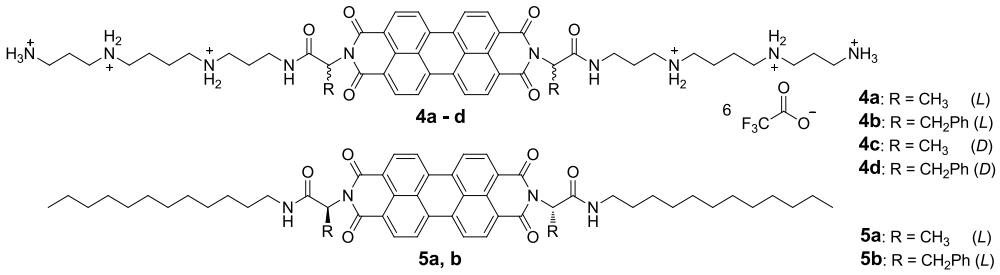

Abbildung 3. Chirale Perylenbisimid-Farbstoffe **4a–d** für Untersuchungen in Wasser und **5a,b** für Studien in Chloroform.

Der Aggregationsprozess der positiv geladenen Bola-Amphiphile wurde im Rahmen einer Verdünnungsreihe per UV/Vis-Spektroskopie untersucht. Dabei konnte für **4a–d** ein relativ ähnliches Aggregationsverhalten wie bei den achiralen Perylenbisimiden **2** und **3a–c** beobachtet werden. In der niedrigsten Konzentration lag ein vibronisch sehr gut aufgelöster, elektronischer S_0-S_1 Übergang vor. Die Absorptionsmaxima lagen hier bei 534 nm und 497 nm. Mit zunehmender Konzentration verbreiterte sich das Absorptionsspektrum mit einem hypsochrom verschobenen Maximum bei 492 nm. Auch hier trat wieder eine weitere Absorptionsbande zwischen 550 nm und 600 nm auf, die ebenfalls auf eine *H*-Aggregation mit rotatorischem Versatz der Chromophore schließen lässt. Analog zu den achiralen Perylenbisimiden traten isosbestische Punkte bei 548 nm und 515 nm auf, die auf ein Monomer-Dimer-Gleichgewicht im niedrigen Konzentrationsbereich bis zu 5×10^{-4} M schließen lassen. Bei entsprechend höherer Konzentration kreuzen die Spektren diese Punkte nicht mehr, was auf die Bildung höherer Oligomere hindeutet (Figure 61A und B). Vergleicht man dabei die UV/Vis-Spektren von **4a** und **4b** mit dem achiralen Glycin-basierten System **3a** bei der gleichen

Konzentration, kann man den direkten Einfluss der Aminosäureseitenkette auf die Aggregation erkennen: je größer der sterische Anspruch dieser Raumgruppe ist, umso geringer ist der Grad der Aggregation (Figure 62A). Die Ergebnisse der Fluoreszenz-Spektroskopie untermauern diese Annahme. PBI **4a** weist eine Fluoreszenzquantenausbeute von 0.72 auf, wohingegen PBI **4b** einen Wert von 0.79 besitzt. Letzteres basiert auf der größeren Anzahl von freien Monomeren, deren Fluoreszenz im Vergleich zum Aggregat nicht gelöscht wurde (Figure 62B). Im Anschluss daran wurde das Aggregationsverhalten der chiralen Bola-Amphiphile in reinem Wasser mit CD-Spektroskopie untersucht. Temperaturabhängige Messungen von PBI **4a** zeigen, kommend von der höheren Wellenlänge, ein bisignantes Signal mit einem zuerst negativen Cotton-Effekt und zwei Maxima bei 552 nm und 522 nm auf. Der sich daran anschließende, positive Cotton-Effekt hat ein Maximum bei 494 nm (Figure 63A). Das hier beobachtete Signal resultiert aus der exzitonischen Kopplung der rotatorisch versetzten Übergangsdipolmomente der Perylenbisimid-Chromophore, die in einem Aggregat mit bevorzugter Helizität angeordnet sind (*M*-Konfiguration). Im Gegensatz zu den CD-Spektren von **4a** zeigt PBI **4b** eine verschiedene Signatur und Form des Cotton-Effekts (Figure 63B). Das Maximum des Signals für den ersten Cotton-Effekt ist positiv und liegt bei 574 nm, wobei der zweite, negative Cotton-Effekt ein Maximum bei 506 nm besitzt. Die Umkehr der Signatur deutet auf eine gegenläufige Helizität der Aggregate von **4a** und **4b** hin. Aggregate basierend auf PBI **4b** haben dementsprechend eine *P*-Konfiguration. CD-Experimente mit **5a** und **5b** in Chloroform zeigen analog zu **4a** in Wasser eine *M*-Konfiguration (Figure 63C und D). Dieses Verhalten ist in klarem Kontrast zu den wasserlöslichen Perylenbisimiden. Für den direkten Nachweis der helikalen Anordnung in den Aggregaten wurden AFM- und TEM-Aufnahmen von chiralen Bola-Amphiphilen gemacht (Figure 64, links und Figure 65). Im völligen Gegensatz zu den achiralen Bausteinen **2** und **3a–c** konnten für die chiralen Bausteine jedoch keine wurmartigen Strukturen nachgewiesen werden, sondern nur kleine kugelförmige Partikel. Dieses veränderte Verhalten ist auf den direkten Einfluss der Aminosäureseitenketten zurückzuführen.

Der in **Kapitel 5** vorgestellte Multichromophor **6** (Abbildung 4) enthält eine planare Perylenbisimid- und zwei Acridin-Einheiten, die über flexible Ethylenglykol-Linker

miteinander verbunden sind. Die bei UV/Vis-Messungen festgestellten spektralen Änderungen bei steigender Konzentration von 10^{-7} bis 10^{-2} M in Chloroform deuten auf einen Selbstassoziierungsprozess der Perylenbisimid-Chromophore in Form von H-Aggregaten hin. Bei Fluoreszenzmessungen wurden sowohl bei Anregung des Acridin-Chromophors (Anregungswellenlänge 340 nm) als auch bei Anregung des Perylenbisimid-Chromophors (Anregungswellenlänge 500 nm) zwei Emissions-Banden bei 536 und 605 nm festgestellt. Während die Bande bei 536 nm durch die Emission vom vibratorischen Grundzustand des Perylen-S_1-Zustands herrührt, könnte die Bande bei 605 nm durch die Emission eines Acridin-Perylen-Exziplexes hervorgerufen worden sein, welches durch die Faltung des angeregten Moleküls entstanden ist. Dagegen ist die Acridin-Emission bei 392 nm nach der Anregung von **6** in der Absorptionsbande des Acridins bei 340 nm nur sehr schwach ausgeprägt. Diese Ergebnisse weisen auf einen effizienten Energietransfer von den Acridin-Chromophoren auf den Perylen-Chromophor hin.

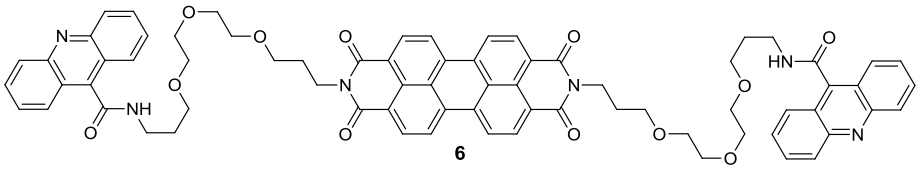

6

Abbildung 4. PBI **6**, welches drei Chromophore enthält.

Die Ergebnisse einer NMR-Verdünnungsreihe deuten aufgrund der signifikanten Verschiebung der Perylen-Protonen im gemessenen Konzentrationsbereich auf zwischenmolekulare π-π-Wechselwirkungen unter den Perylen-Chromophoren hin. Die Signale der Acridin-Protonen dagegen sind nur bei der höchsten gemessenen Konzentration maßgeblich verschoben, was die Beteiligung des Acridin-Chromophors sowohl an π-π-Wechselwirkungen als auch an Wasserstoffbrückenbindungen nahelegt. Mit den spektroskopischen Messungen übereinstimmende Berechnungen eines Monomers und eines Dimers von **6** (Abbildung 5) weisen auf einen Übergang der M2- zur D1-Anordnung hin, bei der zwei Perylen-Einheiten direkt miteinander wechselwirken und die Acridin-Einheiten eine Anordnung ähnlich der von Nukleobasen aufweisen.

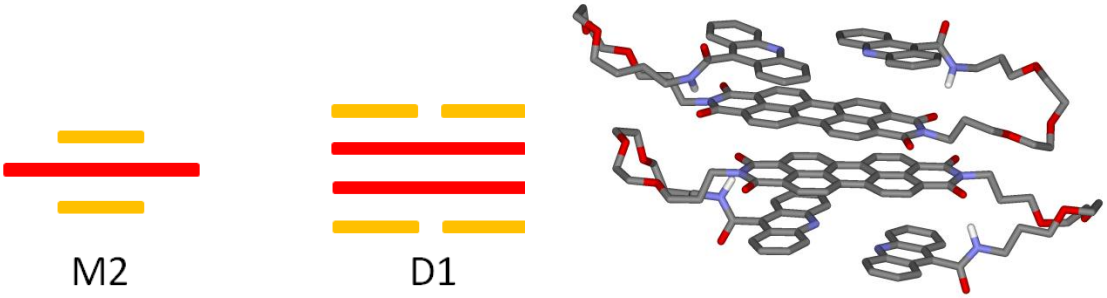

Abbildung 5. Schematische Darstellung der bevorzugten Monomer- und Dimer-Anordnung (M2, D1, links) und die berechnete Dimer-Anordnung D1 des Multichromophors **6** (rechts).

Diese Dissertation liefert einen effizienten Ansatz, die stark hydrophoben Perylenebisimid-Chromophore löslich zu machen, um sie in polaren Lösungen für Selbstaggregationsprozesse zu nutzen. Das Konzept der bola-amphiphilen Architektur wurde eingesetzt, um gestapelte PBI-Strukturen zu erzeugen, die neben einem hydrophoben Kern eine positiv geladene Hülle zur Löslichkeitsförderung in reinem Wasser besitzen. Im Rahmen dieser Arbeit war es möglich, die Aggregatgröße und -struktur zu kontrollieren, indem man zwischen dem Chromophor und den geladenen Spermin-Ketten unterschiedliche Linker einbaute. Die Untersuchung eines im Vergleich dazu weniger hydrophilen Multichromophors mit Perylenbisimid- und Acridin-Einheiten konnte erste Einblicke in dessen sehr interessantes Aggregationsverhalten in Chloroform liefern.

Chapter 8

Experimental Section

8.1 Materials and Methods

Solvents and reagents were purchased from commercial sources, unless otherwise stated, and purified and dried according to standard procedures.[212] Reactions were monitored by thin-layer chromatography (TLC) on silica gel plates (Merck TLC Silica gel 60 F_{254} aluminum sheets). All perylene bisimide derivatives are colored, thus no additional visualization of the spots was necessary. Amines were visualized by spraying the TLC plate with ninhydrine solution.[213] Column chromatography was performed on silica gel (Merck Silica 60, particle size 0.04–0.063 mm). Semi-preparative high-performance liquid chromatography (HPLC) was performed on a Jasco system (PU 2080 PLUS) with a UV/Vis detector (UV 2077 PLUS) using a semi-preparative NUCLEOSIL® C8 column (Macherey & Nagel). NMR experiments were conducted at 298.8 K (unless otherwise stated) on a Bruker Avance 400 or DMX 600 with TMS or residual undeuterated solvent as internal standard. The chemical shifts are reported in ppm referring to TMS (δ scale). The apparent coupling constants *J* are given in Hertz (Hz). The signal fine structures are abbreviated as: s = singlet, br. s = broad signal, d = doublet, br. d = broad doublet, t = triplet, q = quartet, dt = doublet of triplet, tt = triplet of triplet, m = multiplet. IR spectra were measured as KBr pellets on a Jasco FT-IR 410 spectrophotometer. The maxima are classified in three intensities: s (strong), m (middle), w (weak) and are reported in wavenumbers (cm^{-1}).[214] Melting points were

measured with a Linkam TP 94 heating stage and are uncorrected. Mass spectra were performed on Bruker MALDI-TOF (autoflex II) and Bruker ESI-TOF (microTOF focus) spectrometers. For the measurements of PBI **6** in $CHCl_3$ and $CDCl_3$, respectively, the solvent was neutralized over an aluminum oxide column.

UV/Vis Spectroscopy

Absorption spectra were measured on a Perkin-Elmer Lambda 950 spectrometer equipped with a Peltier system as temperature controller in conventional quartz cells of appropriate path length. The spectral bandwidth and the scan rate were 2 nm and 140 nm/min, respectively. Either spectroscopically pure dichloromethane (Uvasol®) or Milli-Q® water (deionized water) was used for the measurements. The stock solutions for the concentration-dependent measurements of spermine-functionalized PBIs were prepared by accurately weighing the respective ^{t}Boc-protected precursors. After conducting the deprotection step the fluffy red solids were dissolved in an appropriate amount of MilliQ® water giving the stock solution. The stock solutions for the concentration-dependent measurements of PBIs **5a**,**b** were prepared by accurately weighing and dissolving in an appropriate volume of chloroform. Dilutions of these stock solutions were used for absorption measurements over the indicated concentration range.

Fluorescence Spectroscopy

Emission spectra were recorded on a PTI QM4-2003 fluorescence spectrometer and were corrected against photomultiplier and lamp intensity. A long wavelength range emission corrected Hamamatsu photomultiplier R928 was used. Quartz glass cuvettes with a thickness of 10 mm were used for the measurements. Fluorescence quantum yields Φ_{fl} were determined in MilliQ water vs. fluorescein (Φ_{fl} = 0.92 in 0.1 N NaOH) as reference.[33,215] The reported quantum yields are averaged from values measured at three different excitation wavelengths with OD 0.02–0.05 in the absorption maximum (standard deviation σ = 1–3 %).

Time-resolved Fluorescence Lifetime

Fluorescence lifetimes were measured with a PTI LaserStrobe fluorescence spectrometer system containing a PTI GL-3300 nitrogen laser (337.1 nm, pulse width 600 ps, pulse energy 1.45 mJ) coupled with a dye laser PTI GL302 (pulse width 500 ps, pulse energy

220 µJ at 550 nm) as an excitation source and stroboscopic detection. Laser output was tuned within the emission curves of the laser dyes supplied by the manufacturer (PLD 500). Details of the Laser Strobe systems are described on the manufacturer's web site and in the literature.[216,217] The instrument S10 response function was collected by scattering the exciting light of a dilute, aqueous suspension of colloidal Silica (LUDOX). Decay curves were evaluated using the software supplied with the instrument applying least square regression analysis. The quality of the fit was evaluated by analysis of $\chi 2$, DW factor and *Z* value and by inspection of residuals and autocorrelation function.

Circular Dichroism (CD) Spectroscopy

CD spectra were measured on a Jasco J-810 circular dichroism spectrometer. Quartz glass cuvettes with the appropriate thickness of 0.1–10 mm were used for the measurements. The stock solutions prepared for the UV/Vis measurements and dilutions of them were used for the CD experiments.

Atomic Force Microscopy (AFM)

AFM investigations were performed under ambient conditions using a Veeco MultiMode™ Nanoscope IV system operating in tapping mode in air. Silicon cantilevers (Olympus Corporation, Japan) with a resonance frequency of ~300 kHz were used. Samples of PBIs **2** and **3a–c** were prepared by spin-coating either a fresh or an aged solution (stored for one month at room temperature in sealed tube) in Milli-Q® water onto freshly cleaved mica at 7000 rpm. Samples of PBIs **4a** and **4b** were prepared by spin-coating of their freshly prepared solutions in Milli-Q® water onto freshly cleaved mica at 7000 rpm.

Transmission Electron Microscopy (TEM)

TEM measurements were performed on a Siemens Elmiskop 101 Electron Microscope, operating at an acceleration voltage of 80 kV. For the observation of aggregates, a drop of sample suspension (PBI **3c**, $c = 1 \times 10^{-3}$ M in water; PBI **4a**, $c = 5 \times 10^{-3}$ M in water) was placed on 400-mesh formvar copper grids coated with carbon. About 2 min after the deposition, the grid was tapped with filter paper to remove surface water. Negative staining was performed by addition of a drop of uranyl acetate aqueous solution (0.5 %) onto the copper grid. After 1 min, the surface water on the grid was removed by taping with filter paper.

Molecular Modeling

Molecular modeling studies reported in Chapters 3 and 4 were performed with the MacroModel Suite V9.6 (Schrödinger LLC). Amber* was used as force field together with the GB/SA (Generalized-Born/Surface-Area) model for water. The electrostatic treatment was chosen as constant with a dielectric coefficient of 1.0 for the molecular dynamics simulation. Charges were assigned by the force field itself, the cutoff values were kept extended with 8.0 Å for van-der-Waals interactions, 20.0 Å for electrostatic interactions and 4.0 Å for hydrogen bonds. Pre-optimization of the single molecules was performed by energy minimizations with the PRCG (Polak-Ribier Conjugate Gradient) method and a maximum of 50.000 iterations (convergence on gradient with a threshold of 0.001). The minimizations for the molecular dynamics simulation were also performed with the PRCG method, but a maximum of 500 iterations was set for the pre-minimized structure (convergence on gradient with a threshold of 0.05). For the dynamics simulation the molecular dynamics method was chosen with the SHAKE option for all bonds. Simulation temperature was adjusted to 300 K. The total simulation time was 500 ps with a time-step of 1.5 fs and an equilibration time of 1.5 ps.

The force field calculations reported in Chapter 5 were performed with the Amber* force field using the solvent model for chloroform (Schrödinger Suite MacroModel 2012). Conformational search procedures (10.000 steps) were performed after minimizing the plotted molecules (50.000 steps, threshold: 0.05).

8.2 Synthesis and Chemical Characterization

Synthesis of compounds in Chapter 3

Synthesis of threefold ^{t}Boc-protected spermine **53**[169]

A solution of spermine (1.00 g, 4.96 mmol) in methanol (70 mL) was cooled to -78 °C under argon atmosphere. Trifluoroacetic acid ethylester (0.59 mL, 0.70 g, 4.96 mmol) was added dropwise to the solution within 30 min. The colorless suspension was stirred for 60 min at -78 °C and subsequently warmed up to 0 °C within 3 h. A solution of di-^{t}butyldicarbonate (4.33 g, 19.5 mmol) in methanol (10 mL) was added dropwise within five minutes. The reaction solution was stirred for additional 20 h under argon

atmosphere at room temperature. After this time period, the pH value of the solution was adjusted to 11 with concentrated aqueous ammonia solution (30 mL). The solution was stirred again for 24 h at room temperature. After removal of the solvent in vacuo (45 °C, 11 mbar) the highly viscous oil was purified by column chromatography (SiO_2, CH_2Cl_2 : MeOH : conc. aq. NH_3 = 70 : 10 : 1 v/v/v) to obtain **53** as colorless oil in 30 % yield (0.75 g, 1.49 mmol). MW ($C_{25}H_{50}N_4O_6$) = 502.69 g/mol; R_f = 0.5 (CH_2Cl_2 : MeOH : conc. aqua. NH_3 = 50:10:1); ^{1}H NMR ($CDCl_3$): δ = 3.36-3.04 (m, 10H), 2.71 (t, *J* = 6.6, 2H), 1.74-1.55 (m, 4H), 1.52-1.35 (m, 33H); HRMS (ESI pos.): *m/z* = 503.3808; calcd. for $C_{25}H_{50}N_4O_6 + H^+$: 503.3808.

PBI **55**: Perylene tetracarboxylic acid bisanhydride **54** (138 mg, 3.52 µmol) and threefold ^{t}Boc-protected spermine **53**[169] (390 mg, 7.76 µmol) were suspended in dry DMF (3 mL) and stirred for 3.5 h at 80 °C. The reaction solution was transferred into a separatory funnel and diluted with water (10 mL) and CH_2Cl_2 (70 mL). The organic phase was washed with water (3 × 40 mL). After phase separation the aqueous phase was extracted with CH_2Cl_2 (2 × 15 mL). The organic phases were combined and dried over magnesium sulphate. The solvent was removed *in vacuo* and the residual crude product was purified by column chromatography (SiO_2, CH_2Cl_2 : MeOH = 97 : 3) and HPLC (Nucleosil®, CH_2Cl_2 : MeOH = 98 : 2) obtaining the fully protected precursor **55** as a red solid in 36 % yield (170 mg, 1.25 µmol). MW ($C_{74}H_{104}N_8O_{16}$) = 1361.66 g/mol; R_f = 0.31 (CH_2Cl_2 : MeOH = 98:2); m.p.: 128 °C; ^{1}H NMR ($CDCl_3$): δ = 8.69 (d, *J* = 8.0, 4H), 8.62 (d, *J* = 8.1, 4H), 4.23 (dt, J_{CHCH} = 7.1, 4H), 3.33, 3.25, 3.15 and 3.09 (br. s, 20H), 2.01 (tt, *J* = 7.7, *J* = 7.0, 4H), 1.66 (br. s, 4H), 1.52 (br. s, 8H), 1.45 (s, 18H), 1.43 (s, 36H); the carbamate NH signal is not detectable due to the fast exchange with the deuterated solvent; HRMS (ESI pos.): *m/z* = 1383.7467; calcd for $C_{74}H_{104}N_8O_{16} + Na^+$: 1383.7467; MS (MALDI, matrix: DCTB): 1360.755 $[M]^{\bullet-}$, calcd for $C_{74}H_{104}N_8O_{16} + e^-$: 1360.757; UV/Vis (CH_2Cl_2): λ_{max} (nm) [ε_{max} ($M^{-1}cm^{-1}$)] = 525 [80500].

General Procedure for the Synthesis of PBI dicarboxylic acids **57a–c**[37]

Perylene tetrycarboxylic bisanhydride **54** (1.3 mmol, 1 equiv.) was suspended in DMSO (50 mL) and the suspension was heated to 100 °C. The appropriate amino acid

(20 equiv.) and KOH (20 equiv.), dissolved (for **57a** and **57b**) or suspended (for **57c**) in water respectively, were added dropwise. The mixture was stirred for 3 h at 100 °C, cooled down to room temperature and adjusted to pH 5 with aqueous hydrochloric acid. The precipitate was centrifuged, washed with water (2 × 50 mL) and methanol (2 × 50 mL) and centrifuged again after each wash. The red solid was boiled in 2 M HCl (100 mL) and the solution was filtrated hotly. The residue was washed with hot 2 M HCl (50 mL) and water (50 mL). Afterwards the red solid was dried in vacuo (60 °C, 2 x 10^{-3} mbar).

PBI **57a**: Yield: 0.54 g (1.07 mmol, 77 %) of a red solid; MW ($C_{28}H_{14}N_2O_8$) = 506.42 g/mol; m.p.: > 400 °C; MS (LDI neg.): *m/z* = 506.07; calcd for $C_{28}H_{14}N_2O_8 + e^-$: 506.08; FT-IR (KBr): 3400 (m), 3068 (w), 3007 (w), 1695 (s), 1662 (vs), 1592 (s), 1365 (m), 1334 (m), 1247 (m), 1174 (w), 1004 (w).

PBI **57b**: Yield: 0.57 g (0.96 mmol, 77 %) of a red solid; MW ($C_{34}H_{26}N_2O_8$) = 590.58 g/mol; m.p.: 394 – 401 °C; MS (ESI neg.): *m/z* = 589.16; calcd for $C_{34}H_{26}N_2O_8 – H^+$: 589.16; FT-IR (KBr): 3400 (m), 2980 (w), 2928 (w), 2860 (w), 1692 (s), 1658 (vs), 1592 (s), 1574 (s), 1445 (w), 1405 (m), 1380 (w), 1347 (m), 1265 (w), 1070 (w), 810 (w), 750 (w).

PBI **57c**: Yield: 0.82 g (1.08 mmol, 83 %) of a red solid; MW ($C_{46}H_{50}N_2O_8$) = 758.90 g/mol; m.p.: 297 – 305 °C; MS (ESI neg.): m/z = 757.35; calcd for $C_{46}H_{50}N_2O_8 – H^+$: 757.35; FT-IR (KBr): 3063 (w), 3038 (w), 2926 (m), 2850 (m), 1770 (w), 1696 (s), 1656 (s), 1593 (s), 1439 (m), 1404 (m), 1343 (s), 1253 (m), 1099 (w), 809 (m), 747 (m).

General Procedure for the Synthesis of fully *t*Boc-protected Precursors PBIs **58a–c**

The respective dicarboxylic acid PBI derivative **57a–c** (0.20 mmol, 1 equiv.), threefold ^{t}Boc-protected spermine **53** (2.2 equiv.), DCC (3 equiv.) and HOBt (0.5 equiv.) were stirred in dry DMF (3 mL) at 40 °C for 20 h under inert gas. The reaction solution was diluted with water and extracted with CH_2Cl_2 (3 × 50 mL). The organic phases were dried over magnesium sulphate and concentrated *in vacuo*. The residue was purified by column chromatography and HPLC.

PBI **58a**: Column chromatography: SiO_2, CH_2Cl_2 : MeOH = 98 : 2; HPLC: Nucleosil®, CH_2Cl_2 : MeOH = 97 : 3; yield: 141 mg (0.1 mmol, 48 %) of a red solid; MW ($C_{78}H_{110}N_{10}O_{18}$) = 1475.76 g/mol; R_f = 0.27 (CH_2Cl_2 : MeOH = 98 : 2); m.p.: 289 °C (decomp.); ^{1}H NMR ([D_6]DMSO): δ = 8.86 (d, J = 7.2, 4H), 8.62 (d, J = 7.9, 4H), 8.17 (br. s, 2H), 6.72 (br. s, 2H), 4.64 (s, 4H), 3.10 (br. s, 20H), 2.87 (dt, J_{CHCH} = 6. 4, J_{NHCH} = 6.2, 4H), 1.60 and 1.55 (br. s, 8H), 1.36 (s, 18H), 1.35 (s, 36H), 1.28 (s, 16H); the amide and carbamate NH signals are broadened due to the fast exchange with the deuterated solvent; HRMS (ESI pos.): m/z = 1497.7924; calcd for $C_{78}H_{110}N_{10}O_{18}$ + Na^+ : 1497.7892; UV/Vis (CH_2Cl_2): λ_{max} (nm) [ε_{max} ($M^{-1}cm^{-1}$)] = 525 [84100].

PBI **58b**: Column chromatography: SiO_2, CH_2Cl_2 : MeOH = 98 : 2 to 97 : 3; HPLC: Nucleosil®, CH_2Cl_2 : MeOH = 97 : 3; yield: 68.5 mg (0.044 mmol, 22 %) of a red solid; MW ($C_{84}H_{122}N_{10}O_{18}$) = 1559.92 g/mol; R_f = 0.31 (CH_2Cl_2 : MeOH = 98 : 2); m.p.: 120-121 °C; ^{1}H NMR ($CDCl_3$): δ = 8.62 (d, J = 8.0, 4H), 8.54 (d, J = 8.1, 4H), 4.23 (dt, J_{CHCH} = 6.4, 4H), 3.22, 3.14, 3.10 and 3.09 (m, 24H), 2.30 (dt, J_{CHCH} = 7.2, 4H), 1.81 (br. s, 8H), 1.65 (br. s, 8H), 1.48 (br. s, 8H), 1.44 and 1.43 (m, 56H); the amide and carbamate NH signals are not detectable due to the fast exchange with the deuterated solvent; HRMS (ESI pos.): m/z = 1581.8793; calcd for $C_{84}H_{122}N_{10}O_{18}$ + Na^+ : 1581.8833; UV/Vis (CH_2Cl_2): λ_{max} (nm) [ε_{max} ($M^{-1}cm^{-1}$)] = 525 [82000].

PBI **58c**: Column chromatography: SiO_2, CH_2Cl_2 : MeOH = 97 : 3; HPLC: (Nucleosil®, CH_2Cl_2 : MeOH = 97 : 3); yield: 60.0 mg (0.036 mmol, 18 %) of a red solid; MW ($C_{96}H_{146}N_{10}O_{18}$) = 1728.24 g/mol; R_f = 0.30 (CH_2Cl_2 : MeOH = 98 : 2); m.p.: 140 °C; ^{1}H NMR ($CDCl_3$): δ = 8.71 (d, J = 8.0, 4H), 8.65 (d, J = 8.2, 4H), 4.20 (dt, J_{CHCH} = 7.6, 4H), 3.21, 3.13 and 3.10 (br. s, 24H), 2.17 (dt, J_{CHCH} = 7.3, 4H), 1.76 (tt, J = 5.8, J = 8.6, 4H), 1.63 (br. s, 12H), 1.45 and 1.43 (br. s, 56H), 1.27 (br. s, 32H); the amide and carbamate NH signals are not detectable due to the fast exchange with the deuterated solvent.; HRMS (ESI pos.): m/z = 1750.0602; calcd for $C_{96}H_{146}N_{10}O_{18}$ + Na^+ : 1750.0709; UV/Vis (CH_2Cl_2): λ_{max} (nm) [ε_{max} ($M^{-1}cm^{-1}$)] = 525 [82800].

General Procedure for the Synthesis of Target PBIs **2** and **3a–c**

The respective ^{t}Boc-protected precursor PBI **55** and **58a–c** (10 µmol) was dissolved in CH_2Cl_2 (1 mL). Trifluoroacetic acid (1 mL) was added and the mixture was stirred at room temperature for 2 h. The solvent and excess trifluoroacetic acid (TFA) were removed *in vacuo* giving a dark red film, which was dissolved in water. The resulted red solution was lyophilized twice from water to remove traces of residual TFA. The red voluminous solid was used without further purification. Yield: quantitative for each, as a red fluffy solid.

PBI **2**: MW ($C_{56}H_{62}N_8O_{16}F_{18}$) = 1445.11 g/mol; ^{1}H NMR ([D$_6$]DMSO): δ = 9.01 (d, J = 8.2, 4H), 8.46 (d, J = 7.8, 4H), 8.55 (br. s, 4H), 7.85 (br. s, 6H), 4.17 (t, J = 6.0, 4H), 3.06 (br. s, 4H), 2.94 and 2.88 (br. s, 16H), 2.05 (tt, J = 5.4, J = 7.2, 4H), 1.87 (tt, J = 8.4, J = 6.9, 4H), 1.61 (br. s, 8H); the broad signals of the ammonium group protons (8H) superimpose one signal of the perylene CH (4H); HRMS (ESI pos.): *m/z* = 761.4494; calcd for $C_{44}H_{56}N_8O_4 + H^+$: 761.4497; UV/Vis (H_2O, c = 7 x 10^{-6} M): λ_{max} (nm) [ε_{max} ($M^{-1}cm^{-1}$)] = 496 [46000], 533 [70000]; fluorescence (H_2O, λ_{ex} = 475 nm): λ_{max} (nm) = 546; Φ_{fl} = 0.90.

PBI **3a**: MW ($C_{60}H_{68}N_{10}O_{18}F_{18}$) = 1559.21 g/mol; ^{1}H NMR ([D$_6$]DMSO): δ = 8.87 (d, J = 8.0, 4H), 8.68 (br. s, 8H), 8.51 (d, J = 7.9, 4H), 8.44 (t, J = 5.0, 2H), 7.94 (br. s, 6H), 4.7 (s, 4H), 3.18 (dt, J_{CHNH} = 5.9, J_{CHCH} = 6.0, 4H), 3.00 – 2.86 (m, 20H), 1.89 (tt, J = 7.9, J = 7.0, 4H), 1.78 (tt, J = 7.7, J = 7.0, 4H), 1.65 – 1.62 (m, 8H); the broad signals of the ammonium group protons (8H and 6H, respectively) superimpose the signals of the perylene CH (2 × 4H) and the amide NH (2H); HRMS (ESI pos.): *m/z* = 875.4911; calcd for $C_{48}H_{62}N_{10}O_6 + H^+$: 875.4927; UV/Vis (H_2O, c = 1 x 10^{-6} M): λ_{max} (nm) [ε_{max} ($M^{-1}cm^{-1}$)] = 496 [45300], 533 [70000]; fluorescence (H_2O, λ_{ex} = 475 nm): λ_{max} (nm) = 546; Φ_{fl} = 0.78.

PBI **3b**: MW ($C_{66}H_{80}N_{10}O_{18}F_{18}$) = 1643.37 g/mol; ^{1}H NMR ([D$_6$]DMSO): δ = 8.58 (d, J = 8.0, 4H), 8.30 (d, J = 7.7, 4H), 8.03 (t, J = 5.4, 2H), 4.03 (br. s, 4H), 3.11 (dt, J_{CHNH} = 6.3, J_{CHCH} = 6.0, 4H), 2.98 (t, J = 7.6, 4H), 2.92 – 2.86 (m, 16H), 2.18 (t, J = 7.0, 4H), 1.89 (tt, J = 8.0, J = 7.1, 4H), 1.78 (tt, J = 7.7, J = 6.9, 4H), 1.63 (br. s, 16H); the broad signals of the ammonium group protons (8H and 6H, respectively) superimpose the signals of the perylene CH (2 × 4H) and the amide NH (2H); HRMS (ESI pos.): *m/z* = 959.5867; calcd for

$C_{54}H_{74}N_{10}O_6$ +H^+ : 959.5866; UV/Vis (H_2O, c = 5 x 10^{-7} M): λ_{max} (nm) [ε_{max} ($M^{-1}cm^{-1}$)] = 496 [42100], 533 [63000]; fluorescence (H_2O, λ_{ex} = 475 nm): λ_{max} (nm) = 546; Φ_{fl} = 0.72.

PBI **3c**: MW ($C_{78}H_{104}N_{10}O_{18}F_{18}$) = 1811.89 g/mol; ^{1}H NMR ([D_6]DMSO): δ = 8.68 (br. s, 8H), 8.35 (d, J = 7.5, 4H), 8.13 (d, J = 7.4, 4H), 7.97 (t, J = 5.4, 2H), 3.94 (br. s, 4H), 3.15 (dt, J_{CHNH} = 6.5, J_{CHCH} = 6.0, 4H), 2.98 (t, J = 7.5, 4H), 2.91 – 2.86 (m, 16H), 2.07 (t, J = 7.2, 4H), 1.89 (tt, J = 7.7, J = 7.3, 4H), 1.71 (tt, J = 6.4, J = 7.6, 4H), 1.68 (br. s, 12H), 1.49 (tt, J = 7.4, J = 6.9, 4H), 1.36 and 1.27 (br. s, 26H); the broad signals of the ammonium group protons (8H and 6H, respectively) superimpose the signals of the perylene CH (2 × 4H) and the amide NH (2H); HRMS (ESI pos.): m/z = 1127.7742; calcd for $C_{66}H_{98}N_{10}O_6$ + H^+ : 1127.7744; UV/Vis (H_2O, c = 5 x 10^{-7} M): λ_{max} (nm) [ε_{max} ($M^{-1}cm^{-1}$)] = 497 [43200], 534 [57300]; fluorescence (H_2O, λ_{ex} = 475 nm): λ_{max} (nm) = 548; Φ_{fl} = 0.39.

Synthesis of compounds in Chapter 4

The synthesis of threefold ^{t}Boc-protected spermine **53**[169] can be found on pages 112/113.

General procedure for the synthesis of PBI dicarboxylic acids **60a–d**[37,206,207]
Perylene tetracarboxylic bisanhydride **54** (2.5 mmol, 1 equiv.), the appropriate α-amino acid **59a–d** (2.1 equiv.) and imidazole (40 equiv.) were mixed in a flask which was flooded with argon gas for 15 minutes. The mixture was heated to 120 °C for 30 minutes and then cooled down to 85 °C. The pH value of the reaction mixture was adjusted to 3-4 with 1 N HCl. The precipitate was collected by suction filtration, washed with water and dried in high vacuum (2 × 10^{-3} mbar, 60 °C).

PBI **60a**: Yield: 1.32 g (2.47 mmol, 97 %) of a red solid; MW ($C_{30}H_{18}N_2O_8$) = 534.47 g/mol; m.p.: > 400 °C; ^{1}H NMR ([D_6]DMSO): δ = 8.23 (d, J = 8.0, 4H), 8.18 (d, J = 8.0, 4H), 5.59 (q, J = 7.0, 2H), 1.68 (d, J = 7.1, 6H); the carboxylic acid protons are not detectable; MS (MALDI, matrix: DCTB): m/z = 534.101; calcd for $C_{30}H_{18}N_2O_8$ + e^- : 534.106.

PBI **60b**: Yield: 1.75 g (2.55 mmol, 100 %) of a red solid; MW ($C_{42}H_{26}N_2O_8$) = 686.66 g/mol; m.p.: > 400 °C; ^{1}H NMR ([D$_6$]DMSO): δ = 8.87 (d, *J* = 8.2, 4H, perylene protons), 8.51 (d, *J* = 7.8, 4H, perylene protons), 7.19 (d, *J* = 1.3, 4H, Ph-H), 7.15 (t, *J* = 7.2, 4H, Ph-H), 7.04 (t, *J* = 7.2, 2H, Ph-H), 5.92 (q, *J* = 5.3, 2H, CH), 3.60 (dd, *J* = 14.8, *J* = 5.9, 2H, CH_2), 3.38 (dd, *J* = 14.2, *J* = 9.5, 2H, CH_2, partially superimposed by the water peak); MS (MALDI, matrix: DCTB): *m/z* = 686.176; calcd for $C_{42}H_{26}N_2O_8 + e^-$: 686.189.

PBI **60c**: Yield: 1.32 g (2.47·mmol, 97 %) of a dark red solid; MW ($C_{30}H_{18}N_2O_8$) = 534.47 g/mol; m.p.: > 400 °C; ^{1}H NMR ([D$_6$]DMSO): δ = 8.23 (d, *J* = 7.3, 4H), 8.18 (d, *J* = 8.0, 4H), 5.59 (q, *J* = 7.0, 2H), 1.68 (d, *J* = 7.1, 6H); MS (MALDI, matrix: DCTB): *m/z* = 534.101; calcd for $C_{30}H_{18}N_2O_8 + e^-$: 534.106.

PBI **60d**: Yield: 1.85 g (2.70 mmol, 100 %) of a red solid; MW ($C_{42}H_{26}N_2O_8$) = 686.66 g/mol; m.p.: > 400 °C; ^{1}H NMR ([D$_6$]DMSO): δ = 8.84 (d, *J* = 8.3, 4H, perylene protons), 8.50 (d, *J* = 7.6, 4H, perylene protons), 7.20 (d, *J* = 1.3, 4H, Ph-H), 7.15 (t, *J* = 7.2, 4H, Ph-H), 7.05 (t, *J* = 7.2, 2H, Ph-H), 5.91 (dd, *J* = 5.4, 2H, Ph-H), 3.60 (dd, *J* = 14.4, *J* = 5.9, 2H, CH_2), 3.40 (dd, *J* = 14.0, *J* = 9.5, 2H, CH_2); MS (MALDI, matrix: DCTB): *m/z* = 686.160; calcd for $C_{42}H_{26}N_2O_8 + e^-$: 686.189.

General procedure for the synthesis of the fully Boc-protected PBIs **61a–d**

A solution of the respective PBI **60a–d** (0.28 mmol, 1 equiv.), threefold ^{t}Boc-protected spermine **54** (2.1 equiv.), DCC (3 equiv.), HOBt (0.8 equiv.) and Hünig's base (0.1 mL) were stirred in DMF (5 mL) at 80 °C for 4 h. After the mixture was cooled down to room temperature, water (50 mL) and CH_2Cl_2 (50 mL) were added. The phases were separated and the aqueous phase was extracted with CH_2Cl_2 (2 × 50 mL). The combined organic phases were washed with water (200 mL) and concentrated under reduced pressure. The crude product was purified by column chromatography (SiO_2, CH_2Cl_2 : MeOH = 99 : 1 to 97 : 3) and subsequent HPLC (Nucleosil®, CH_2Cl_2 : MeOH = 97 : 3).

PBI **61a**: Yield: 187 mg (0.12 mmol, 44 %) of a red solid; MW ($C_{80}H_{114}N_{10}O_{18}$) = 1503.82 g/mol; R_f = 0.22 (SiO_2, CH_2Cl_2 : MeOH = 97 : 3); m.p.: 100 – 102 °C; ^{1}H NMR

($CDCl_3$): δ = 8.69 (d, *J* = 8.0, 4H), 8.63 (d, *J* = 8.0, 4H), 7.62 (br. s, 2H), 5.78 (q, *J* = 6.7, 2H), 3.26 – 3.02 (m, 24H), 1.79 (d, *J* = 7.2, 6H), 1.62 (br. s, 8H), 1.42 (s, 46H), 1.01 (s, 16H); the amide and carbamate NH signals are broadened due to the fast exchange with the deuterated solvent; HRMS (APCI pos.): *m/z* = 1537.7994; calcd for $C_{80}H_{114}N_{10}O_{18}$ + Cl^- : 1537.8007; UV/Vis (CH_2Cl_2, *c* = 5 × 10^{-5} M): λ_{max} (nm) [ε_{max} ($M^{-1}cm^{-1}$)] = 458.5 [18500], 489.5 [51200], 526.5 [85000].

PBI **61b**: Yield: 76 mg (0.46 mmol, 29 %) of a pink solid; MW ($C_{92}H_{122}N_{10}O_{18}$) = 1656.01 g/mol; R_f = 0.26 (SiO_2, CH_2Cl_2 : MeOH = 97 : 3); m.p.: 91 – 93 °C; ^{1}H NMR ($CDCl_3$): δ = 8.51 (d, *J* = 8.0, 4H), 8.44 (s, *J* = 8.3; 4H), 7.62 (br. s, 2H), 7.19 – 6.93 (m, 10H), 6.00 (dd, *J* = 5.9, *J* = 4.6, 2H), 3.79 – 3.74 (m, 2H), 3.60 – 3.54 (m, 2H), 3.24 – 2.90 (m, 24H), 1.56 (m, 8H), 1.42 (s, 46H), 0.80 (s, 16H); the amide and carbamate NH signals are broadened due to the fast exchange with the deuterated solvent; HRMS (ESI pos.): *m/z* = 1677.8836; calcd for $C_{92}H_{122}N_{10}O_{18}$ + Na^+ : 1677.8831; UV/Vis (CH_2Cl_2, *c* = 5 × 10^{-5} M): λ_{max} (nm) [ε_{max} ($M^{-1}cm^{-1}$)] = 459 [18400], 490.5 [50800], 527 [85000].

PBI **61c**: Yield: 327 mg (0.21 mmol, 61 %) of a red solid; MW ($C_{80}H_{114}N_{10}O_{18}$) = 1503.82 g/mol; R_f = 0.22 (SiO_2, CH_2Cl_2 : MeOH = 97 : 3); m.p.: 99 – 102 °C; ^{1}H NMR ($CDCl_3$): δ = 8.69 (d, *J* = 7.6, 4H), 8.63 (d, *J* = 8.0, 4H), 7.62 (br. s, 2H), 5.79 (q, *J* = 6.9, 2H), 3.27 – 3.02 (m, 24H), 1.79 (d, *J* = 7.2, 6H), 1.62 (br. s, 8H), 1.42 (s, 46H), 1.01 (s, 16H); the amide and carbamate NH signals are broadened due to the fast exchange with the deuterated solvent; HRMS (ESI pos.): *m/z* = 1503.8371; calcd for $C_{80}H_{114}N_{10}O_{18}$ + H^+ : 1503.8389; UV/Vis (CH_2Cl_2, *c* = 5 × 10^{-5} M): λ_{max} (nm) [ε_{max} ($M^{-1}cm^{-1}$)] = 458.5 [18500], 489.5 [51100], 526.5 [85000].

PBI **61d**: Yield: 430 mg (0.26 mmol, 72 %) of a pink solid; MW ($C_{92}H_{122}N_{10}O_{18}$) = 1656.01 g/mol; R_f = 0.26 (SiO_2, CH_2Cl_2 : MeOH = 97 : 3); m.p.: 92 – 93 °C; ^{1}H NMR ($CDCl_3$): δ = 8.57 (d, *J* = 8.3, 4H), 8.44 (s, *J* = 6.6; 4H), 7.69 (br. s, 2H), 7.23 – 7.00 (m, 10H), 6.06 (dd, *J* = 4.2, *J* = 5.0, 2H), 3.85 – 3.82 (m, 2H), 3.68 – 3.61 (m, 2H), 3.31 – 2.97 (m, 24H), 1.61 (m, 8H), 1.42 (s, 46H), 0.87 (s, 16H); the amide and carbamate NH signals are broadened due to the fast exchange with the deuterated solvent; HRMS (ESI pos.): *m/z* =

1677.8852; calcd for $C_{92}H_{122}N_{10}O_{18}$ + Na^+ : 1677.8831; UV/Vis (CH_2Cl_2, c = 5 × 10^{-5} M): λ_{max} (nm) [ε_{max} ($M^{-1}cm^{-1}$)] = 459 [18200], 490.5 [50600], 527 [85000].

General procedure for the synthesis of the target deprotected PBIs **4a–d**

A solution of the respective Boc-protected PBI **61a–d** (8 × 10^{-6} mol, 1 equiv.) in trifluoroacetic acid (3 mL) was stirred for 2 h at room temperature and subsequently concentrated *in vacuo*. MilliQ water (5 mL) was added to the residue, yielding a dark red solution, which was lyophilized twice to obtain pure compound. Yield: quantitatively for each, as a red fluffy solid.

PBI **4a**: MW ($C_{62}H_{72}F_{18}N_{10}O_{18}$) = 1587.26 g/mol; m.p.: > 400 °C; ^{1}H NMR ([D_6]DMSO): δ = 9.02 (d, *J* = 8.0, 4H), 8.72 (br. s, 4H), 8.62 (d, *J* = 7.8, 4H), 8.52 (br. s, 4H), 8.13 (t, *J* = 5.9, 2H), 7.88 (br. s, 6H), 5.56 (q, *J* = 6.9, 2H), 3.15 (dt, *J* = 7.8, *J* = 5.76), 2.99 – 2.86 (m, 20H), 1.89 (tt, *J* = 7.8, *J* = 7.4, 4H), 1.72 (tt, *J* = 7.6, *J* = 6.0, 4H), 1.64 (br. s, 8H), 1.58 (d, *J* = 7.0, 6H); HRMS (ESI pos.): *m/z* = 903.5239; calcd for $C_{50}H_{66}N_{10}O_6$ + H^+ : 903.5239; UV/Vis (H_2O, c = 5 × 10^{-7} M): λ_{max} (nm) [ε_{max} ($M^{-1}cm^{-1}$)] = 466 [18000], 497 [48500], 534 [77200]; fluorescence (H_2O, λ_{ex} = 475 nm): λ_{max} (nm) = 547; Φ_{fl} = 0.72.

PBI **4b**: MW ($C_{74}H_{80}F_{18}N_{10}O_{18}$) = 1739.45 g/mol; m.p.: > 400 °C; ^{1}H NMR ([D_6]DMSO): δ = 8.95 (d, *J* = 8.0, 4H, perylene protons), 8.72 (br. s, 4H, NH), 8.53 (br. d, *J* = 7.6, 6H, perylene protons, NH), 8.22 (t, *J* = 6.0, 2H, CH), 7.88 (br. s, 4H, NH_2), 7.05 (m, 10H, Ph-H), 5.82 (dd, *J* = 10.0, *J* = 5.2, 2H, CH_2), 3.65 (dd, *J* = 14.0, *J* = 5.6, 2H, CH_2), 3.17 (m, 4H, CH_2), 2.91 (m, 20H, CH_2), 1.89 (quintet, *J* = 7.2, 4H, CH_2), 1.73 (m, 4H, CH_2), 1.66 (br. s, 8H, CH_2); HRMS (ESI pos.): *m/z* = 1055.5865; calcd for $C_{62}H_{74}N_{10}O_6$ + H^+ : 1055.5866; UV/Vis (H_2O, c = 5 × 10^{-6} M): λ_{max} (nm) [ε_{max} ($M^{-1}cm^{-1}$)] = 469 [19400], 500 [52600], 537 [84900]; fluorescence (H_2O, λ_{ex} = 475 nm): λ_{max} (nm) = 549; Φ_{fl} = 0.79.

PBI **4c**: MW ($C_{62}H_{72}F_{18}N_{10}O_{18}$) = 1587.26 g/mol; m.p.: > 400 °C; ^{1}H NMR ([D_6]DMSO): δ = 9.01 (d, *J* = 8.6, 4H), 8.74 (br. s, 4H), 8.62 (d, *J* = 7.4, 4H), 8.53 (br. s, 4H), 8.13 (t, *J* = 6.4, 2H), 7.89 (br. s, 6H), 5.56 (q, *J* = 6.9, 2H), 3.15 (dt, *J* = 7.5, *J* = 8.0), 3.01 – 2.84 (m, 20H), 1.89 (tt, *J*

= 7.4, *J* = 7.5, 4H), 1.76 – 1.68 (m, 4H), 1.65 (br. s, 8H), 1.58 (d, *J* = 6.9, 6H); HRMS (ESI pos.): *m/z* = 903.5239; calcd for $C_{50}H_{66}N_{10}O_6 + H^+$: 903.5240.

PBI **4d**: MW ($C_{74}H_{80}F_{18}N_{10}O_{18}$) = 1739.45 g/mol; m.p.: > 400 °C; ^{1}H NMR ([D$_6$]DMSO): δ = 8.95 (d, *J* = 8.0, 4H, perylene protons), 8.78 (br. s, 4H, NH), 8.58 (br. s, 2H, NH), 8.53 (d, *J* = 8.0, 4H, perylene protons), 8.21 (t, *J* = 6.0, 2H, CH), 7.91 (br s, 4H, NH_2), 7.06 (m, 10H, Ph-H), 5.82 (dd, *J* = 10.4, *J* = 5.6, 2H, CH_2), 3.66 (dd, *J* = 14.4, *J* = 5.6, 2H, CH_2), 3.17 (br. s, 4H, CH_2), 2.93 (m, 20H, CH_2), 1.91 (quintet, *J* = 8.0, 4H CH_2), 1.73 (m, 4H, CH_2), 1.66 (br. s, 8H, CH_2); HRMS (ESI pos.): *m/z* = 1055.5866; calcd for $C_{62}H_{74}N_{10}O_6 + H^+$: 1055.5866.

General procedure for the synthesis of the neutral PBIs **5a** and **5b**[206]

A solution of the respective ^{t}Boc-protected *α*-amino acid **62a**, **b** (2.50 mmol, 1 equiv.), HATU (1 equiv.), dodecylamine (**63**, 1.2 equiv.) and Hünig's base (10 mL) in CH_2Cl_2 (150 mL) were stirred for 6 h at room temperature under argon atmosphere. The reaction solution was concentrated under reduced pressure. The oily residue was diluted with diethylether to obtain a precipitate, which was filtered and washed with diethylether. The combined organic phases were concentrated under reduced pressure and elutriated with *n*-hexane. The resulting solid was filtrated, dried under high vacuum and used without further purification. A solution of the crude product in CH_2Cl_2 (20 mL) and trifluoroacetic acid (3 mL) was stirred at room temperature. The reaction solution was concentrated under reduced pressure to yield the trifluoroacetate salts **64a**, **b** of the free amine.

64a: Yield: 85 % for both steps; MW ($C_{17}H_{33}F_3N_2O_3$) = 370.45 g/mol; ^{1}H NMR ($CDCl_3$): δ = 8.08 (br. s, 3H), 7.29 (t, *J* = 5.4, 1H), 4.15 (q, *J* = 6. 6, 1H), 3.28 - 3.07 (m, 2H), 1.48 (d, *J* = 6.9, 3H), 1.31 (br. s, 20H), 0.87 (t, *J* = 6.7, 3H); MS (MALDI, matrix: DCTB): *m/z* = 257.268; calcd for $C_{15}H_{32}N_2O + H^+$: 257.259.

64b: Yield: 72 % for both steps; MW ($C_{23}H_{37}F_3N_2O_3$) = 446.55 g/mol; ^{1}H NMR ($CDCl_3$): δ = 7.96 (br. s, 3H), 7.34 - 7.18 (m, 5H), 6.54 (t, *J* = 5.4, 1H), 4.15 (dd, *J* = 6.2, *J* = 2.6, 1H), 3.25

– 2.94 (m, 2H + 2H), 1.48 (d, *J* = 6.9, 3H), 1.24 (br. s, 20H), 0.88 (t, *J* = 6.7, 3H); MS (MALDI, matrix: DCTB): *m/z* = 333.304; calcd for $C_{26}H_{31}N_2O + H^+$: 333.290.

Perylene tetracarboxylic bisanhydride **54** (0.156 mmol, 1 equiv.), the appropriate *α*-ammonium dodecylamide trifluoroacetate salt **64a**, **b** (2 equiv.) and imidazole (430 mg) were mixed in a flask, which was flooded with argon for 15 minutes. The mixture was heated to 120 °C for 1 h and then cooled down to 90 °C. MeOH was added and the resulting precipitate was filtrated, washed with methanol and dried under high vacuum. The crude product was purified by column chromatography (SiO_2, CH_2Cl_2 : MeOH = 98.5 : 1.5).

PBI **5a**: Yield: 44 % (60 mg, 0.07 mmol) of an orange solid; R_f = 0.33 (SiO_2, CH_2Cl_2 : MeOH = 98.5 : 1.5); MW ($C_{54}H_{68}N_4O_6$) = 869.14 g/mol; m.p.: 321 °C; ^{1}H NMR ([D$_6$]DMSO): δ = 8.68 (d, *J* = 8.1, 4H), 8.50 (d, *J* = 7.9, 4H), 7.81 (t, *J* = 5.3, 2H), 5.46 (q, *J* = 7.0, 2H), 3.12 – 2.92 (m, 4H), 1.59 (d, *J* = 7.0, 6H), 1.62 (br. s, 4H), 1.67 (br. s, 36H), 0.79 (t, *J* = 6.8, 6H); HRMS (ESI pos.): *m/z* = 869.5211; calcd for $C_{54}H_{68}N_4O_6 + H^+$: 869.5212; UV/Vis ($CHCl_3$): λ_{max} (nm) [ε_{max} ($M^{-1}cm^{-1}$)] = 460 [18900],491 [52300], 528 [86600].

PBI **5b**: Yield: 19 % (31 mg, 0.03 mmol) of a deep red solid; R_f = 0.44 (SiO_2, CH_2Cl_2 : MeOH = 98.5 : 1.5); MW ($C_{66}H_{76}N_4O_6$) = 1021.33 g/mol; m.p.: 123 °C; ^{1}H NMR ([D$_6$]DMSO): δ = 8.76 (d, *J* = 8.6, 4H), 8.43 (d, *J* = 8.0, 4H), 7.93 (t, *J* = 5.4, 2H), 7.15 – 6.98 (m, 10H), 5.76 (dd, *J* = 5.3, *J* = 5.4, 2H), 3.67 (dd, *J* = 5.4, *J* = 8.6, 2H), 3.16 – 2.96 (m, 4H), 1.36 (br. s, 4H), 1.33 and 1.89 (br. s, 36H), 0.78 (t, *J* = 6.7, 6H); one proton signal (2H) is superposed by the signal of water; HRMS (ESI pos.): *m/z* = 1043.5657; calcd for $C_{66}H_{76}N_4O_6 + Na^+$: 1043.5657; UV/Vis ($CHCl_3$): λ_{max} (nm) [ε_{max} ($M^{-1}cm^{-1}$)] = 461 [19500],492 [53600], 528 [86000].

Synthesis of compounds in Chapter 5

66: Di-*t*-butyl dicarbonate (7.28 mL, 34.0 mmol) dissolved in CH_2Cl_2 (150 mL) was dropped within one hour to a mixture of 1,13-diamino-4,7,10-trioxatridecane (**65**, 15.0 g, 15.0 mL, 68.1 mmol) and *N*,*N*'-diisopropylethylamine (6.12 mL, 36.0 mmol) under

an argon atmosphere. The mixture was stirred for two more hours and concentrated under vacuum. The residue was purified by column chromatography (SiO_2, CH_2Cl_2 : MeOH : NEt_3 = 8.7 : 0.8 : 0.5; R_f = 0.5) to obtain a slightly yellowish oil in 62 % yield (6.76 g, 21.1 mmol). MW ($C_{15}H_{32}N_2O_5$) = 320.42 g/mol; R_f = 0.5 (CH_2Cl_2 : MeOH : NEt_3 = 8.7 : 0.8 : 0.5); ^{1}H NMR ($CDCl_3$): δ = 5.13 (br. s, 1H, CON*H*), 3.67 – 3.51 (m, 12H, OC*H*$_2$), 3.22 (d, 2H), 2.84 (t, 2H, *J* = 6.6), 2.39 (s, 2H, N*H*$_2$), 1.82 – 1.68 (m, 4H, $CH_2CH_2CH_2$), 1.44 (s, 9H); HRMS (ESI pos.): *m/z* = 321.23780, calcd for $C_{15}H_{32}N_2O_5 + H^+$: 321.23891.

PBI **67**: Perylene tetracarboxylic acid bisanhydride (**54**, 200 mg, 0.51 mmol) and **66** (1.96 g, 6.12 mmol) were stirred in DMF (5 mL) at 80 °C under an argon atmosphere for 3 h. The reaction mixture was purified by column chromatography (SiO_2, CH_2Cl_2 : MeOH = 19 : 1). A red solid was obtained in 70 % yield (356 mg, 0.357 mmol). MW ($C_{54}H_{68}N_4O_{14}$) = 997.14; R_f = 0.8 (CH_2Cl_2 : MeOH = 9 : 1); m.p. 193 – 204 °C; ^{1}H NMR ($CDCl_3$): δ = 8.60 (d, *J* = 8.0, 4H, Pery-H), 8.50 (d, *J* = 8.2, 4H, Pery-H), 5.03 (br. s, 2H, CON*H*), 4.31 (t, *J* = 7.2, 4H, NC*H*$_2$), 3.68 – 3.50 (m, 24H, OC*H*$_2$), 3.21 (m, 4H), 2.08 (quintet, *J* = 6.8, 4H), 1.74 (quintet, *J* = 6.2, 4H), 1.43 (s, 18H); HRMS (ESI pos.): *m/z* = 1019.46378, calcd for $C_{54}H_{68}N_4O_{14}$ + Na: 1019.46262.

PBI **68**: To a solution of **67** (104 mg, 0.11 mmol) in dry CH_2Cl_2 (4.0 mL) freshly distilled trifluoroacetic acid (1.0 mL) was added under an argon atmosphere. The mixture was stirred for 2 h at room temperature and concentrated under vacuum. Water (20 mL) was added and the solution lyophilized (20 h, 0.001 mbar). A red solid (83.5 mg, 0.08 mmol) was obtained in 78 % yield. It was used without further purification. MW ($C_{48}H_{54}F_6N_4O_{14}$) = 1024.95; ^{1}H NMR ([D_6]DMSO): δ = 8.75 (d, *J* = 8.4, 4H, perylene-H), 8.44 (d, *J* = 8.0, 4H, perylene-H), 7.62 (br. s, 4H, NH_2), 4.13 (t, *J* = 7.1, 4H), 3.6 – 3.4 (m, 28H), 1.91 (quintet, *J* = 6.8, 4H), 1.74 (quintet, *J* = 6.7, 4H).

PBI **6**: Acridin-9-carboxylic acid hydrate (**69**, 63.6 mg, 0.26 mmol) and 1-[bis(dimethylamino)methylene]-1H-1,2,3-triazolo[4,5-b]pyridinium 3-oxid hexafluoro-phosphate (HATU, 107 mg, 0.28 mmol, 1.1 equiv.) were suspended in DMF (1.60 mL). *N*,*N*'-diisopropylethylamine (0.07 mL, 0.41 mmol, 1.6 equiv.) was added to the bright

yellow suspension. About 3 min. after addition of the base a clear yellow solution was formed. After about 5 more minutes a yellow solid precipitated. The diamine PBI **68** (128 mg, 0.13 mmol) was added to this suspension. After about 10 min a red solution has been formed. The reaction solution was stirred for 20 min and transferred into a separatory funnel with CH_2Cl_2 (50 mL). The organic phase was washed with water (3 x 50 mL). The organic phase was dried over magnesium sulphate and the solvent was removed *in vacuo*. The residual crude product was purified by column chromatography (SiO_2, CH_2Cl_2 : MeOH = 19 : 1) to obtain PBI **6** as a red solid (130 mg, 0.11 mmol) in 86 % yield. MW ($C_{72}H_{66}N_6O_{12}$) = 1207.33; m.p.: 107 °C; ^{1}H NMR ($CDCl_3$): δ = 8.30 (d, ^3J = 8.0, 4H, perylene-H), 8.23 (d, ^3J = 8.1, 4H, perylene-H), 8.03 (d, ^3J = 8.6, 4H, acridine-H),7.95 (d, ^3J = 8.8, 4H, acridine-H), 7.63 (m, 4H, acridine-H), 7.50 (m, 4H, acridine-H), 4.11 (t, ^3J = 7.9, 4H, NCH_2), 3.87 (q, ^3J = 6.2, 4H), 3.73 (t, ^3J = 5.7, 4H), 3.57 – 3.55 (m, 4H), 3.43 – 3.40 (m, 8H), 3.15 (s, 8H), 2.11 (quintet, 4H), 1.90 (quintet, 4H). HRMS (ESI-pos): 1207.48430, calcd for $C_{72}H_{66}N_6O_{12}$ +H = 1207.48115; UV/Vis (6 x 10^{-7} M; $CHCl_3$): λ_{max} (nm) [ε_{max} ($M^{-1}cm^{-1}$)] = 528 [83000], 492 [52000], 460 [19900]; fluorescence ($CHCl_3$): λ_{max} (nm) = 536; Φ_{fl} = 0.66 ± 0.15 (against perylene standard); elemental analysis, found: C 69.90, H 5.51, N 6.69; calcd for $C_{72}H_{66}N_6O_{12}\cdot 1.5\ H_2O$ = M + 1.5 H_2O: C 70.06, H 5.63, N 6.81.

References

[1] T. D. Hamilton, L. R. MacGillivray, in *Encycl. Supramol. Chem.* (Eds.: L. Atwood, J.W. Steed), Dekker, New York, **2004**, p. 1257.

[2] F. Würthner, *Chem. Commun.* **2004**, 1564–1579.

[3] Z. Chen, A. Lohr, C. R. Saha-Möller, F. Würthner, *Chem. Soc. Rev.* **2009**, *38*, 564–584.

[4] S. Nakazono, S. Easwaramoorthi, D. Kim, H. Shinokubo, A. Osuka, *Org. Lett.* **2009**, 11–14.

[5] S. Nakazono, Y. Imazaki, H. Yoo, J. Yang, T. Sasamori, N. Tokitoh, T. Cédric, H. Kageyama, D. Kim, H. Shinokubo, A. Osuka, *Chem. Eur. J.* **2009**, *15*, 7530–7533.

[6] T. Teraoka, S. Hiroto, H. Shinokubo, *Org. Lett.* **2011**, *13*, 2532–2535.

[7] C. Kohl, T. Weil, J. Qu, K. Müllen, *Chem. Eur. J.* **2004**, *10*, 5297–5310.

[8] J. Qu, C. Kohl, M. Pottek, K. Müllen, *Angew. Chem. Int. Ed.* **2004**, *43*, 1528–1531.

[9] T. Weil, T. Vosch, J. Hofkens, K. Peneva, K. Müllen, *Angew. Chem. Int. Ed.* **2010**, *49*, 9068–9093.

[10] C. D. Schmidt, A. Hirsch, in *Ideas Chem. Mol. Sci. Adv. Synth. Chem.*, Wiley-VCH, Weinheim, **2010**, pp. 283–304.

[11] C. Li, H. Wonneberger, *Adv. Mater.* **2012**, *24*, 613–636.

[12] J. L. Finney, *Philos. Trans. R. Soc. Lond. B. Biol. Sci.* **2004**, *359*, 1145–1163.

[13] P. Ball, *Chem. Rev.* **2008**, *108*, 74–108.

[14] T. H. Lilley, *Philos. Trans. R. Soc. Lond. B. Biol. Sci.* **2004**, *359*, 1321–1322.

[15] T. Rehm, C. Schmuck, *Chem. Commun.* **2008**, 801–813.

[16] T. H. Rehm, C. Schmuck, *Chem. Soc. Rev.* **2010**, *39*, 3597–3611.

[17] H. Ringsdorf, B. Schlarb, J. Venzmer, *Angew. Chem. Int. Ed.* **1988**, *27*, 113–158.

[18] J. H. Fuhrhop, D. Fritsch, *Acc. Chem. Res.* **1986**, *19*, 130–137.

[19] G. H. Escamilla, G. R. Newkome, *Angew. Chem. Int. Ed.* **2008**, *33*, 1937–1940.

[20] J.-H. Fuhrhop, T. T. Wang, *Chem. Rev.* **2004**, *104*, 2901–2937.

[21] F. J. M. Hoeben, P. Jonkheijm, E. W. Meijer, A. P. H. J. Schenning, *Chem. Rev.* **2005**.

[22] J. K. Klosterman, Y. Yamauchi, M. Fujita, *Chem. Soc. Rev.* **2009**, *38*, 1714–1725.

[23] S. Grimme, *Angew. Chem. Int. Ed.* **2008**, *47*, 3430–3434.

[24] C. A. Hunter, K. R. Lawson, J. Perkins, C. J. Urch, *J. Chem. Soc. Perkin Trans. 2* **2001**, 651–669.

[25] M. L. Waters, *Curr. Opin. Chem. Biol.* **2002**, *6*, 736–741.

[26] B. W. Blokzijl, J. B. F. N. Engberts, *Angew. Chem. Int. Ed.* **1993**, *32*, 1545–1579.

[27] E. Meyer, R. Castellano, F. Diederich, *Angew. Chem. Int. Ed.* **2003**, *42*, 1210–1250.

[28] K. Igarashi, K. Kashiwagi, *Int. J. Biochem. Cell Biol.* **2010**, *42*, 39–51.

[29] A. E. Pegg, *IUBMB Life* **2014**, *66*, 8–18.

[30] R. Montañez, F. Sánchez-Jiménez, J. F. Aldana-Montes, M. Á. Medina, *Amino Acids* **2007**, *33*, 283–289.

[31] W. E. Ford, *J. Photochem.* **1987**, *37*, 189–204.

[32] Z. Chen, V. Stepanenko, V. Dehm, P. Prins, L. D. a Siebbeles, J. Seibt, P. Marquetand, V. Engel, F. Würthner, *Chem. Eur. J.* **2007**, *13*, 436–449.

[33] J. R. Lakowicz, *Principles of Fluorescence Spectroscopy*, Kluwer Academic Plenum Publishers, New York, **1999**.

[34] T. Deligeorgiev, D. Zaneva, I. Petkov, I. Timcheva, R. Sabins, *Dyes Pigments* **1994**, *24*, 75–81.

[35] R. A. Bissell, A. P. de Silva, H. Q. N. Gunaratne, P. L. M. Lynch, G. E. M. Maguire, K. R. A. S. Sandanayake, *Chem. Soc. Rev.* **1992**, *21*, 187–195.

[36] L. M. Daffy, A. P. de Silva, H. Q. N. Gunaratne, C. Huber, P. L. M. Lynch, T. Werner, O. S. Wolfbeis, *Chem. Eur. J.* **1998**, *4*, 1810–1815.

[37] G. Schnurpfeil, J. Stark, D. Wöhrle, *Dyes Pigments* **1995**, *27*, 339–350.

[38] Y. Nagao, *Prog. Org. Coatings* **1997**, *31*, 43–49.

[39] N. I. Georgiev, A. R. Sakr, V. B. Bojinov, *Dyes Pigments* **2011**, *91*, 332–339.

[40] W. Zhang, S.-Y. Gan, F.-H. Li, D.-X. Han, Q.-X. Zhang, L. Niu, *RSC Adv.* **2015**, *5*, 2207–2212.

[41] M. Marcia, P. Singh, F. Hauke, M. Maggini, A. Hirsch, *Org. Biomol. Chem.* **2014**, *12*, 7045–58.

[42] H. Wu, H. Wang, L. Xue, Y. Shi, X. Li, *J. Phys. Chem. B* **2010**, *114*, 14420–14425.

[43] B. Wang, F. Wang, H. Jiao, X. Yang, C. Yu, *Analyst* **2010**, *135*, 1986–1991.

[44] B. Wang, Q. Zhu, D. Liao, C. Yu, *J. Mater. Chem.* **2011**, *21*, 4821–4826.

[45] B. Wang, C. Yu, *Angew. Chem. Int. Ed.* **2010**, *49*, 1485–1488.

[46] Z. Lv, J. Liu, W. Bai, S. Yang, A. Chen, *Biosens. Bioelectron.* **2015**, *64*, 530–534.

[47] X. Yang, F. Pu, J. Ren, X. Qu, *Chem. Commun.* **2011**, *47*, 8133–8135.

[48] R. Zhou, B. Li, N. Wu, G. Gao, J. You, J. Lan, *Chem. Commun.* **2011**, *47*, 6668–6670.

[49] S. Malkondu, *Tetrahedron* **2014**, *70*, 5580–5584.

[50] S. Malkondu, S. Erdemir, *Dyes Pigments* **2015**, *113*, 763–769.

[51] J. Lin, C. Zhu, X. Liu, B. Chen, Y. Zhang, J. Xue, J. Liu, *Chinese J. Chem.* **2014**, *32*, 1116–1120.

[52] L. Yan, L. Yang, J. Lan, J. You, *Sci. China, Ser. B Chem.* **2009**, *52*, 518–522.

[53] X. Liu, N. Zhang, J. Zhou, T. Chang, C. Fang, D. Shangguan, *Analyst* **2013**, *138*, 901–906.

[54] J. Lydon, *J. Mater. Chem.* **2010**, *20*, 10071–10099.

[55] J. Lydon, *Curr. Opin. Colloid Interface Sci.* **2004**, *8*, 480–490.

[56] J. Lydon, *Handbook of Liquid Crystals*, Wiley-VCH, Weinheim, **1998**.

[57] I. K. Iverson, S.-W. Tam-Chang, *J. Am. Chem. Soc.* **1999**, 5801–5802.

[58] I. K. Iverson, S. M. Casey, W. Seo, S. W. Tam-Chang, B. A. Pindzola, *Langmuir* **2002**, *18*, 3510–3516.

[59] S. W. Tam-Chang, I. K. Iverson, J. Helbley, *Langmuir* **2004**, *20*, 342–347.

[60] S. W. Tam-Chang, J. Helbley, I. K. Iverson, *Langmuir* **2008**, *24*, 2133–2139.

[61] J. J. Naidu, Y. Bae, K. Jeong, S. H. Lee, S. Kang, M. Lee, *Bull. Korean Chem. Soc.* **2009**, *30*, 935–937.

[62] Y. Guan, Y. Zakrevskyy, J. Stumpe, M. Antonietti, C. F. J. Faul, *Chem. Commun.* **2003**, 894–895.

[63] Y. Zakrevskyy, C. F. J. Faul, Y. Guan, J. Stumpe, *Adv. Funct. Mater.* **2004**, *14*, 835–841.

[64] Y. Huang, Y. Yan, B. M. Smarsly, Z. Wei, C. F. J. Faul, *J. Mater. Chem.* **2009**, *19*, 2356–2362.

[65] T. Ma, C. Li, G. Shi, *Langmuir* **2008**, *24*, 43–48.

[66] M. Kumar, S. J. George, *Chem. Sci.* **2014**, *5*, 3025–3030.

[67] T. A. Everett, D. A. Higgins, *Langmuir* **2009**, *25*, 13045–13051.

[68] C. R. Weitzel, T. A. Everett, D. A. Higgins, *Langmuir* **2009**, *25*, 1188–1195.

[69] C. Rodríguez-Abreu, C. Aubery-Torres, C. Solans, A. López-Quintela, G. J. T. Tiddy, *ACS Appl. Mater. Interfaces* **2011**, *3*, 4133–4141.

[70] Q. Chen, B. J. Worfolk, T. C. Hauger, U. Al-Atar, K. D. Harris, J. M. Buriak, *ACS Appl. Mater. Interfaces* **2011**, *3*, 3962–3970.

[71] K. V. Rao, S. J. George, *Chem. Eur. J.* **2012**, *18*, 14286–14291.

[72] M. Supur, S. Fukuzumi, *Phys. Chem. Chem. Phys.* **2013**, *15*, 2539–2546.

[73] M. Supur, S. Fukuzumi, *J. Phys. Chem. C* **2012**, *116*, 23274–23282.

[74] M. Supur, K. Ohkubo, S. Fukuzumi, *Chem. Commun.* **2014**, *50*, 13359–13361.

[75] Y. Huang, B. Quan, Z. Wei, G. Liu, L. Sun, *J. Phys. Chem. C* **2009**, 3929–3933.

[76] B. Russ, M. J. Robb, F. G. Brunetti, P. L. Miller, E. E. Perry, S. N. Patel, V. Ho, W. B. Chang, J. J. Urban, M. L. Chabinyc, C. J. Hawker, R. A. Segalman, *Adv. Mater.* **2014**, *26*, 3473–3477.

[77] L. Zhao, T. Ma, H. Bai, G. Lu, C. Li, G. Shi, *Langmuir* **2008**, *24*, 4380–4387.

[78] G. M. Blackburn, M. J. Gait, D. Loakes, D. M. Williams, Eds., *Nucleic Acids in Chemistry and Biology*, RSC Publishing, Cambridge, **2006**.

[79] M. Demeunynck, C. Bailly, W. Wilson, Eds., *Small Molecule DNA and RNA Binders: From Synthesis to Nucleic Acid Complexes*, Wiley-VCH, Weinheim, **2002**.

[80] S. M. Kerwin, *Curr. Pharm. Des.* **2000**, *6*, 441–471.

[81] J.-L. Mergny, C. Hélène, *Nat. Med.* **1998**, *4*, 1366–1367.

[82] Z. Xu, K. Guo, J. Yu, H. Sun, J. Tang, J. Shen, K. Müllen, W. Yang, M. Yin, *Small* **2014**, *10*, 4087–4092.

[83] O. Y. Fedoroff, M. Salazar, H. Han, V. V Chemeris, S. M. Kerwin, L. H. Hurley, *Biochemistry* **1998**, *37*, 12367–12374.

[84] S. Neidle, M. A. Read, *Biopolymers* **2001**.

[85] H. Han, L. H. Hurley, *Trends Pharmacol. Sci.* **2000**, *21*, 136–142.

[86] W. Tuntiwechapikul, T. Taka, M. Béthencourt, L. Makonkawkeyoon, T. Randall Lee, *Bioorganic Med. Chem. Lett.* **2006**, *16*, 4120–4126.

[87] J. T. Kern, P. W. Thomas, S. M. Kerwin, *Biochemistry* **2002**, *41*, 11379–11389.

[88] S. M. Kerwin, G. Chen, J. T. Kern, P. W. Thomas, *Bioorg. Med. Chem. Lett.* **2002**, *12*, 447–450.

[89] L. Rossetti, M. Franceschin, S. Schirripa, A. Bianco, G. Ortaggi, M. Savino, *Bioorg. Med. Chem. Lett.* **2005**, *15*, 413–420.

[90] M. Franceschin, C. M. Lombardo, E. Pascucci, D. D'Ambrosio, E. Micheli, A. Bianco, G. Ortaggi, M. Savino, *Bioorg. Med. Chem.* **2008**, *16*, 2292–2304.

[91] D. D'Ambrosio, P. Reichenbach, E. Micheli, A. Alvino, M. Franceschin, M. Savino, J. Lingner, *Biochimie* **2012**, *94*, 854–863.

[92] S. Krauß, M. Lysetska, F. Würthner, *Lett. Org. Chem.* **2005**, *2*, 349–353.

[93] C. W. Tabor, H. Tabor, *Metab. Clin. Exp.* **1984**, 749–790.

[94] G. Iacomino, G. Picariello, L. D'Agostino, *Biochim. Biophys. Acta - Mol. Cell Res.* **2012**, *1823*, 1745–1755.

[95] V. Vijayanathan, E. Agostinelli, T. Thomas, T. J. Thomas, *Amino Acids* **2014**, *46*, 499–509.

[96] H. Szelke, S. Schübel, J. Harenberg, R. Krämer, *Chem. Commun.* **2010**, *46*, 1667–1669.

[97] H. Szelke, S. Schübel, J. Harenberg, R. Krämer, *Bioorganic Med. Chem. Lett.* **2010**, *20*, 1445–1447.

[98] F. Würthner, V. Stepanenko, Z. Chen, C. R. Saha-Möller, N. Kocher, D. Stalke, *J. Org. Chem.* **2004**, 7933–7939.

[99] R. K. Dubey, A. Efimov, H. Lemmetyinen, *Chem. Mater.* **2011**, *23*, 778–788.

[100] T. H. Rehm, M. R. Stojković, S. Rehm, M. Škugor, I. Piantanida, F. Würthner, *Chem. Sci.* **2012**, *3*, 3393–3397.

[101] J. Gershberg, M. R. Stojković, M. Škugor, S. Tomić, T. H. Rehm, S. Rehm, C. R. Saha-Möller, I. Piantanida, F. Würthner, *Chem. Eur. J.* **2015**, *21*, 7886–7895.

[102] S. Rehm, V. Stepanenko, X. Zhang, T. H. Rehm, F. Würthner, *Chem. Eur. J.* **2010**, *16*, 3372–3382.

[103] H. Zollinger, *Color Chemistry*, Wiley-VCH, Weinheim, **2003**.

[104] W. Herbst, K. Hunger, *Industrial Organic Pigments: Production, Properties, Applications*, Wiley-VCH, Weinheim, **1997**.

[105] H. Langhals, *Heterocycles* **1995**, *40*, 477–500.

[106] F. C. De Schryver, T. Vosch, M. Cotlet, M. Van Der Auweraer, K. Müllen, J. Hofkens, *Acc. Chem. Res.* **2005**, *38*, 514–522.

[107] C. Flors, I. Oesterling, T. Schnitzler, E. Fron, G. Schweitzer, M. Sliwa, A. Herrmann, M. Van Der Auweraer, F. C. De Schryver, K. Müllen, J. Hofkens, *J. Phys. Chem. C* **2007**, *111*, 4861–4870.

[108] D. Wöhrle, D. Meissner, *Adv. Mater.* **1991**, *3*, 129–138.

[109] C. J. Brabec, N. S. Sariciftci, J. C. Hummelen, *Adv. Funct. Mater.* **2001**, *11*, 15–26.

[110] L. Schmidt-Mende, A. Fechtenkötter, K. Müllen, E. Moons, R. H. Friend, J. D. MacKenzie, *Science* **2001**, *293*, 1119–1122.

[111] M. Sommer, M. Thelakkat, *Eur. Phys. J. Appl. Phys.* **2006**, *36*, 245–249.

[112] P. Ranke, I. Bleyl, J. Simmerer, D. Haarer, A. Bacher, H. W. Schmidt, *Appl. Phys. Lett.* **1997**, *71*, 1332–1334.

[113] C. Ego, D. Marsitzky, S. Becker, J. Zhang, A. C. Grimsdale, K. Müllen, J. D. MacKenzie, C. Silva, R. H. Friend, *J. Am. Chem. Soc.* **2003**, *125*, 437–443.

[114] F. Jaiser, D. Neher, A. Meisel, H. G. Nothofer, T. Miteva, A. Herrmann, K. Müllen, U. Scherf, *J. Chem. Phys.* **2008**, *129*, 114901(1–9).

[115] P. R. L. Malenfant, C. D. Dimitrakopoulos, J. D. Gelorme, L. L. Kosbar, T. O. Graham, A. Curioni, W. Andreoni, *Appl. Phys. Lett.* **2002**, *80*, 2517–2519.

[116] B. A. Jones, M. J. Ahrens, M. H. Yoon, A. Facchetti, T. J. Marks, M. R. Wasielewski, *Angew. Chem. Int. Ed.* **2004**, *43*, 6363–6366.

[117] R. Schmidt, M. M. Ling, J. H. Oh, M. Winkler, M. Könemann, Z. Bao, F. Würthner, *Adv. Mater.* **2007**, *19*, 3692–3695.

[118] V. Gorteau, G. Bollot, J. Mareda, S. Matile, *Org. Biomol. Chem.* **2007**, *5*, 3000–3012.

[119] A. Perez-Velasco, V. Gorteau, S. Matile, *Angew. Chem. Int. Ed.* **2008**, *47*, 921–923.

[120] S. Hagihara, L. Gremaud, G. Bollot, J. Mareda, S. Matile, *J. Am. Chem. Soc.* **2008**, *130*, 4347–4351.

[121] J. Mareda, S. Matile, *Chem. – A Eur. J.* **2009**, *15*, 28–37.

[122] J. Hofkens, T. Vosch, M. Maus, F. Köhn, M. Cotlet, T. Weil, A. Herrmann, K. Müllen, F. C. De Schryver, *Chem. Phys. Lett.* **2001**, *333*, 255–263.

[123] A. C. Grimsdale, K. Müllen, *Angew. Chem. Int. Ed.* **2005**, *44*, 5592–5629.

[124] M. Sliwa, C. Flors, I. Oesterling, J. Hotta, K. Müllen, F. C. De Schryver, J. Hofkens, *J. Phys. Condens. Matter* **2007**, *19*, 445004 (1–14).

[125] S. M. Melnikov, E. K. L. Yeow, H. Uji-i, M. Cotlet, K. Müllen, F. C. De Schryver, J. Enderlein, J. Hofkens, *J. Phys. Chem. B* **2007**, *111*, 708–719.

[126] K. Peneva, G. Mihov, F. Nolde, S. Rocha, J. Hotta, K. Braeckmans, J. Hofkens, H. Uji-i, A. Herrmann, K. Müllen, *Angew. Chem. Int. Ed.* **2008**, *47*, 3372–3375.

[127] N. Rahe, C. Rinn, T. Carell, *Chem. Commun.* **2003**, 2119–2121.

[128] W. Wang, W. Wan, H.-H. Zhou, S. Niu, A. D. Q. Li, *J. Am. Chem. Soc.* **2003**, *125*, 5248–5249.

[129] Y. Zheng, H. Long, G. C. Schatz, F. D. Lewis, *Chem. Commun.* **2005**, 4795–4797.

[130] C. Wagner, H. A. Wagenknecht, *Org. Lett.* **2006**, *8*, 4191–4194.

[131] D. Baumstark, H.-A. Wagenknecht, *Angew. Chem. Int. Ed.* **2008**, *47*, 2612–2614.

[132] D. Baumstark, H. A. Wagenknecht, *Chem.Eur. J.* **2008**, *14*, 6640–6645.

[133] T. A. Zeidan, R. Carmieli, R. F. Kelley, T. M. Wilson, F. D. Lewis, M. R. Wasielewski, *J. Am. Chem. Soc.* **2008**, *130*, 13945–13955.

[134] M. Hariharan, Y. Zheng, H. Long, T. A. Zeidan, G. C. Schatz, J. Vura-Weis, M. R. Wasielewski, X. Zuo, D. M. Tiede, F. D. Lewis, *J. Am. Chem. Soc.* **2009**, *131*, 5920–5929.

[135] X. Zhang, Z. Chen, F. Würthner, *J. Am. Chem. Soc.* **2007**, *129*, 4886–4887.

[136] E. Shirman, A. Ustinov, N. Ben-Shitrit, H. Weissman, M. A. Iron, R. Cohen, B. Rybtchinski, *J. Phys. Chem. B* **2008**, *112*, 8855–8858.

[137] J. Baram, E. Shirman, N. Ben-Shitrit, A. Ustinov, H. Weissman, I. Pinkas, S. G. Wolf, B. Rybtchinski, *J. Am. Chem. Soc.* **2008**, *130*, 14966–14967.

[138] G. Golubkov, H. Weissman, E. Shirman, S. G. Wolf, I. Pinkas, B. Rybtchinski, *Angew. Chem. Int. Ed.* **2009**, *48*, 926–930.

[139] E. Krieg, E. Shirman, H. Weissman, E. Shimoni, S. G. Wolf, I. Pinkas, B. Rybtchinski, *J. Am. Chem. Soc.* **2009**, *131*, 14365–14373.

[140] X. Zhang, S. Rehm, M. M. Safont-Sempere, F. Würthner, *Nat. Chem.* **2009**, *1*, 623–629.

[141] A. Ebel, W. Donaubauer, F. Hampel, A. Hirsch, *Eur. J. Org. Chem.* **2007**, *2007*, 3488–3494.

[142] C. Backes, C. D. Schmidt, F. Hauke, C. Böttcher, A. Hirsch, *J. Am. Chem. Soc.* **2009**, *131*, 2172–2184.

[143] C. D. Schmidt, C. Böttcher, A. Hirsch, *Eur. J. Org. Chem.* **2007**, 5497–5505.

[144] C. Backes, F. Hauke, C. D. Schmidt, A. Hirsch, *Chem. Commun.* **2009**, 2643–2645.

[145] C. Ehli, C. Oelsner, D. M. Guldi, A. Mateo-Alonso, M. Prato, C. Schmidt, C. Backes, F. Hauke, A. Hirsch, *Nat. Chem.* **2009**, *1*, 243–249.

[146] C. D. Schmidt, C. Bòttcher, A. Hirsch, *Eur. J. Org. Chem.* **2009**, 5337–5349.

[147] H. Langhals, W. Jona, F. Einsiedl, S. Wohnlich, *Adv. Mat.* **1998**, *10*, 1022–1024.

[148] Y. Jeon, T. Lim, C. Lee, J. Cheon, M. Gong, *J. Indian Chem. Soc.* **2007**, *13*, 518–522.

[149] Y. Liu, K.-R. Wang, D.-S. Guo, B.-P. Jiang, *Adv. Funct. Mater.* **2009**, *19*, 2230–2235.

[150] H.-A. Klok, J. R. Hernández, S. Becker, K. Müllen, *J. Polym. Sci. Part A Polym. Chem.* **2001**, *39*, 1572–1583.

[151] T. Weil, M. A. Abdalla, C. Jatzke, J. Hengstler, K. Müllen, *Biomacromolecules* **2005**, *6*, 68–79.

[152] J. T. Kern, S. M. Kerwin, *Bioorg. Med. Chem. Lett.* **2002**, *12*, 3395–3398.

[153] J. Zhou, G. Yuan, J. Liu, C.-G. Zhan, *Chem. Eur. J.* **2007**, *13*, 945–949.

[154] R. Samudrala, X. Zhang, R. M. Wadkins, D. L. Mattern, *Bioorg. Med. Chem.* **2007**, *15*, 186–93.

[155] A. Margineanu, J. Hofkens, M. Cotlet, S. Habuchi, A. Stefan, J. Qu, C. Kohl, K. Müllen, J. Vercammen, Y. Engelborghs, T. Gensch, F. C. De Schryver, *J. Phys. Chem. B* **2004**, *108*, 12242–12251.

[156] R. A. Casero, P. M. Woster, *J. Med. Chem.* **2009**, *52*, 4551–4573.

[157] M. A. Grillo, *Int. J. Biochem.* **1985**, *17*, 943–948.

[158] A. U. Khan, Y. H. Mei, T. Wilson, *PNAS* **1992**, *89*, 11426–11427.

[159] V. A. Bloomfield, *Biopolymers* **1997**.

[160] J. S. Lewis, T. J. Thomas, A. Shirahata, T. Thomas, *Biomacromolecules* **2000**, *1*, 339–349.

[161] C. Wang, J.-G. Delcros, J. Biggerstaff, Phanstiel, *J. Med. Chem.* **2003**, *46*, 2663–2671.

[162] V. M. Johansson, M. F. Miniotis, C. Hegardt, G. Jönsson, J. Staaf, P. S. H. Berntsson, S. M. Oredsson, K. Alm, *Cell Biol. Int.* **2008**, *32*, 1467–1477.

[163] A. R. Khomutov, T. A. Keinanen, N. A. Grigorenko, M. T. Hyvonen, A. Uimari, M. Pietila, M. Cerrada-Gimenez, A. R. Simonian, M. A. Khomutov, J. Vepsalainen, L. Alhonen, J. Janne, *Mol. Biol.* **2009**, *43*, 249–259.

[164] L. Rossetti, M. Franceschin, A. Bianco, G. Ortaggi, M. Savino, *Bioorg. Med. Chem. Lett.* **2002**, *12*, 2527–2533.

[165] M. Franceschin, A. Alvino, G. Ortaggi, A. Bianco, *Tetrahedron Lett.* **2004**, *45*, 9015–9020.

[166] A. Alvino, M. Franceschin, C. Cefaro, S. Borioni, G. Ortaggi, A. Bianco, *Tetrahedron* **2007**, *63*, 7858–7865.

[167] E. Micheli, C. M. Lombardo, D. D'Ambrosio, M. Franceschin, S. Neidle, M. Savino, *Bioorg. Med. Chem. Lett.* **2009**, *19*, 3903–3908.

[168] G. H. Escamilla, G. R. Newkome, *Angew. Chem. Int. Ed.* **1994**, *33*, 1937–1940.

[169] A. J. Geall, I. S. Blagbrough, *Tetrahedron* **2000**, *56*, 2449–2460.

[170] F. Würthner, C. Thalacker, S. Diele, C. Tschierske, *Chem.Eur. J.* **2001**, *7*, 2245–2253.

[171] Z. Chen, U. Baumeister, C. Tschierske, F. Würthner, *Chem. Eur. J.* **2007**, *13*, 450–465.

[172] C. Hippius, I. H. M. van Stokkum, E. Zangrando, R. M. Williams, M. Wykes, D. Beljonne, F. Würthner, *J. Phys. Chem. C* **2008**, *112*, 14626–14638.

[173] J. J. Han, A. D. Shaller, W. Wang, A. D. Q. Li, *J. Am. Chem. Soc.* **2008**, *130*, 6974–6982.

[174] E. Schwartz, V. Palermo, C. E. Finlayson, Y.-S. Huang, M. B. J. Otten, A. Liscio, S. Trapani, I. González-Valls, P. Brocorens, J. J. L. M. Cornelissen, K. Peneva, K. Müllen, F. C. Spano, A. Yartsev, S. Westenhoff, R. H. Friend, D. Beljonne, R. J M Nolte, P. Samorì, A. E. Rowan, *Chem. Eur. J.* **2009**, *15*, 2536–2547.

[175] D. Aikens, S. Bunce, F. Onasch, R. Parker, C. Hurwitz, S. Clemans, *Biophys. Chem.* **1983**, *17*, 67–74.

[176] H. Geneste, M. Hesse, *Chem. unserer Zeit* **1998**, *32*, 206–218.

[177] Z. R. Liu, R. L. Rill, *Anal. Biochem.* **1996**, *236*, 139–145.

[178] J. Suh, H. J. Paik, B. K. Hwang, *Bioorg. Chem.* **1994**, *22*, 318–327.

[179] H.-J. Schneider, L. Tianjun, N. Lomadze, *Angew. Chem. Int. Ed.* **2003**, *42*, 3544–3546.

[180] R. F. Fink, J. Seibt, V. Engel, M. Renz, M. Kaupp, S. Lochbrunner, H.-M. Zhao, J. Pfister, F. Würthner, B. Engels, *J. Am. Chem. Soc.* **2008**, *130*, 12858–12859.

[181] H. G. Hansma, *J. Vac. Sci. Technol. B Microelectron. Nanom. Struct.* **1996**, *14*, 1390–1394.

[182] J. Tamayo, R. García, *Langmuir* **1996**, *12*, 4430–4435.

[183] J. M. Berg, J. L. Tymoczko, L. Stryer, *Biochemistry*, Palgrave MacMillan, New York, **2006**.

[184] A. Klug, *Philos. Trans. R. Soc. Lond. B. Biol. Sci.* **1999**, *354*, 531–535.

[185] T. L. Schlick, Z. Ding, E. W. Kovacs, M. B. Francis, *J. Am. Chem. Soc.* **2005**, *127*, 3718–3723.

[186] R. Corradini, S. Sforza, T. Tedeschi, R. Marchelli, *Chirality* **2007**, *19*, 269–294.

[187] J. W. Steed, J. L. Atwood, *Supramolecular Chemistry*, Wiley & Sons, Chichester, **2009**.

[188] F. Vögtle, *Supramolekulare Chemie*, Teubner Verlag, Stuttgart, **1992**.

[189] H.-J. Schneider, A. Yatsimirsky, *Principles and Methods in Supramolecular Chemistry*, Wiley & Sons, Chichester, **2000**.

[190] D. Adam, P. Schuhmacher, J. Simmerer, L. Haussling, K. Siemensmeyer, K. H. Etzbachi, H. Ringsdorf, D. Haarer, *Nature* **1994**, *371*, 141–143.

[191] J. Wu, M. D. Watson, L. Zhang, Z. Wang, K. Müllen, *J. Am. Chem. Soc.* **2004**, *126*, 177–186.

[192] H. Engelkamp, S. Middelbeek, R. J. M., Nolte, *Science* **1999**, *284*, 785–788.

[193] G. D. Pantoş, P. Pengo, J. K. M. Sanders, *Angew. Chem. Int. Ed.* **2007**, *46*, 194–197.

[194] G. D. Pantoş, J.-L. Wietor, J. K. M. Sanders, *Angew. Chem. Int. Ed.* **2007**, *46*, 2238–2240.

[195] J.-L. Wietor, G. D. Pantoş, J. K. M. Sanders, *Angew. Chem. Int. Ed.* **2008**, *47*, 2689–2692.

[196] B. M. Bulheller, G. D. Pantos, J. K. M. Sanders, J. D. Hirst, *Phys. Chem. Chem. Phys.* **2009**, *11*, 6060–6065.

[197] P. Osswald, D. Leusser, D. Stalke, F. Würthner, *Angew. Chem. Int. Ed.* **2005**, *44*, 250–253.

[198] P. Osswald, M. Reichert, G. Bringmann, F. Würthner, *J. Org. Chem.* **2007**, *72*, 3403–3411.

[199] P. Osswald, F. Würthner, *Chem. Eur. J.* **2007**, *13*, 7395–7409.

[200] M. M. Safont-Sempere, P. Osswald, K. Radacki, F. Würthner, *Chem. Eur. J.* **2010**, *16*, 7380–7384.

[201] V. Dehm, Z. Chen, U. Baumeister, P. Prins, L. D. A. Siebbeles, F. Würthner, *Org. Lett.* **2007**, *9*, 1085–1088.

[202] F. Würthner, C. Bauer, V. Stepanenko, S. Yagai, *Adv. Mater.* **2008**, *20*, 1695–1698.

[203] A. Wicklein, S. Ghosh, M. Sommer, F. Würthner, M. Thelakkat, *ACS Nano* **2009**, *3*, 1107–1114.

[204] S. Ghosh, X.-Q. Li, V. Stepanenko, F. Würthner, *Chem. Eur. J.* **2008**, *14*, 11343–11357.

[205] C. Thalacker, F. Würthner, *Adv. Funct. Mater.* **2002**, *12*, 209–218.

[206] Y. Xu, S. Leng, C. Xue, R. Sun, J. Pan, J. Ford, S. Jin, *Angew. Chem. Int. Ed.* **2007**, *46*, 3896–3899.

[207] T. D. Carson, S. M. Casey, I. K. Iverson, W. Seo, S. W. Tam-Chang, PCT Int. Appl. **2005**, WO 2005089094.

[208] N. Berova, K. Nakanishi, R. W. Woody, Eds., in *Circ. Dichroism*, **2000**, pp. 337–383.

[209] H. Ihmels, D. Otto, *Supermolecular Dye Chem.* **2005**, *258*, 161–204.

[210] I. Tinoco, *J. Am. Chem. Soc.* **1960**, *82*, 4785–4790.

[211] N. L. Vekshin, *J. Biol. Phys.* **1999**, *25*, 339–354.

[212] D. D. Perrin, W. L. F. Armarego, *Purification of Laboratory Chemicals*, Pergamon Press, Oxford, **1981**.

[213] J. Leonard, B. Lygo, G. Procter, *Praxis der Organischen Chemie*, Wiley-VCH, Weinheim, **1996**.

[214] M. Hesse, H. Meier, B. Zeeh, *Spektroskopische Methoden in der Organischen Chemie*, Thieme Verlag, Stuttgart, **2005**.

[215] G. A. Crosby, J. N. Demas, *J. Phys. Chem.* **1971**, *75*, 991–1024.

[216] Photon Technology International, Inc., can be found under www.pti-nj.com.

[217] R. G. Bennett, *Rev. Sci. Instrum.* **1960**, *31*, 1275–1279.

Acknowledgement/Danksagung

Herrn Professor Dr. Frank Würthner danke ich für die Überlassung des interessanten Themas, für wertvolle Anregungen und hilfreiche Diskussionen, für die ausgezeichneten Arbeitsbedingungen sowie für seine Unterstützung und Geduld in der Endphase der Doktorarbeit.

Herrn Dr. Chantu Saha-Möller danke ich für seine exzellente und zuverlässige Überarbeitung von Manuskripten und Teilen der vorliegenden Arbeit.

Herrn Dr. Vladimir Stepanenko, Herrn Dr. Xin Zhang und Herrn Dr. Thomas Rehm danke ich für die Durchführung der AFM und TEM Messungen bzw. der Kraftfeldrechnungen sowie für die daraus entstanden interessanten Diskussionen.

Herrn Joachim Bialas und Frau Manuela Kaiser danke ich für ihre tatkräftige Unterstützung und ihre unschätzbare Hilfe im Laboralltag.

Herrn Dr. Matthias Grüne und Frau Elfriede Ruckdeschel danke ich für die Aufnahme der NMR- Spektren sowie für hilfreiche Diskussionen.

Herrn Dr. Michael Büchner und Herrn Fritz Dadrich danke ich für die Aufnahme der Massenspektren.

Frau Lieselotte Michels danke ich für die Durchführung der Elementaranalysen.

Herrn Dipl.-Ing. Bernd Brunner danke ich für die immer rasche und kompetente Hilfe bei Computerproblemen.

Frau Christiana Toussaint danke ich für ihre Unterstützung in allen formalen und organisatorischen Belangen und Frau Ana-Maria Krause für ihre stete Hilfsbereitschaft.

Den Auszubildenden Frau Sabine Apel, Frau Tatjana Unger, Herrn Eugen Ehrlich und Herrn Kai Hammond danke ich für ihre engagierte Arbeit.

Meinen ehemaligen Kolleginnen und Kollegen, insbesondere Rüdiger, Peter, Volker, Conny, Andy, Valerie, Catharina, Johann, Theo, Manuela und Matthias sowie den Schmucks danke ich für ihre Unterstützung in allen Belangen und unsere gemeinsame, zwar manchmal anstrengende aber auch immer humorvolle Zeit.

Allen, die mich zur Fertigstellung dieser Arbeit ermutigt und mich bei deren Abschluss unterstützt haben, bin ich zu außerordentlichem Dank verpflichtet.

Meinen Eltern und meiner gesamten Familie gilt mein besonderer Dank für ihre großartige Unterstützung.

Thomas, Julian und Charlotte danke ich zutiefst für einfach alles!